UC Riverside
UC Riverside Electronic Theses and Dissertations

Title
Surface Chemistry in Chemical Deposition of Manganese-Based Thin Films on Silicon Substrates

Permalink
https://escholarship.org/uc/item/3vd9j111

Author
Sun, Huaxing

Publication Date
2013

Peer reviewed|Thesis/dissertation

eScholarship.org
Powered by the California Digital Library
University of California

UNIVERSITY OF CALIFORNIA
RIVERSIDE

Surface Chemistry in Chemical Deposition of Manganese-Based Thin Films on Silicon Substrates

A Dissertation submitted in partial satisfaction
of the requirements for the degree of

Doctor of Philosophy

in

Chemistry

by

Huaxing Sun

December 2013

Dissertation Committee:

Dr. Francisco Zaera, Chairperson
Dr. Leonard Mueller
Dr. Richard Hooley

Copyright by
Huaxing Sun
2013

The Dissertation of Huaxing Sun is approved:

Committee Chairperson

University of California, Riverside

ACKOWLEDGEMENTS

First of all, I would like to thank my research advisor, Professor Francisco Zaera, who is a distinguished professor of chemistry, and also a famous scientist in surface chemistry. I really appreciate his instructing, supervising and helping me throughout my graduate studies. Without his guidance and support, this research would have been impossible and I would have never made it. His valuable comments and discussions in the replies to my monthly reports gave me the light of what to do and how to make my research forward. He is always there to give a hand whenever I encountered a problem, academic or personal.

Also, I would like to thank Professor Leonard Mueller and Professor Richard Hooley for their advice on my dissertation and the final defense.

I am also grateful to my labmates: Dr. Xiangdong Qin, for supervising me and later helping me setting up the equipment, designing the experiments, analyzing data and fixing problems with the system in the 5 years; Dr Ilkeun Lee, for being able to help me and guide to use the system in the beginning; Stan Sheldon, for his help in the electronic and mechanic instruments, and home-made equipments; Dr. Qiang Ma, for his help for assisting me in the equipment repairing and results discussion; and to all the other persons in the lab that make my stay in the lab one of my greatest experiences in my life, whose names are Chris, Shinji, Xin, Menno, Taeseung, Yunxi, Karakalos, Aashani, Zhihuan, Lei, Yang,

Maryam, Lanxia, Xiaoliang, Dan, Timothy, Golam, Yurri, Alexander, Carlos, Yujun, Jie. Thank to all the labmates for their help with my graduate study.

I appreciate all the help provided in all the times by Linda Edwards, Christina Youhas, Barbara Outzen, Wayne Kaylor, Jeffery W Lefler, and Tina Enriquez.

Last but not least, I would like to thank all the support that was given by my family and friends. Without their support and encouragement, I would not have made this possible.

COPYRIGHT ACKKNOWLEDGMENTS

The text of this dissertation, in part or in full, is a reprint of the material as is appears in the publications below. Dr. Francisco Zaera directed and supervised the research which forms the basis for this dissertation. Dr. Xiangdong Qin helped me set up equipment and maintain the system, and supervised me in the first two years.

[1] H. Sun. X. Qin, F. Zaera, *Journal of Physical Chemistry Letters,* **2011**, 2, 2525;

[2] H. Sun, X. Qin, F. Zaera, *Journal of Physical Chemistry Letters*, **2012**, 3, 2523;

[3] H. Sun, F. Zaera, *Journal of Physical Chemistry*, C **2012**, 116, 23585.

ABSTRACT OF THE DISERTATION

Surface Chemistry in Chemical Deposition of
Manganese-Based Thin Films on Silicon Substrates

by

Huaxing Sun

Doctor of Philosophy, Graduate Program in Chemistry
University of California, Riverside, December 2013
Dr. Francisco Zaera, Chairperson

Manganese films have been identified as potential candidates for the self-formation of barriers to prevent the diffusion of copper interconnects into the underlying silicon substrate. Given the complex topography of the modern integrated circuits where these diffusion barriers are to be used and the unique nature of chemical vapor deposition (CVD) and atomic layer deposition (ALD), those methods are considered to replace the traditional physical deposition approach, forming more conformal diffusion barriers layers.

In this project, the growth of manganese-based films on silicon substrates via chemical deposition of two Mn metalorganic complexes, bis(N,N'-diisopropyl-pentylamidinato) Mn(II)) (Mn Amidinate) and methylcyclopentadienyl-manganese(I) tricarbonyl (MeCpMn(CO)$_3$, was characterized and contrasted by using an instrument equipped with a reactor coupled to a X-ray photoelectron

spectroscopy (XPS) analytical chamber. The goal of this project is to develop a molecular-level understanding of the surface chemistry for the precursor to improve the selection of manganese precursors.

In our initial studies on the nature of films prepared by chemical means using $MeCpMn(CO)_3$ as the precursor, it was found that a manganese silicate layer grows first and a thin manganese silicide film develops latter at the SiO_2/Si (100) interface between approximately 550 and 750 K. It was also found that a typical nude ion gauge is capable of enhancing the deposition through gas-phase activation of $MeCpMn(CO)_3$ by electron bombardment. Finally, Mn Amidinate was proved to be highly reactive, affording the deposition of Mn at reasonable rates, higher at higher temperatures, but also leading to the incorporation of nitrogen and additional carbon in the grown Mn(0) films; $MeCpMn(CO)_3$, by contrast, was quite unreactive, but did not leave nitrogen contaminants on the surface. As with the carbonyl precursor, deposition with the Mn amidinate leads to the formation of a nonstoichiometric mixture of MnOx + SiOx and Mn silicate first, possibly followed by the formation of a thin subsurface Mn silicide layer. The combined Mn silicate/Mn silicide structure acts as an effective diffusion barrier, after which Mn(0) metallic films can be grown on top.

One copper precursor, copper (I)-*N,N'*-di-*sec*-butylacetamidinate, was also deposited on the as-formed manganese thin film above with different ratios of Mn(0) and Mn silicate. Details of the results from this work are discussed.

TABLE OF CONTENTS

Pages

ACKNOWLEDGEMENTS……iv

ABSTRACT……vii

TABLE OF CONTENTS……ix

LIST OF FIGURES……xiii

CHAPTER ONE

Introduction and Overview……1

1.1 Copper interconnect……1

1.2 Atomic layer deposition……3

1.3 Manganese precursors……5

1.4 Dissertation work……6

1.5 References: ……9

CHAPTER TWO

Experimental……11

2.1 Introduction……11

2.2 X-ray photoelectron spectroscopy (XPS)……11

2.3 XPS experimental setup……13

2.4 References……17

CHAPTER THREE

Activation of $MeCpMn(CO)_3$ by Electron Bombardment in Gas Phase for Enhanced Deposition of Solid Films……18

3.1 Introduction……………………………………………………………………………...18

3.2 Experimental methods………………………………………………………………19

3.3 Results and discussion………………………………………………………………20

3.4 Conclusion……………………………………………………………………………...33

3.5 References……………………………………………………………………………...35

CHATPER FOUR

Manganese Deposition on Si with Native Oxide Using MeCp(CO)$_3$……………...37

4.1 Introduction……………………………………………………………………………...37

4.2 Preliminary results……………………………………………………………………38

4.3 Results……………………………………………………………………………………...43

4.3.1 Deposition of MeCpMn(CO)$_3$ at different temperatures…………....43

4.3.2 Angle-resolved XPS for MeCpMn(CO)$_3$ on Si with native oxide….46

4.3.3 Uptake study of MeCpMn(CO)$_3$ on Si with native oxide……………53

4.4 Uptake of MeCpMn(CO)$_3$ on Si with different thick silicon oxide……….53

4.5 Discussions and conclusions……………………………………………………...56

4.6 References……………………………………………………………………………...61

CHAPTER FIVE

Chemical Vapor Deposition of Manganese Metallic Films on Silicon Oxide Substrates……………………………………………………………………………………64

5.1 Introduction……………………………………………………………………………...64

5.2 Results……………………………………………………………………………………...65

5.2.1 Deposition of Mn Amidinate on Si with 300 nm silicon oxide…...65

5.2.2 Deposition of MeCpMn(CO)$_3$ on Si with 300 nm silicon oxide…...75

5.2.3 Deposition vs diffusion in manganese deposition……………………..83

5.2.4 Optimized deposition sequence……………………………………………87

5.3 Discussion…………………………………………………………………………..89

5.4 Conclusion…………………………………………………………………………..98

5.5 References…………………………………………………………………………101

CHAPTER SIX

Chemical Deposition of Copper on the As-deposited Manganese Films…..103

6.1 Introduction………………………………………………………………………103

6.2 Results……………………………………………………………………………..103

6.2.1 Preparation of as-deposited Mn thin film…………………………….103

6.2.2 CuAM on MnSiOx/300 nm SiO_2 at 625 K……………………………..104

6.2.3 CuAM on Mn(0)/MnSiOx/300 nm SiO_2 at 625 K……………………113

6.2.4 CuAM on 300 nm SiO_2 vs Mn(0)/MnSiOx/300 nm SiO_2 at 425K135……………………………………………………………………116

6.3 Discussion and Conclusion……………………………………………………..120

6.4 References………………………………………………………………………...122

CHAPTER SEVEN

General Conclusions and Future Work……………………………………………123

7.1 General conclusions……………………………………………………………..123

7.2 Future work………………………………………………………………………..126

7.2.1 Studies using temperature programmed desorption……………..126

7.2.2 Studies on manganese thin film deposition…………………………..127

7.2.3 Studies on Cu deposition on the manganese thin films…………...127

7.2.4 Electronic properties measurements……………………………………..128

7.3 References………………………………………………………………………...129

LIST OF FIGURES

CHAPTER ONE

Figure 1.1 Schematic process of atomic layer deposition (ALD)…………………….....4

Figure 1.2 Chemical formulas of the two precursor molecules: top, methylcyclo pentadienylmanganese(I) tricarbonyl ($MeCpMn(CO)_3$); bottom, bis(N,N'-diiso propylpentylamidinato)manganese(II)……………………………………………………7

CHAPTER TWO

Figure 2.1 A picture of the UHV system used in this dissertation……………………..12

CHAPTER THREE

Figure 3.1 Mn 2p (left) and C 1s (right) XPS data from 300 nm silicon dioxide films exposed to defined doses of $MeCpMn(CO)_3$ at 625 K………………………………21

Figure 3.2 O 1s XPS data from 300 nm SiO_2 films exposed to defined doses of $MeCpMn(CO)_3$ at 625 K…………………………………………………………………………..22

Figure 3.3 Si 2p XPS data from 300 nm SiO_2 films exposed to defined doses of $MeCpMn(CO)_3$ at 625 K…………………………………………………………………………..23

Figure 3.4 Mn 2p XPS traces from sputterred Si(100) with completely removal of native oxide exposed to $MeCpMn(CO)_3$……………………………………………………..26

Figure 3.5 Deposition of $MeCpMn(CO)_3$ on 300nm SiO_2 at room temperature with IG on…………………………………………………………………………………………………..27

Figure 3.6 Electron-impact mass spectrum for $MeCpMn(CO)_3$……………………...29

Figure 3.7 Schematic chart of gas-phase activation of $MeCpMn(CO)_3$ by electron bombardment ……………………………………………………………………………………34

CHATPER FOUR

Figure 4.1 Mn 2p XPS for deposition of $MeCpMn(CO)_3$ on Si with native oxide at 425 K with separate dosings……………………………………………………………….…39

Figure 4.2 Mn 2p XPS for deposition of $MeCpMn(CO)_3$ on Si with native oxide at 600 K with separate dosings…………………………………………………………………..40

Figure 4.3 Mn 2p XPS intensity for $MeCpMn(CO)_3$ at 425K *vs* 600K…………………41

Figure 4.4 Left: Mn 2p XPS for $MeCpMn(CO)_3$ (0.15 m Torr for 2000 s) on a Si(100) sample covered with its native oxide layer(~1 nm) as a function of temperature……………………………………………………………………………………..44

Figure 4.5 Angle-resolved Mn 2p (left) and Si 2p (right) XPS for $MeCpMn(CO)_3$ (0.08 mTorr for 3780 s) on a Si(100) sample covered with its native oxide layer(~1 nm) at 625 K as a function of detection (takeoff) angle, measured from the surface normal………………………………………………………………………………..48

Figure 4.6 Angle-resolved C 1s XPS for $MeCpMn(CO)_3$ (0.08 mTorr for 3780 s) on a Si(100) sample covered with its native oxide layer(~1 nm) at 625 K as a function of detection (takeoff) angle, measured from the surface normal………...49

Figure 4.7 Summary of XPS peak intensities in Figure 4.5 and 4.6 as a function of detection angle (symbols with error bars) and a proposed layered model structure on the basis of the angular dependence displayed in this figure…........51

Figure 4.8 Left: Uptake Mn 2p XPS data from a SiO_2/Si(100) surface dosed with 0.15 mTorr of $MeCpMn(CO)_3$ at 675 K as a function of dosing time. Right: Summary of peak intensities for the Mn species in the left panel……………………..54

Figure 4.9 Mn 2p XPS for $MeCpMn(CO)_3$ on silicon surfaces dosed with ~2 $x10^6$ L

at 625 K (left) and after annealing at 725 K (right)……………………………………….55

Figure 4.10 Schematic chart for the formation of the layered structure in the uptake of $MeCpMn(CO)_3$ on the Si with native oxide substrate……………………...60

CHAPTER FIVE

Figure 5.1 Mn 2p XPS data for the evolution of a silicon oxide substrate upon exposure to 0.4 mTorr of Mn Amidinate at 625 K…………………………………………66

Figure 5.2. Summary of the Mn 2p XPS signal intensities obtained in Mn uptake studies such as that illustrated in Figure 5.1 as a function of substrate temperature using the Mn Aamidinate precursor……………………………………..…..69

Figure 5.3. C 1s XPS data for the same experiment reported in Figure 5.1. The raw data were deconvoluted into three Gaussian components, corresponding to, from low to high binding energies: carbidic, and two organic components. ….…72

Figure 5.4 N 1s XPS data for the same experiment reported in Figure 5.1….……73

Figure 5.5 Summary of the N 1s XPS signal intensities obtained in Mn Amidinate uptake experiments such as that shown in Figure 5.4 for three substrate temperatures. ………………………………………………………………………………………74

Figure 5.6 Mn 2p XPS uptake spectra for films grown on SiO_2 using ($MeCpMn(CO)_3$) at three deposition temperatures: 625 (left), 675 (center), and 725 (right) K……………………………………………………………………………………77

Figure 5.7 Summary of the XPS signal intensities seen during the uptake of $MeCpMn(CO)_3$ on SiO_2 at 725 K. Data are reported for the O 1s, Si 2p, and Mn 2p XPS signals……………………………………………………………………………………....79

Figure 5.8 Depth profile for the as-formed thin films with Ar^+ sputtering as function of time……………………………………………………………………………..…………..82

Figure 5.9 Mn 2p XPS for the annealing of the as-deposited thin film grown by Mn Amidinate precursor…………………………………………………………………………..84

Figure 5.10 Summary of the XPS signal intensities seen during the uptake of $MeCpMn(CO)_3$ on SiO_2 at 625 K at different dosing pressures……………………….86

Figure 5.11 Manganese deposition using Mn Amidinate first, and then $MeCpMn(CO)_3$ on Si with 300 nm thick silicon oxide………………………………..…..88

CHAPTER SIX

Figure 6.1 Copper precursor: copper(I)-*N,N'*-di-*sec*-butylacetamidinate………..105

Figure 6.2 Mn 2p XPS for the deposition of $MeCpMn(CO)_3$ on 300nm SiO_2 at 625 K as function of dosing time(60, 120, 180, 240, and 300 minutes)…………………106

Figure 6.3 XPS Mn 2p for CuAM deposition on 300n SO_2 covered by Mn silicate at 625 K and sputtering after deposition……………………………………………………108

Figure 6.4 XPS Cu 2p for CuAM deposition on 300n SO_2 covered by Mn silicate at 625 K and sputtering after deposition……………………………………………………109

Figure 6.5 XPS C 1s for CuAM deposition on 300n SO_2 covered by Mn silicate at 625 K and sputtering after deposition. ………………………………………………….110

Figure 6.6 XPS Mn 2p for $MeCpMn(CO)_3$ on the as-deposited Cu thin film made by 30 minutes dosing of CuAM……………………………………………………………112

Figure 6.7 XPS Mn 2p for the mixed depositions(a to e) using $MeCpMn(CO)_3$ and CuAM…………………………………………………………………………………………114

Figure 6.8 XPS Mn 2p for the mixed depositions(a to e) using $MeCpMn(CO)_3$ and CuAM……………………………………………………………………………………………………..115

Figure 6.9 XPS Cu 2p for CuAM on bare 300 nm SiO_2 vs Mn(0)/MnSiOx/300 nm SiO_2 at 425 K………………………………………………………………………………………….117

Figure 6.10 XPS N 1s for CuAM on bare 300 nm SiO_2 vs Mn(0)/MnSiOx/300 nm SiO_2 at 425 K………………………………………………………………………………………….118

CHAPTER ONE

Introduction and Overview

1.1 Copper interconnect

There have been great changes in the semiconductor industries in recent decades. For example, personal computers have become more and more powerful while they are cheaper and cheaper. One reason for this is that the chips inside computers are shrinking all the time when the poer of the transistors inside the chips are increasing as the technology develops. This observation, described by Moore's law, reflects the history of computing hardware in recent 50 years, predicating that the number of transistors on the integrated circuits doubles approximately every 18 months [1]. Usually integrated circuits are arranged on a 2-dimensional wafer surface. As the demands and requirements for high-speed central processing units (CPU) increase, 3-D integration has replaced 2-D integration to be able to pack many more transistors in the same unit size. Conductive interconnects are necessary to connect the different layers as well as transistors inside one single layer, which makes the stacking multiple units together possible.

Copper (Cu) is replacing aluminum as the standard material for connecting transistors in integrated circuits due to its relatively low resistivity and excellent electromigration properities [2,3]. Barriers must be placed surrounding the Cu wires to prevent its diffusion to the insulating materials and its oxidation by

oxygen and water in the environment [3]. In the current technology map [4], sputtered tantalum nitride (TaN) serves as an effective diffusion barrier, and tantalum (Ta) is sputtered on top of TaN to enhance the adhesion of Cu, and improve the durability of 3-D structures.

The non-conformal nature of the sputtering method for TaN and Ta layers has caused problems as the dimensions of the integrated circuits shrinking. Sputtering makes thicker layer near the top opening, leading to the formation of voids in the following electroplating process for Cu on the inside regions that are shielded from the line of sight to the sputtering target.

The material properties are dependent on the fabrication method. Physical vapor deposition methods have been applied to deposit these layers in the current technology, but it is difficult to sputter completely conformal and uniform barrier and adhesion layers. Other materials have also recently tested as diffusion barriers. In particular, manganese films have been identified as potential candidates for the self-formation of barriers to prevent the diffusion of copper interconnects into the underlying silicon substrates [5-9]. A few nm thick barrieries, in the form of amorphous manganese silicate (MnSixOy), could be formed by sputtering a Mn-Cu alloy and annealing at 450°C [10]. However, the sputtering method used in those studies stills suffers from the problem of conformity. Thus there is a need for finding a method to form more conformal diffusion barriers. Given the complex topography of the modern integrated circuits where these diffusion barriers are to be used and the unique nature of

chemical vapor deposition (CVD) and atomic layer deposition (ALD), those methods are considered ideal to replace the traditional physical deposition approach [11].

1.2 Atomic layer deposition

CVD is a chemical process used to produce solid materials in high purity and high performance, and it is often used in the semiconductor industry to produce thin films. In a typical CVD process, one or more precursors are introduced to react and/or decompose on the substrate surface to produce the desired deposit, while volatile by-products are usually also produced and removed by gas flow through the reaction chamber. In particular, conformal self-aligned MnSixOy bariers for Cu interconnects made using CVD of manganese metal have shown to be good barriers against the diffusion of Cu, O_2 and H_2O [12]. However, the nature of the final films in that case appears to be complex, and it is not fully understood.

Atomic layer deposition (ALD), is a modified version of chemical vapor deposition introduced by T. Suntola in Finland [13]. ALD has been shown to be capable of growing conformal and uniform thin films with precise thickness control by sequentially introducing two self-limiting and complementary half-cycle reactions to grow a monolayer at a time. A thin film can be built up by repeating the cycles, which enables the precise thickness control of a thin film by

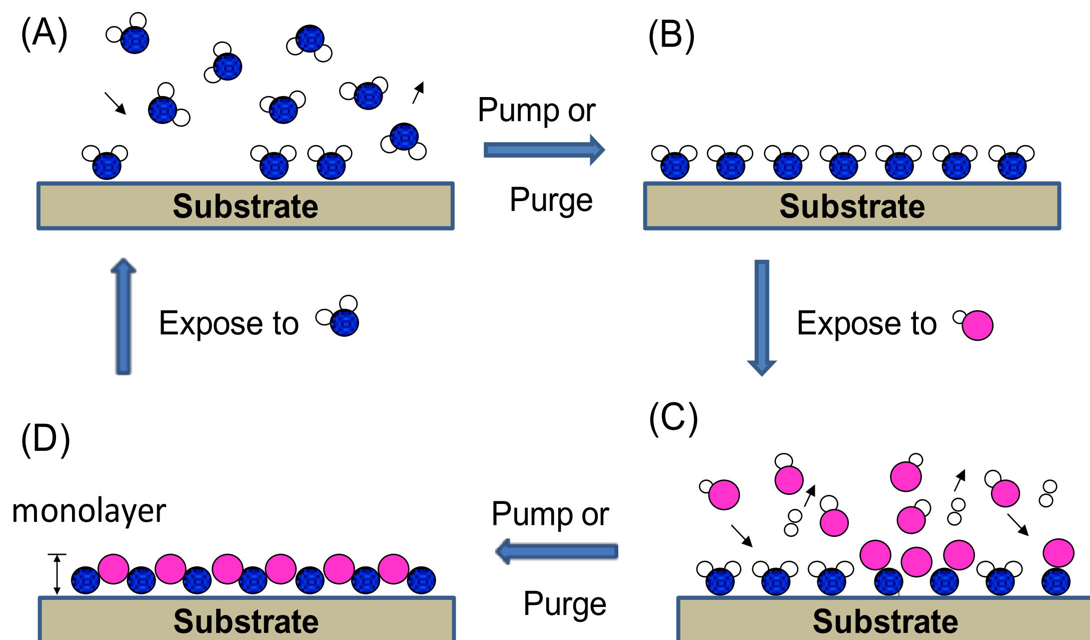

Figure 1.1 Schematic process of atomic layer deposition (ALD)

the number of reaction cycles. At the same time, uniform thin films can be easily deposited over large and complex substrates because gas molecules can react over the whole surfaces in the reaction zone. As a result, ALD is becoming a promising method for the production of very thin films in the integrated circuits in the semiconductor industry [14]. It would be highly desirable to find appropriate precursors and apply the ALD method to the formation of manganese silicate barriers to produce uniform and conformal thin film.

Despite the fact that ALD offers many advantages, including great control over film thickness, it does have some limitations, such as the incorporation of impurities, and low growth rate [15]. The key to solving these issues is to advance the understanding of the ALD process at a molecular level.

1.3 Manganese precursors

One of the biggest challenges in CVD and ALD is to find the appropriate precursor. The precursor selected needs to be volatile and stable enough to be delivered into the ALD reactor as a gas at relatively low temperatures, yet it also needs to be prevented from undergoing extensive decomposition and depositing impurities. Of course, it must also be able to proceed via the required self-limiting half reactions in the ALD process to reach saturated chemisorption of precursor molecules on the surface. Many Mn metalorganic complexes have been tested for CVD Mn [16-19], but only a few have ever been tested for ALD of

manganese oxide [20,21], and none have yet been identified as to have ideal behavior for this application.

In our research, we chose two of the most promising manganese precursors used in the CVD of manganese oxide, methylcyclopentadienylmanganese(I) tricarbonyl ($MeCpMn(CO)_3$) and bis(N,N'-diisopropylpentylamidinato)Mn(II) (Mn Amidinate), to investigate the surface chemistry of ALD process on different silicon substrates. Though $MeCpMn(CO)_3$ has been shown to be a good precursor for the CVD of Mn [18,22], the ALD process using this precursor has not been tested. The Mn Amidinate precursor used in these studies was provided by Intel, and was synthesized by following a procedure reported by Gordon [23].

Our work focuses on the use of surface science techniques to understand the key criteria for the selection of optimum organometallic manganese precursors on different silicon substrates at different temperatures. One copper compound was also deposited to study the deposition of Copper on the as-deposited manganese-based thin film to test its possibility as a copper diffusion barrier.

1.4 Dissertation work

The work presented in this dissertation has been divided into 7 chapters. An introduction with an overview of the projects is briefly offered in Chapter 1. A discussion of the experimental details including a description of the materials, experimental apparatus, and surface analysis techniques employed is provided

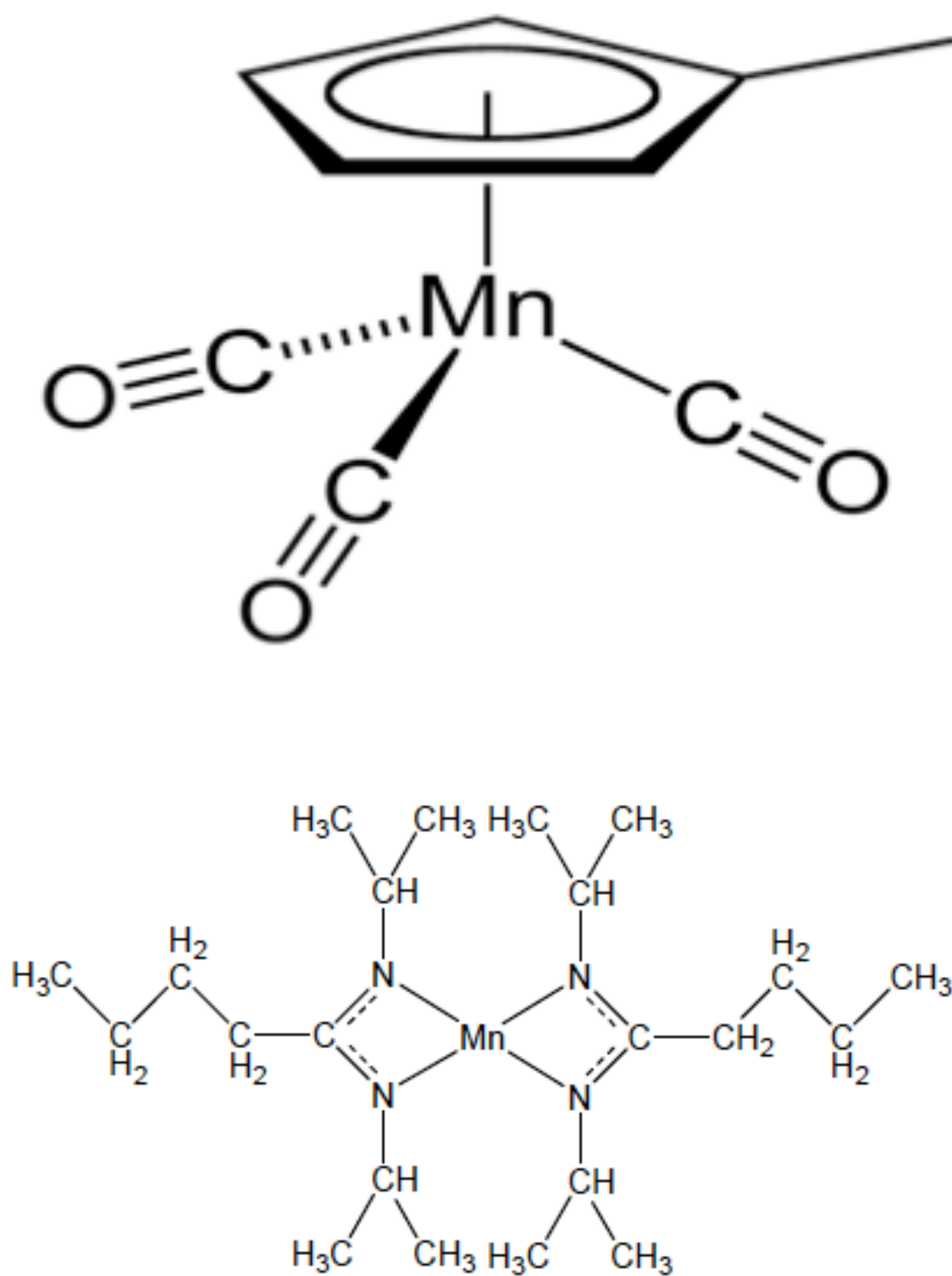

Figure 1.2 Chemical formulas of the two precursor molecules:

top, methylcyclopentadienylmanganese(I) tricarbonyl ($MeCpMn(CO)_3$);

bottom, bis(N,N'-diisopropylpentylamidinato)manganese(II).

in Chapter 2. Chapter 3 presents data on the incorporation of gas-phase electron-impact ionization and activation of the metal-organic compound, $MeCpMn(CO)_3$, for the atomic layer deposition (ALD) process. In Chapter 4, the deposition of $MeCpMn(CO)_3$ on silicon (Si) with a native oxide film is described. In the following Chapter 5, the deposition of two precursors, $MeCpMn(CO)_3$ and Mn Amidinate, on Si with thick silicon oxide films (300 nm) are compared and analyzed, and the optimized deposition sequence of the two different manganese precursors to get the fast growth Mn-based thin film while the surface contaminates are minimized is also demonstrated. Chapter 6 introduces preliminary results from studies on the deposition of copper on the as-deposited Mn-based thin film to test the possibility of those serving as a diffusion barrier for copper. Finally, some general conclusions and proposed future work are given in Chapter 7. Most of the results in the following chapters were published in articles and re-written with permission: Chapter 3 in the *Journal of Physical Chemistry Letters*, 2012, 3, 2523-2527; Chapter 4 in the *Journal of Physical Chemistry Letters*, 2011, 2, 2525-2530; Chapter 5 in the *Journal of Physical Chemistry*, 2012, 116, 23585-23595 (copyright by American Chemical Society). The experiments reported in Chapter 3 and Chapter 4 were finished in collaboration with Dr. Xiangdong Qin.

1.5 References:

[1] G. Moore, *Electronics Magazine*, **1965**, 38, 8;

[2] Z. Li, S. T. Barry, R. G. Gordon, *Inorganic Chemistry*, **2005**, 44, 1728;

[3] Z. Li, A. Rahtu, R. G. Gordon, *J. Electrochem. Soc.*, **2006**, 153, C787;

[4] International Technology Roadmap for Semiconductors, **2008**;

[5] J. Koike, M. Wada, *Appl. Phys. Lett.* **2005**, 87, 041911;

[6] T. Usui, H. Nasu, S. Takahashi, N. Shimizu, T. Nishikawa, M. Yoshimaru, H. Shibata, M. Wada, J. Koike, *IEEE Trans. Electron Devices,* **2006**, 53, 2492;

[7] J. Koike, M. Haneda, J. Iijima, Y. Otsuka, H. Sako, K. Neishi, *J. Appl. Phys.* **2007**, 102, 043527;

[8] M. Haneda, J. Iijima, J.Koike, *Appl. Phys. Lett.* **2007**, 90, 252107;

[9] J. Iijima, Y. Fujii, K. Neishi, J. Koike, *J. Vac. Sci. Technol. B,* **2009**, 27, 1963;

[10] J. Koike, M. Haneda, J. Iijima, Y. Otsuka, H. Sako, and K. Neishi, *J. Appl. Phys.* **2007**, 102, 043527;

[11] H. Sun, F. Zaera, *J. Phys. Chem. C*, **2012**, 116, 23585;

[12] R. G. Gordon, H. Kim, Y. Au, H. Wang, H.B. Bhandari, Y Liu, D. K. Lee, Y Lin, *Advanced Metallization Conference 2008 proceedings*, **2009**, 321;

[13] A. Niskanen, A. Rahtu, T. Sajavaara, K. Arstila, M. Ritala, M. Leskela, *J. Electrochem. Soc.*, **2005**, 152, G25;

[14] A.I. Kingon, J. –P. Maria, S. K. Streiffer, *Nature*, **2000**, 406, 1032;

[16] G.N.Pain, N. Bharatula, G.I. Christiansz, M.H. Kibel, M.S. Kwietniak, C. Sandford, T. Warminski, R.S. Dickson, R.S. Rowe, K. McGregor, *J. Cryst. Growth,* **1990**, 101, 208;

[17] D.K. Russell, I.M.T. Davidson, A.M. Ellis, G.P. Mills, M. Pennington, I.M.

Povey, J.B. Raynor, S. Saydam, *Chem. Vap. Dep*. **1998**, 4, 103;

[18] M.J. Almond, H. Redman, D.A Rice, *J. Mater. Chem.* **2000**, 10, 2842;

[19] S.Wen-bin, K. Durose, A.W. Brinkman, J. Woods, *J. Cryst. Growth*, **1991**,13, 1;

[20] B.B. Burton, F.H. Fabreguette, S.M. George, *Thin Solid Films*, **2009**, 517, 5658;

[21] O. Nilsen, H. Fjellvåg, A. Kjekshus, *Thin Solid Films*, **2003**, 444, 44;

[22] S. Wen-bin, K. Durose, A.W. Brinkman, B.K. Tanner, *Mater. Chem. Phys.* **1997**, 47, 75;

[23] B.S. Lim, A. Rahtu, J.S. Park, R.G. Gordon, *Inorg. Chem.* **2003**, 42, 7951.

CHAPTER TWO

Experimental

2.1 Introduction

All the experiments discussed in this dissertation were carried out inside an ultrahigh vacuum (UHV) chamber equipped with X-ray photoelectron spectroscopy (XPS) to investigate the surface chemistry of manganese precursors and other reactants on three different substrates under different experimental conditions: Si (100) single crystal wafer with native oxide, sputtered Si without native oxide, and Si with thick silicon oxide (300 nm). Mass spectra of the precursor $MeCpMn(CO)_3$ were acquired by using an Agilent 7890/ Waters GCT GC-MS instrument in our lab [1,2]. Figure 2.1 shows a picture of the system.

2.2 X-ray photoelectron spectroscopy (XPS)

X-ray photoelectron spectroscopy (XPS), also known as ESCA (Electron Spectroscopy for Chemical Analysis), is the primary surface sensitive technique used here to characterize the deposition of the precursors in our experiments. XPS is widely used to measure the composition and electronic structure of elements in thin films [3]. By irradiating a material with a beam of X-rays, XPS spectra are obtained through measuring the kinetic energy and number of excited electrons that escape from the surface of the material, which are detected

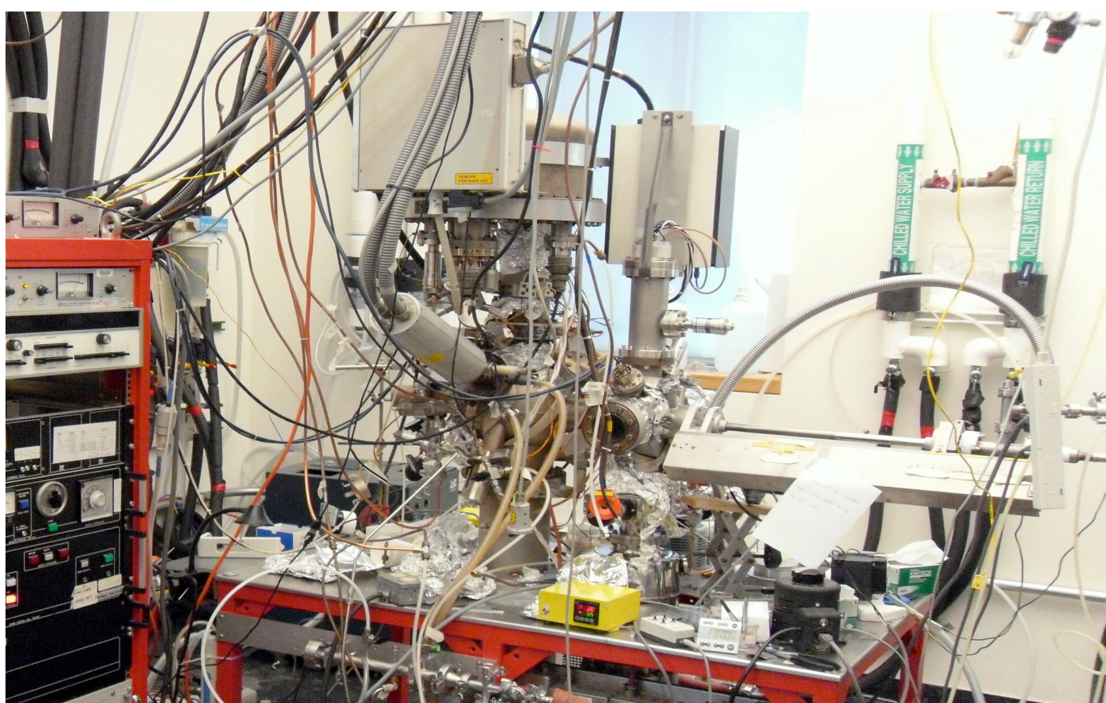

Figure 2.1 A picture of the UHV system used in this dissertation.

by a hemispherical electron energy analyzer under ultra-high vacuum (UHV) conditions. The XPS spectra obtained here display peaks with different binding energies, whose positions are determined by the identity and chemical environments of the elements on the surface. Generally speaking, the intensity of the peaks is proportional to the surface concentration of the elements, while the binding energy might be different with changes in oxidation states.

2.3 XPS experimental setup

All X-ray photoelectron spectroscopy (XPS) experiments discussed in the following chapters were obtained by using a two-chamber stainless-steel ultrahigh vacuum (UHV) apparatus. The main chamber on the left is evacuated to a base pressure of ~1 x 10^{-9} Torr by using a turbomolecular pump for the acquisition of the XPS data. The auxiliary chamber in the middle, which is also evacuated by a separate turbomolecular pump, is mainly designed to transfer the samples fast from the outside into the UHV XPS analytical chamber, while it was also used as a preparation chamber to perform the exposure of the samples to the manganese precursors in this study. As a result, the as-deposited samples can be delivered into the main chamber without obvious vacuum break and exposure to the outside air.

A typical process for the way our experiment are carried out is as follows: first, a silicon substrate (~1 cm x 1 cm) is cleaned by placing it into a small beaker with acetone and, after 10 minutes of ultrasonic cleaning, washing by deionized water

for 2 minutes, and finally blowing dry with compressed air and mounting on a supporting rod. The rod is transferred into the small load lock chamber on the right of the picture, which is evacuated by a mechanic pump; after 10 minutes, it is transferred to the preparation chamber in the middle and kept in the chamber for 2 hours before it is finally delivered into the main XPS chamber to collect the data for the substrate without any deposition, used as a control experiment. The rod can be used to transfer the substrate back to the preparation chamber to be exposed to the precursors for several minutes to hours, and to return the sample to the main chamber for XPS data collection. The rod can be also rotated for alignment and angle-resolved XPS studies. It is capable of cooling down to ~175 K and resistive heating up to close to 1000 K. The temperature of the substrate is monitored with a K-type thermocouple inserted between the sample and the metallic clip that holds the sample in place.

The XPS data were collected using a Leybold EA11 multichannel detection system and a dual Mg–Kα/Al–Kα anode X-ray excitation source; the data reported here were acquired using the aluminum anode (hν = 1486.6 eV) or magnesium anode (hν = 1253.6 eV). The XPS data from the two anodes might have different intensities for the same element with the same oxidation state, but the same anode was used to make the results are comparable with the data reported in each individual chapter. The total resolution of the instrument under the settings used in this study (nonmonochromatized X-ray sources with fixed pass energy at 100.8 eV) was approximately 1.0 eV, but peak positions could be determined within an accuracy of approximately 0.1 eV. After collecting the raw

data using the software provided by *SPECS* for the system, *MS Excel* was used in our work to transfer and briefly process the data, and then software, *XPS Peak 4.1*, was used for the deconvolution of the XPS peaks and the identification of the different components of the overall signals in the spectra of each element [4,5]. All XPS peak positions are reported in binding energies (BE), calibrated against values for the Si 2p XPS peaks [6]. In most analysis, Shirley background subtraction was done first, after which Gaussian peaks were fitted. The binding energies and widths for a given element were fixed across each data set to minimize the number of adjustable parameters. In some cases, two pairs of peaks were used to fit the Mn $2p_{3/2}$ and Mn $2p_{1/2}$ XPS features, corresponding to the Mn(0)/Mn silicide and Mn silicate components, respectively, when those species were detected (which was the case in most sample). In most cases, the signal intensities are reported in arbitrary units, but were corrected by the XPS atomic sensitivity factors reported for concentric hemispherical analyzers in order to allow for relative comparisons across the data for the different elements [7]. Depth profiling was carried out with an ion gun, using argon gas at a pressure of 3×10^{-6} Torr and an emission current of 25 mA.

The methylcyclopentadienyl manganese tricarbonyl (MeCpMn $(CO)_3$) precursor used in these studies was purchased from Strem Chemicals (97% minimum purity), while the bis(N,N'-diisopropylpentylamidinato) Mn(II) precursor used was provided by Intel. The melting point of MeCpMn$(CO)_3$ is -2.2^{o}C, and its vapor pressure at 20°C is about 0.05 Torr, high enough for the delivery and deposition without heating the manifold. Both precursors were purified by a series of

freeze-pump-thaw cycles in situ in our gas-handling manifold, and dosed by introducing its vapor into the chamber using different leak valves. However, Mn Amidinate is a yellow solid under room temperature and it's very air and water sensitive. Several cycles of freeze-pump-thaw were necessary to remove the residual water and oxygen inside the manifold after getting the precursor into the manifold in a glove box. Then it is ready to use. To get sufficient dosing pressure, the manifold for the second precursor, Mn Amidinate, needs to be heated and kept in a 90°C silicone oil bath when the vapor pressure is ~0.07 Torr. Parts of the preparation chamber on the delivery pass including the leak valve for Mn Amidinate needs to keep warm too to avoid the possible deposition on the walls. Gas doses were set by fixing the gas pressure (followed continuously by using a nude ion gauge) and dosing times and reported in units of Langmuirs (1 L = 1 x 10^{-6} Torr for one second).

Zero-grade Argon (Ar, 99.998%) and hydrogen gas (H_2, 99.99%) were purchased from Airgas. Ar was used to sputter the surface of Si with native oxide to obtain the sputtered Si without native oxide, also it was used to do the depth profiling experiments by sputtering the as-deposited thin films for minutes to remove the layers on the surfaces at a speed about 1 monolayer a minute.

2.4 References:

[1] M. Bouman, F. Zaera, *ECS Trans*. **2010**, 33, 291;

[2] M. Bouman, F. Zaera, *J. Electrochem. Soc.* **2011**, 158, D524;

[3] W. M. Lau, X. –W. Wu, *Surf. Sci.* **1991**, 245, 345;

[4] Q. Ma, H. Guo, R.G. Gordon, F. Zaera. *Chem. Mater*. **2011**, 23, 3325;

[5] Q. Ma, F. Zaera, R.G. Gordon, *J. Vac. Sci. Technol.*, A **2012**, 30, 01A114;

[6] C. D. Wagner, W.M. Riggs, L.E. Davis, J.F. Moulder, G.E. Muilenberg, G.E. Eds, *Handbook of X-Ray Photoelectron Spectroscopy*, Perkin-Elmer Corporation: Eden Prairie, MN, **1978**;

[7] D. Briggs, M.P. Seah, *XPS Atomic Sensitivity Factors versus Atomic Number. In Practical Surface Analysis. Auger and X-ray Photoelectron Spectroscopy*, John Wiley and Sons: Chichester, U.K., **1990**, 1.

CHAPTER THREE

Activation of $MeCpMn(CO)_3$ by Electron Bombardment in Gas Phase for Enhanced Deposition of Solid Films

3.1 Introduction

One of the main challenges in CVD and ALD is the selection of an appropriate precursor. That precursor should be sufficiently reactive to dissociatively adsorb on the solid surface and form viable metal-containing surface intermediates [1]. Nevertheless, the precursor needs to be stable enough to be delivered whole to the substrate at sufficient vapor pressure. However, these two requirments are somewhat contradictory: precursors with excessive reactivity easily decompose before reaching the desired surfaces; yet stable compounds may be difficult to activate upon the adsorption on the desired surfaces at all. One solution to the activation problem is to use harsh conditions such as high temperatures in the deposition process, but this is often counterproductive. Because high temperature may affect the integrity of the surface, for instance, the circuits already present on the wafer, leading to undesirable structural changes in the grown films or the incorporation of contaminants. Another solution might be to activate the precursor before it reaches the surface, so such deposition can be finished under mild reaction conditions, such as lower temperature. Electron bombardment is widely used as a method of ionization to produce ions in mass

spectrometry, particularly for gases and volatile organic molecules; it has been reported in films study [2-4]. In the electron bombardment method, electrons produced through thermionic emission by heating a wire filament, are accelerated and attracted to the trap electrode. At the same time, neutral molecules are introduced to interact with these electrons, giving rise to fragment ions by cleavage reactions [5]. These fragments are highly reactive, and might be used in thin film deposition.

In this chapter, we advance an alternative approach, simply turning on the nude ion gauge widely used in UHV systems, for some ALD processes based on the gas-phase activation of the precursor by electron bombardment immediately prior to deposition on the surface.

3.2 Experimental methods

All the conditions are same to the description in Chapter 2, except following ones: the nude ion gauge, placed on the side of the auxiliary chamber (out of sight of the silicon oxide substrate to avoid excitation of the surface), was used for the electron-impact excitation experiments by simply turning on or off and the electron energy used was 150 eV; the substrates for this experiments were Si with 300 nm thick silicon oxide or sputtered Si with removal of the native oxide, which made explanation for the role of ion gauge convincing. For the experiments with ion gauge on, the ion gauge would be kept on all through the deposition of $MeCpMn(CO)_3$ on Si with thick silicon oxide (300 nm) or sputtered

Si with removal of all the native oxide. For the ones with ion gauge off, the ion gauge would be turned on before the deposition starts to measure the dosing pressure of the precursor, then the experiments would not start until 10 minutes after the ion gauge had been turned off. To maintain stable dosing pressure when the ion gauge was off, all the other conditions would be precisely controlled.

3.3 Results and discussion

Figure 3.1 displays the experiments related to the deposition of $MeCpMn(CO)_3$ on 300 nm thick SiO_2 films. The bottom (blue) traces correspond to a 60 minutes exposure with 6×10^{-6} Torr of $MeCpMn(CO)_3$ ($2 \times 10^6 L$) while keeping the ion gauge off, whereas the top (red) data are for a 30 minutes exposure at the same pressure (total 1×10^6 L of exposure) but with the ion gauge on. Two cases are contrasted from experiments where a nude ion gauge (IG), placed on the side of our reactor in the way between the gas delivery entrance and the surface, was turned on versus off during dosing. This ion gauge was used as a source of electrons (with 150 eV energy) for the excitation of the gas-phase molecules when it was turned on. It is clear that turning on the ion gauge during exposure leads to a significantly higher uptake of Mn on the surface, as indicated by the shaded areas under the traces. A quantitative estimation of the relative areas is provided on the left side of each Mn XPS trace shows that the Mn uptake in the case of the IG off amounted to less than a quarter of that obtained with the IG on even though twice the exposure was used. In fact, the experiment with the IG on

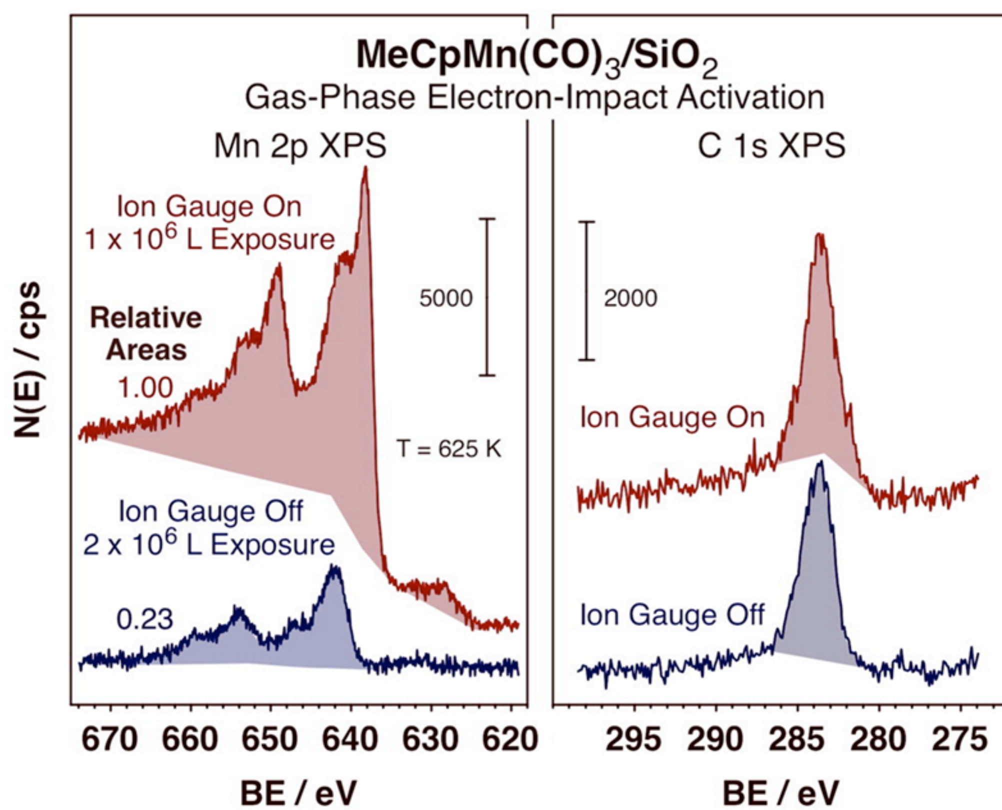

Figure 3.1 Mn 2p (left) and C 1s (right) XPS data from 300 nm silicon dioxide films exposed to defined doses of $MeCpMn(CO)_3$ at 625 K.

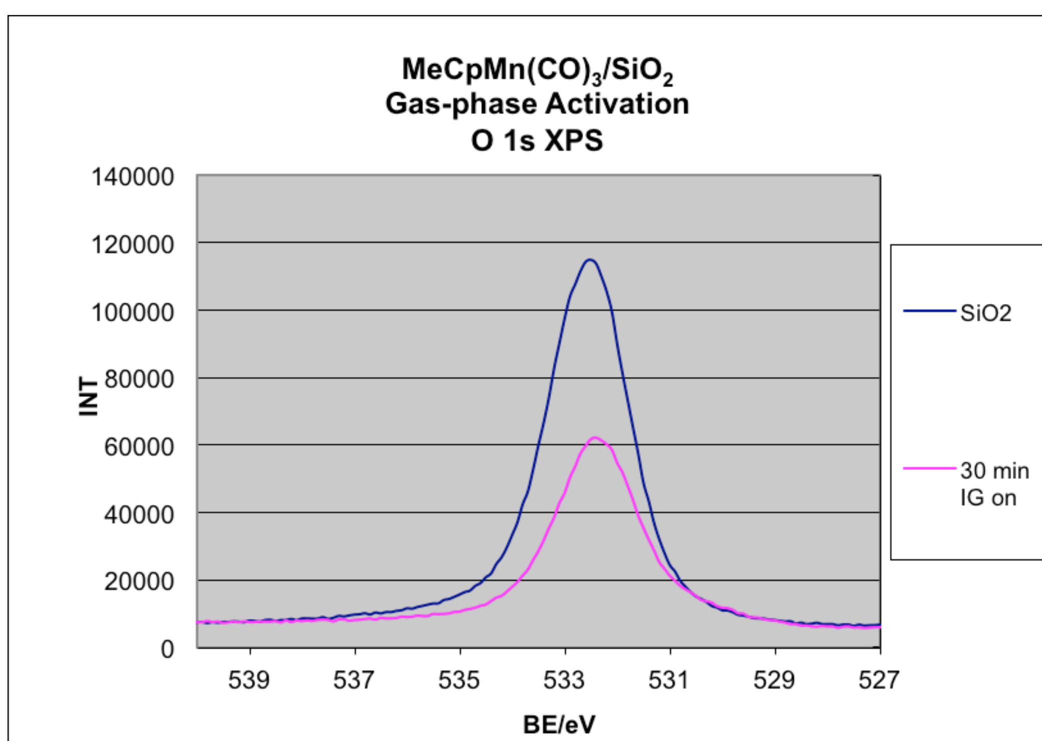

Figure 3.2 O 1s XPS data from 300 nm SiO_2 films exposed to defined doses of $MeCpMn(CO)_3$ at 625 K.

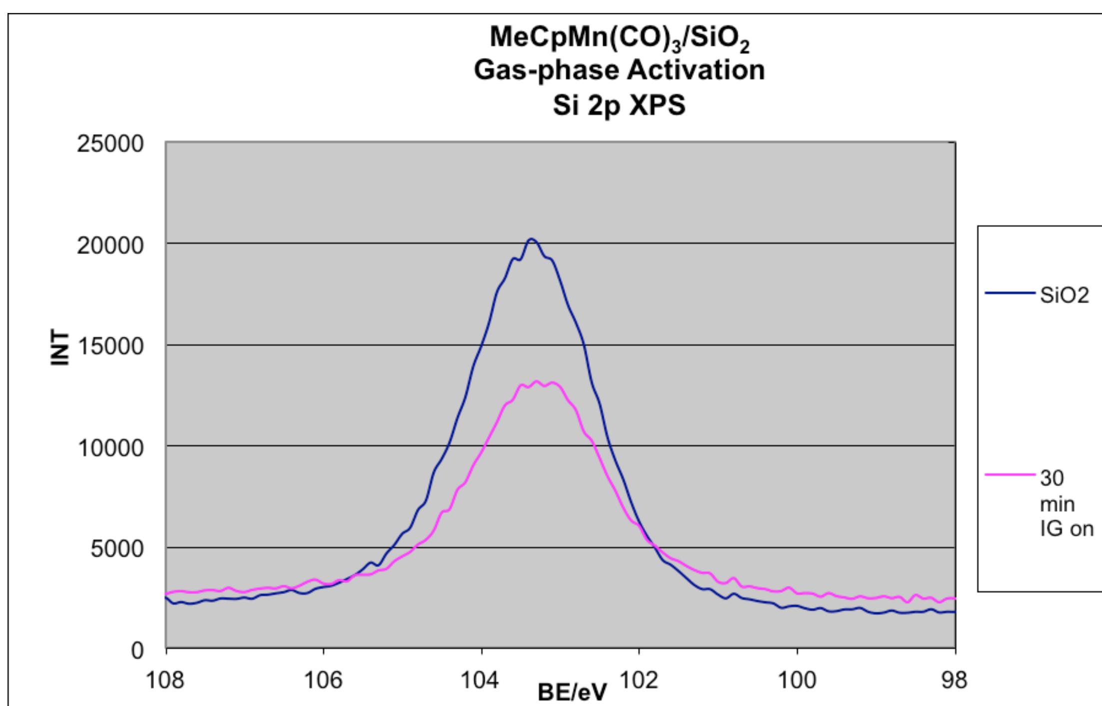

Figure 3.3 Si 2p XPS data from 300 nm SiO_2 films exposed to defined doses of $MeCpMn(CO)_3$ at 625 K.

led to the deposition of multilayers of Mn; on the basis of the attenuation of the measured Si 2p and O 1s XPS signals in Figure 3.2 and 3.3, a manganese film thickness of approximately 9 Å was estimated in this case, the equivalent of three to four layers. It should be noted, this film thickness calculation is not accurate and should only be taken as a gross estimation of the total amount of Mn deposited. Self-limiting deposition, as required for ALD applications, may require lower substrate temperatures.

The C 1s XPS data in the right panel of Figure 3.1 indicate that this electron-impact activation of the precursor does not lead to a significant increase in carbon contamination of the deposited film. In addition, no evidence was ever obtained from the experiments for the survival of CO moieties on the surface; those should have shown up as a separate C 1s XPS peak at around 287 eV. Most if not all of the CO ligands in the original $MeCpMn(CO)_3$ precursor are removed either during electron-impact activation in the gas phase or immediately upon adsorption on the surface. In fact, given the high temperatures of the substrate during the Mn deposition used in these experiments, no CO species are expected to survive on the surface even if initially adsorbed with the Mn-containing species. The carbon XPS signal seen here is most likely due to methylcyclopentadienyl moieties adsorbed on the surface.

The deposition enhancement induced by the gas-phase electron bombardment of the precursor provided by the ion gauge is more dramatic on pure silicon surfaces, where there are no hydroxyl groups to help with the thermal activation

of the precursor [6–8]. This is clearly indicated by the data in Figure 3.4, in which Mn 2p XPS traces are shown as a function of deposition temperature for deposition on sputtered Si (100) with completely removal of native oxide. The bottom spectrum, which corresponds to deposition at 725 K with the IG off, shows only a small signal, indicating very limited deposition even at such high temperatures. With the IG on, by contrast, significant Mn film growth was observed at all temperatures. In fact, Mn uptake was clearly detected with the IG on even at room temperature, as shown in Figure 3.5.

Another interesting observation that derives from Figure 3.4 is that the Mn deposited on the sputtered Si (100) is identified by low-binding-energy Mn 2p XPS peaks, centered at 638.5 ($2p_{3/2}$) and 649.8 ($2p_{1/2}$) eV. These are values typical of metallic manganese but can also be assigned to manganese silicide [9]. The appearance of plasmon resonances in the spectra at approximately 660 and 670 eV with increasing surface temperature demonstrates that low temperature deposition leads mainly to Mn(0) film growth but that some manganese silicide forms by 525 K as well. The ability to deposit metallic manganese at low temperatures is particularly interesting because that requires the reduction of the original Mn(I) centers in the $MeCpMn(CO)_3$ precursors. The reduction of oxidized manganese at higher temperatures, which is quite difficult, may be bypassed by low-temperature ALD by using our proposed gas-phase electron-impact precursor excitation method in applications where metallic films are desired.

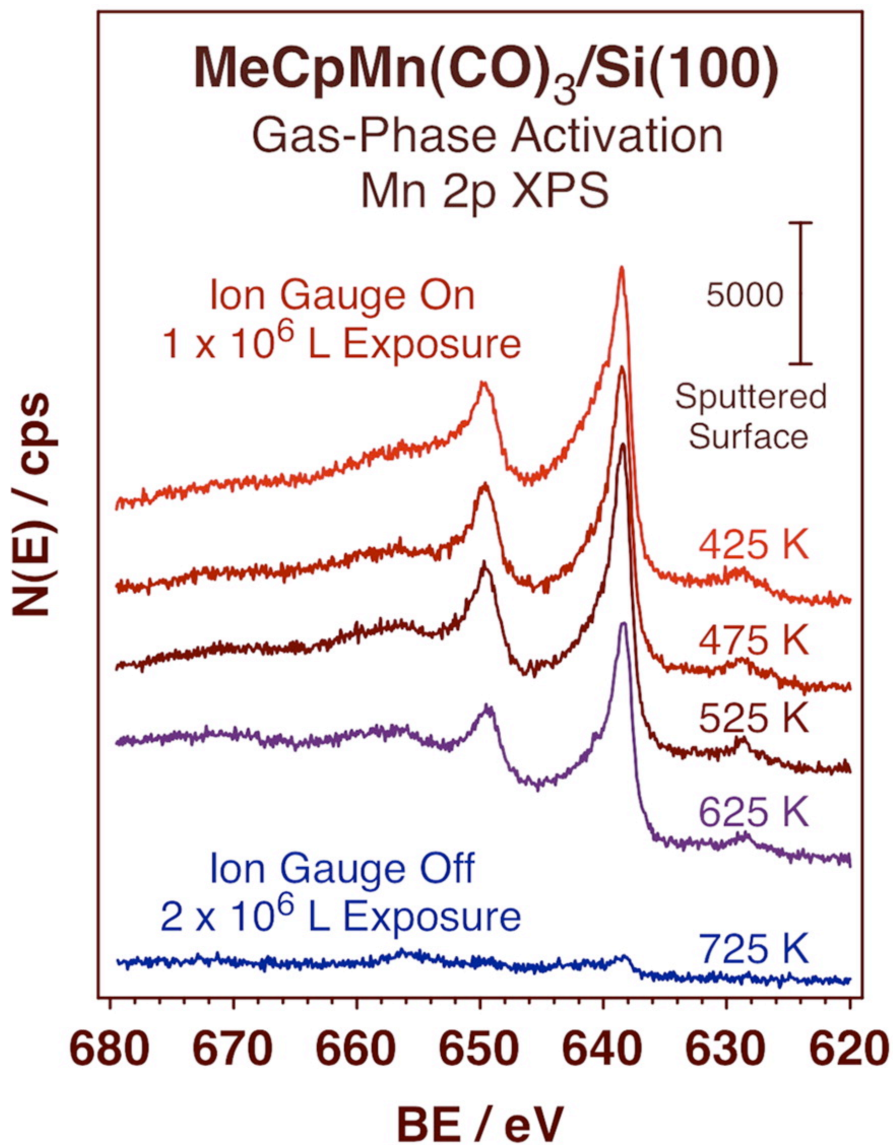

Figure 3.4 Mn 2p XPS traces from sputterred Si(100) with completely removal of native oxide exposed to $MeCpMn(CO)_3$.

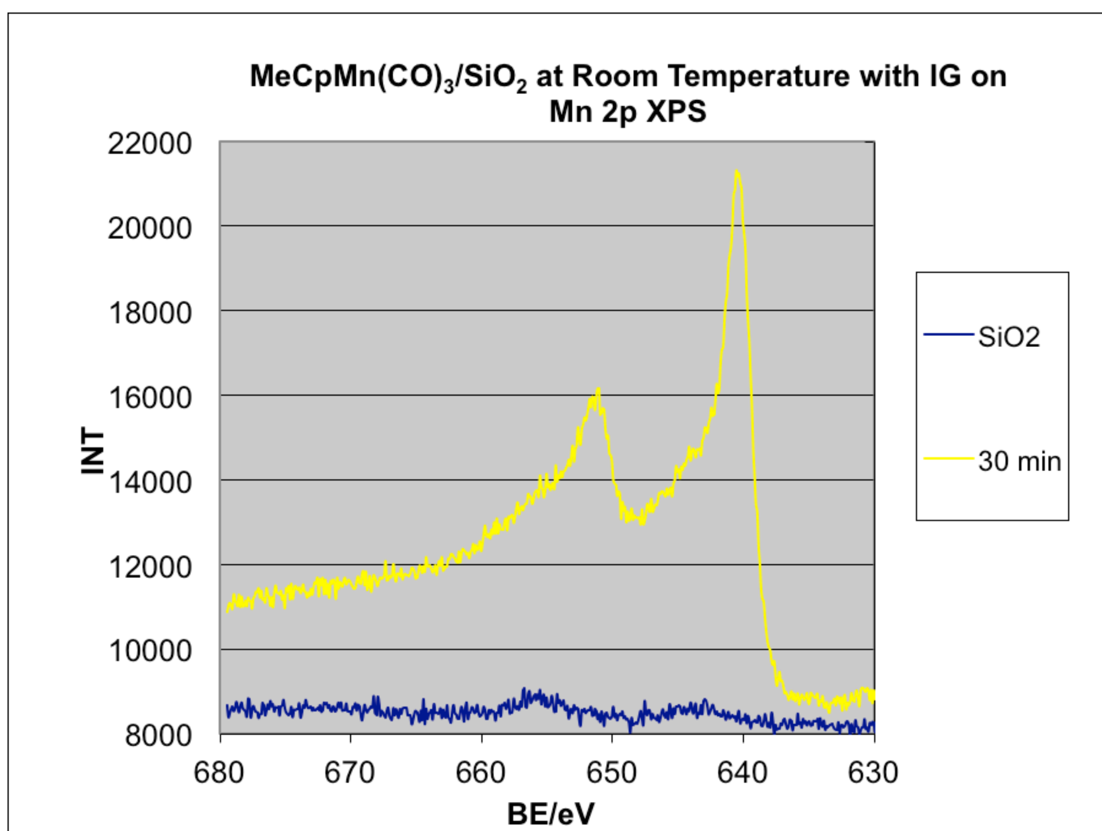

Figure 3.5 Deposition of $MeCpMn(CO)_3$ on 300nm SiO_2 at room temperature with IG on.

The physical explanation for the enhancement in film deposition seen here upon electron bombardment of the precursor in the gas phase is straightforward; molecular excitation by such electrons leads to ionization, fragmentation, and the creation of highly reactive cations and radicals. The composition of the mixture of cations made by electron bombardment can be established by electron-impact mass spectrometry, which uses an excitation source with a design similar to that of the ion gauge employed in the experiments reported here. Figure 3.6 shows the mass spectra obtained for $MeCpMn(CO)_3$, taken with 100 eV electron energy excitation. The cracking pattern of most molecules depends only weakly on electron energy in this voltage range and experiments with the traditional 70 eV electron energy value yielded exactly the same mass spectrum to that from our experiment. This spectrum, which matches previously reported data [10, 11], illuminates clearly why the electron bombardment approach works in this case. A number of manganese-containing highly reactive ions are created, that are likely to stick to the surface upon contact with close to unit probability.

The highlight in Figure 3.6 is that the cracking pattern is reasonably clean and is dominated by $MeCpMn(CO)_x^+$ ions (x = 0−3): the main peak corresponds to $MeCpMn^+$ and accounts for 35% of all ions, and the sum of all of the species that only miss carbonyl ligands amounts to approximately two-thirds of the total mass spectra signal. $MeCpMn(CO)_x^+$ ions are active species for film deposition, because they are likely to lose the remaining carbonyl ligands upon adsorption and retain the methylcyclopentadienyl moiety intact, for controlled removal in

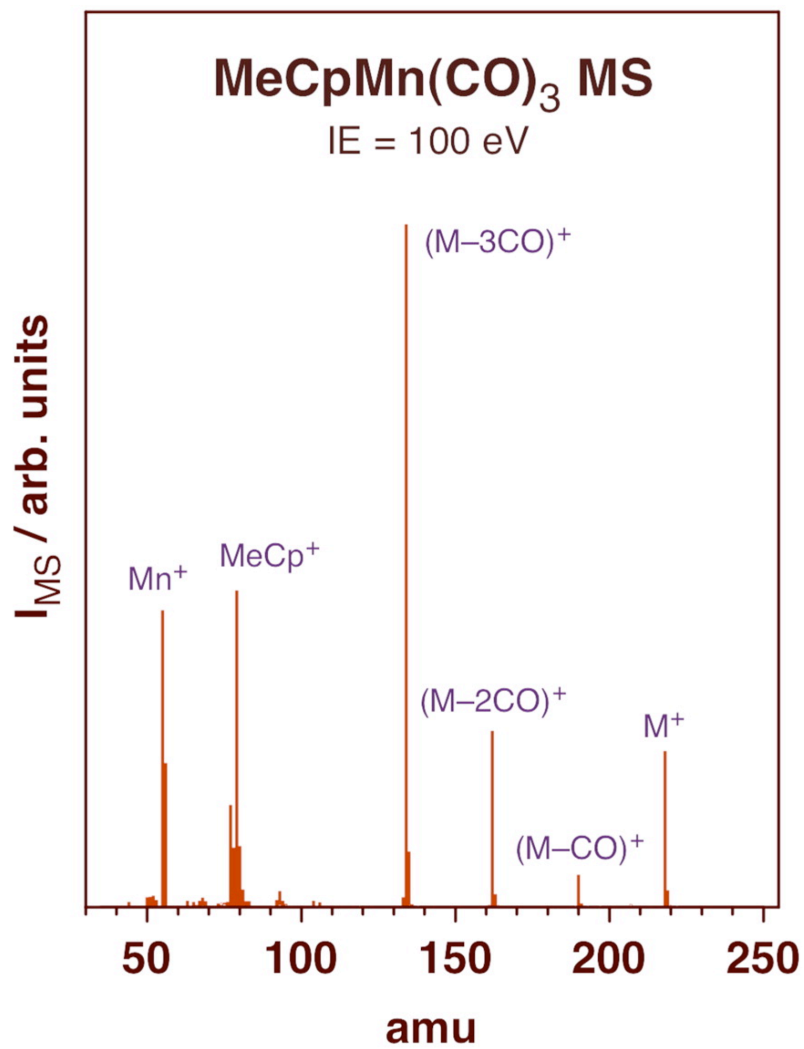

Figure 3.6 Electron-impact mass spectrum for $MeCpMn(CO)_3$.

the second half of the ALD cycle. Previous studies in our laboratory indicate that this is indeed what takes place on the surface.

The preceding discussion hints at the criteria for choosing appropriate precursors for gas-phase electron bombardment excitation in ALD. First, this procedure is only worth implementing if the precursor is too stable to be activated thermally. $MeCpMn(CO)_3$, for instance, decomposes only at temperatures above 675 K. Second, the cracking pattern of the precursor upon electron excitation needs to be reasonably clean, to minimize the deposition of undesirable organic fragments. Metal carbonyls fall into this category, but pure carbonyl complexes tend to be too reactive for ALD [12]; mixed carbonyl–organometallic compounds such as the one studied here are better candidates. Luckily, there are a wide variety of compounds of such nature available with many metals for use in film depositions. Third, the organic ligands in the precursor should be sturdy, so that they do not decompose upon electron excitation. Cyclopentadienyl ligands such as the one used here fit this bill nicely, but others may as well, including arenes and other π-bonded ligands and perhaps also simple σ-bonded ligands such as methyls. In fact, it may be even possible to use noncarbonyl metal–organic precursors as long as all ligands survive electron excitation mostly intact. It is not always obvious which compounds may work for this electron bombardment ALD approach, but a decision can be made relatively quickly based on an analysis of the corresponding mass spectra.

There seems to be only limited precedent for the electron excitation approach described in this chapter. Plasma sources are common in ALD processes but often used to generate radical species such as atomic hydrogen, oxygen, or nitrogen radicals in the second half of the ALD cycle, to clean up the surface from the undesired side products from activation of the main metal precursor and/or to add the missing elements in the deposition of oxides, nitrides, carbides, or other metal-based compounds [13]. Here, gas-phase excitation is introduced in the first half of the ALD cycle to excite the main metal precursor and make it more reactive so that it can adsorb on the surface more efficiently. Electron bombardment was used in our study for this purpose, but other excitation sources such as visible or ultraviolet light, or even beams of other particles, may work as well. However, it is important that the excitation be reasonably selective, so that limited and controlled rather than extensive and nonselective cracking of the precursor takes place. Early examples of the use of gas-phase precursor excitation include use of UV radiation, directly [14] or via the photoelectrons generated by illumination of the surface [15], or plasma excitation [16], and metal carbonyls. Limited if any surface characterization was offered in those reports, and no control on the gas-phase chemistry of the precursor was attempted; the films grown were likely not clean. There are also several reports on the use of high-energy electron beams to deposit metals from gas-phase precursors. The ability to focus and raster those beams offers great opportunities in terms of creating spatially resolved patterns on the surface [17], but the chemistry involved in those systems is extensive, often uncharacterized, and difficult to control, and may lead to the deposition of impurities [18]. The

procedure proposed here is milder and, in combination with ALD designs, more flexible.

Finally, it is worth discussing some possible limitations of the gas-phase electron-impact precursor excitation procedure described in this chapter. Even if the precursor decomposition in the gas phase is relatively clean, as was argued is the case in our example (Figure 3.6), there is always the possibility that further decomposition of the reactive species on the surface may lead to fast deposition rates and to the incorporation of impurities. Certainly, the decarbonylated manganese ions made in the gas phase in our experiments are expected to be quite reactive and to stick to surfaces with high probabilities. The data in Figures 3.1 and 3.4 indicate that much Mn was deposited in these experiments, amounting to the deposition of multilayers. This is behavior expected from CVD, not ALD, processes. It suggests that it may not be easy to design processes using such gas-phase-made ions with the self-limiting deposition characteristics required for ALD. We believe, however, that it may be possible to achieve such ALD behavior at lower temperatures if the remaining ligands, the methylcyclopentadienyl moiety in our example, remain intact and attached to the metal center upon adsorption and if a layer of such organic matter passivates the surface toward further uptake of Mn species from the gas phase; that layer can then be removed by the second ALD agent, in the second half cycle of the ALD process. Our previous experiments on the native oxide of silicon wafers provide some hints that this may in fact be what happens with $MeCpMn(CO)_3$, but the issue requires a more careful temperature dependence study. In any case,

at the very least, electron-impact excitation of stable precursors in the gas phase could be used for CVD film growth at lower temperatures than those relying on thermal activation exclusively.

3.4 Conclusion

In this chapter, the incorporation of gas-phase electron-impact ionization and activation of metal–organic compounds into atomic layer deposition (ALD) processes is reported as a way to enhance film growth with stable precursors. Specifically, it is shown here that gas-phase activation of $MeCpMn(CO)_3$, which was accomplished by using a typical nude ion gauge employed in many ultrahighvacuum (UHV) studies, enhances its dissociative adsorption on silicon surfaces, affording the design of ALD cycles with more extensive Mn deposition and at lower temperatures. Significantly higher Mn uptakes were demonstrated by X-ray photoelectron spectroscopy (XPS) on both silicon oxide films and on Si (100) wafers Ar^+-sputtered to remove their native oxide layer. The effectiveness of this electron-impact activation approach in ALD is explained in terms of the cracking patterns seen in mass spectrometry for the metal–organic precursor used in Figure 3.7, which hints at the criteria for choosing appropriate precursors for gas-phase electron bombardment excitation in ALD, its promising application, and also its limitation due to its nature of electron bombardment on metal organic precursors.

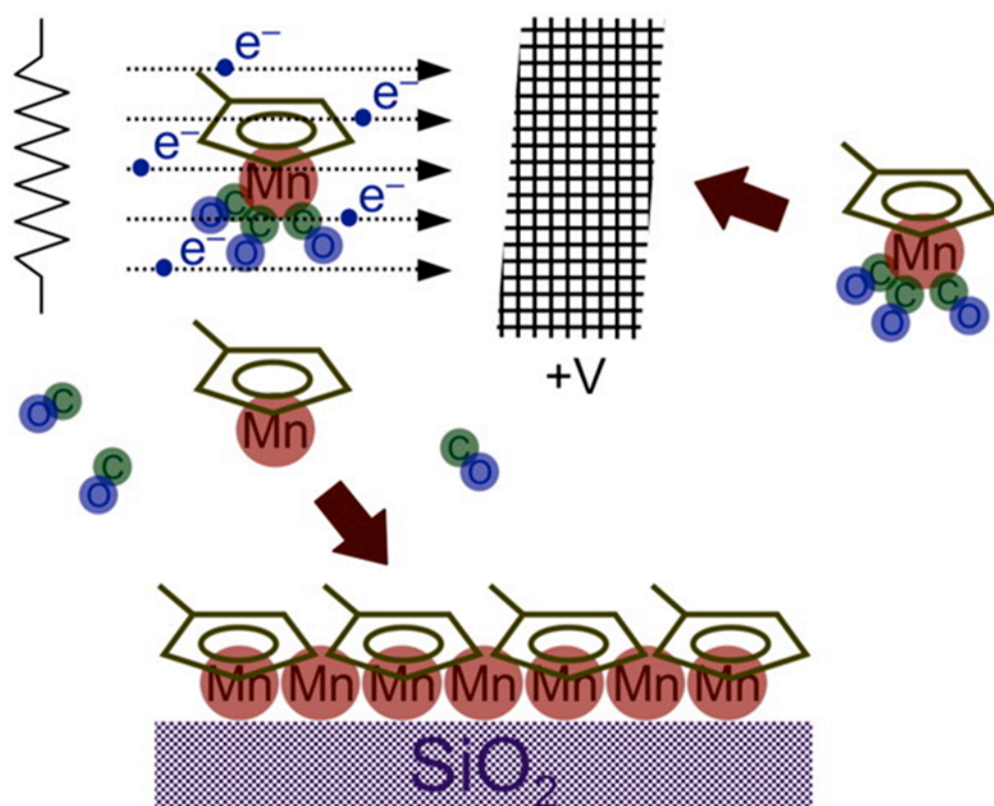

Figure 3.7 Schematic chart of gas-phase activation of $MeCpMn(CO)_3$ by electron bombardment

3.5 References:

[1] F. Zaera, *J. Phys. Chem. Lett.* **2012**, 3, 1301;

[2] D. J. Stirland, *Appl. Phys. Lett.* **1966**, 8, 326;

[3] R. W. Christy, *J. Appl. Phys*. **1960**, 31, 1680;

[4] U. von Staken, D. E. Brodie, *Can. J. Phys.* **1985**, 63, 757;

[5] R. Peterkops, *Theory of ionization of atoms by electron impact.* Boulder, Colo: Colorado Associated University Press. **1977**;

[6] S. Haukka, E. L. Lakomaa, A. Root, *J. Phys. Chem.* **1993**, 97, 5085;

[7] M. J. Kelly, J. H. Han, C. B. Musgrave, G. N. Parsons, *Chem. Mater.* **2005**, 17, 5305;

[8] M. Dai, J. Kwon, M. D. Halls, R. G. Gordon, Y. J. Chabal, *Langmuir* **2010**, 26, 3911;

[9] N. Ohtsu, M. Oku, A. Nomura, T. Sugawara, T. Shishido, K. Wagatsuma, *Appl. Surf. Sci.* **2008**, 254, 3288;

[10] I. R. Lyatifov, I. G. Gulieva, E. I. Mysov, V. N. Babin, *J. Organomet. Chem.* **1987**, 326, 89;

[11] S. Wen-bin, K. Durose, A. W. Brinkman, J. Woods, *J. Cryst. Growth*, **1991**, 113, 1;

[12] X. Qin, H. Sun, F. Zaera, *J. Vac. Sci. Technol., A* **2012**, 30, 01A112;

[13] H. B. Profijt, S. E. Potts, M. C. M. van de Sanden, W. M. M. Kessels, *J. Vac. Sci. Technol., A* **2011**, 29, 050801;

[14] S. E. Blum, K. H. Brown, R. Srinivasan, *Patent US 4451503*, **1984**;

[15] P. M. George, J. L. Beauchamp, *Thin Solid Films*, **1980**, 67, L25;

[16] A. Brocherieux, O. Dessaux, P. Goudmand, L. Gengembre, J. Grimblot, M. Brunel, R. Lazzaroni, *Appl. Surf. Sci.* **1995**, 90, 47;

[17] W. F. van Dorp, C. W. Hagen, *J. Appl. Phys.* **2008**, 104, 081301;

[18] J. D. Wnuk, S. G. Rosenberg, J. M. Gorham, W. F. van Dorp, C. W. Hagen, D. H. Fairbrother, *Surf. Sci.* **2011**, 605, 257.

CHATPER FOUR

Manganese Deposition on Si with Native Oxide using $MeCp(CO)_3$

4.1 Introduction

$MeCpMn(CO)_3$ were widely used as a supplement to the gasoline additive tetraethyllead to increase a fuel's octane rating, and was later used in unleaded gasoline. In the research of chemical deposition of manganese thin flim, $MeCpMn(CO)_3$, has been proved to be useful manganese precursors due to its easy access, and sufficient vapor pressure at room temperature. Metal manganese films have successfully been grown on (100) and (111) GaAs substrates by metal organic chemical vapor deposition using $MeCpMn(CO)_3$ as the Mn source material above 410°C with surface roughness was measured to be ~ 4 nm [1]. Several angstrom (Å) thick silicon native oxide films have been reported to grow on Si surface after 10h exposure to air, and the growth has received an increasing attention since then as the pattern dimension of integrated circuits is decreasing [2-4]. In microelectronics, the native oxide films can act as electric insulators with high chemical stability [4]. MnSixOy barriers were formed by reaction between Mn and SiO_2 on wafers covered by thick SiO_2 made by thermal method or CVD [1, 5], from which we can predict that such MnSixOy complex might be formed by the deposition of manganese on silicon wafers covered by thin native silicon oxide films too. However, the surface

chemistry in the process on Si with their native oxide films might be different with that on thick SiO_2, because SiO_2 in the thin native oxide films is limited.

In this chapter, we report on results from X-ray photoelectron spectroscopy (XPS) studies on the nature of films prepared by chemical means using $MeCpMn(CO)_3$ as the precursor on the Si(100) with native oxide films. The goal is to develop a molecular-level understanding of the surface chemistry in depositing the precursor on Si with native oxide films to improve the selection of manganese precursor.

4.2 Preliminary results

First of all, trials were carried out to find out the proper temperature range for the deposition of $MeCpMn(CO)_3$. Experiments were done at 425 K and 600 K on Si surfaces with their native oxide films with dosing pressure of 4.6×10^{-4} Torr of the Mn precursor, without introducing the second reactant. The ion gauge was kept on all through the deposition process to better activate the carbonyl precursor. It has been reported that no obvious manganese grow on GaAs below 685 K [1], so it is expected that the precursor may decompose above 410°C or higher temperatures. Preliminary results of the uptake of the precursor at two different temperatures are shown in Figures 4.1 to 4.3.

For the deposition of $MeCpMn(CO)_3$ at 425K in Figure 4.1, the growth was slow during the first several dosings, but much faster as the dosing amount increased,

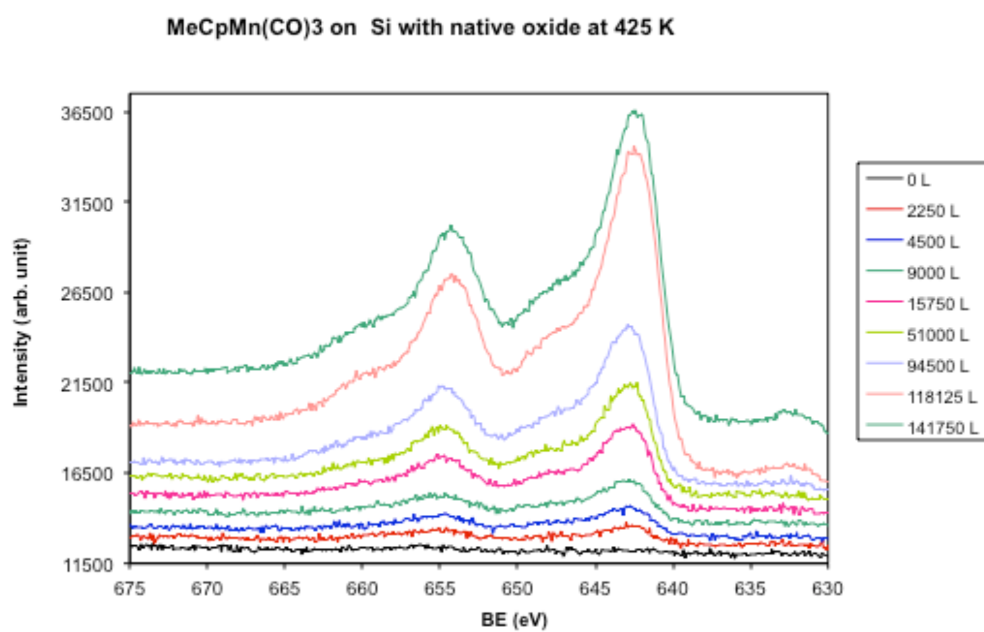

Figure 4.1 Mn 2p XPS for deposition of $MeCpMn(CO)_3$ on Si with native oxide at 425 K with separate dosings.

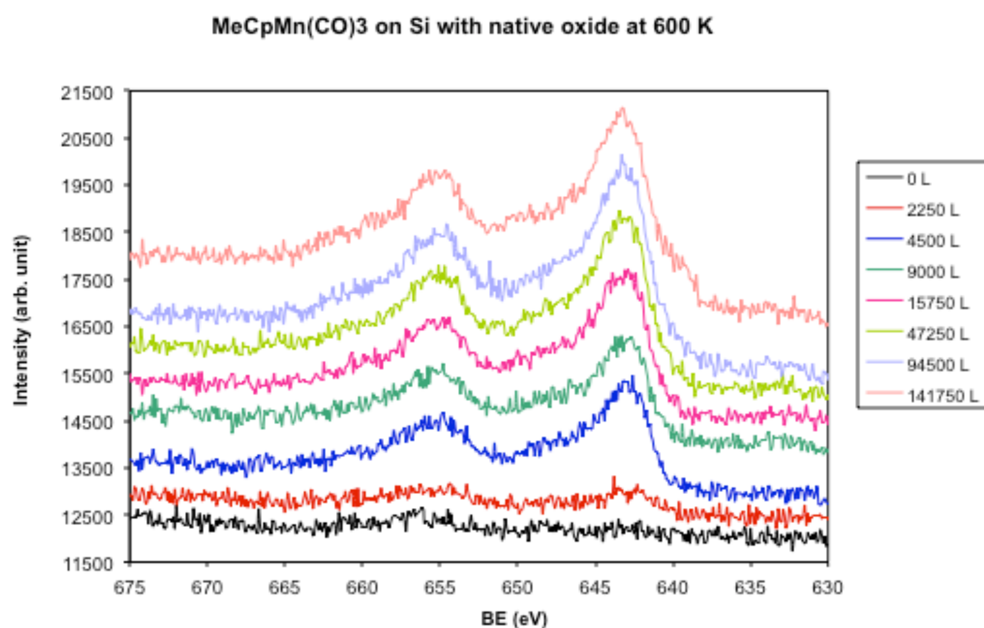

Figure 4.2 Mn 2p XPS for deposition of $MeCpMn(CO)_3$ on Si with native oxide at 600 K with separate dosings.

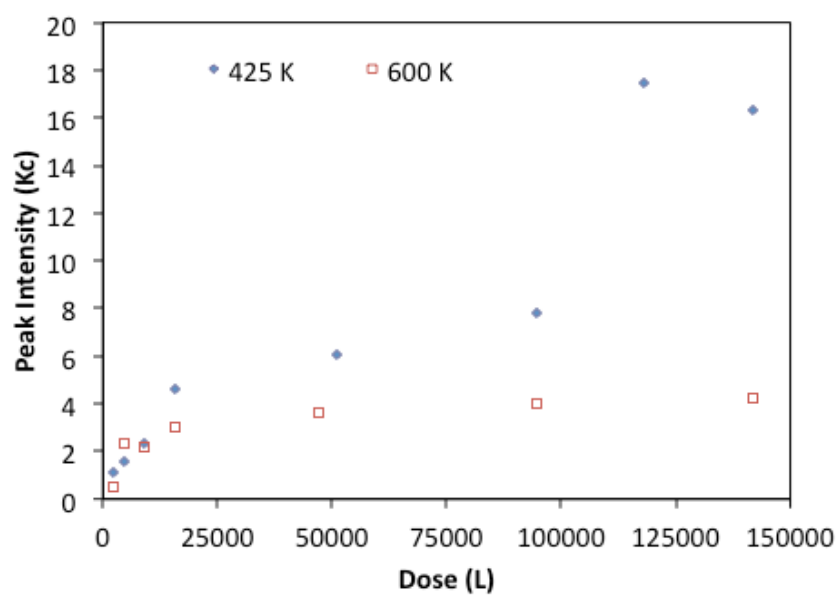

Figure 4.3 Mn 2p XPS intensity for $MeCpMn(CO)_3$ at 425K *vs* 600K

and never reached a saturation on the surface. The main Mn 2p XPS peaks are centered at 641.8 and 653.9 eV, binding energies characteristic of Mn $2p_{3/2}$ and Mn $2p_{1/2}$ photoelectrons from oxidized manganese, respectively [6,7]. The exact nature of the manganese in this case is not straightforward to identify, given that many manganese oxides display similar binding energies, but the additional appearance of satellite peaks at ~645.9 and 659.4 eV strongly suggest the presence of manganese in a +2 oxidation state [8-10]. The oxidized manganese in this deposition at 425K is believed to be MnO.

For the deposition of $MeCpMn(CO)_3$ at 600 K in Figure 4.2, the thin film grew very slowly during the first dosing(2250 L), much faster during the second dosing, and then slowly after the third dosing (15750 L). It seemed that saturation was achieved on the surface, which indicates that this is a self-limiting half reaction, as required for an ALD process. The main Mn 2p XPS peaks show almost the same binding energies to those for deposition at 425 K, except that a pair of shoulders appears at 638.2 and 649.3 eV after the final dosing. Appearance of the new peaks means that a new oxidation state of the same element formed. The nature of the thin film formed in this deposition was also not easy to identify. A detailed analysis of the peaks and oxidation states for the deposition at 600 K will be discussed in the following section, where a series of experiments at different temperatures and with different dosing amounts were carried out.

Figure 4.3 shows the comparison between the two depositions at 425K and 600K. Obviously, the deposition at 600K was slow but reached saturation quickly after the first several dosings, while the deposition at 425K was slower at first, but much faster later. The growth difference in the first 2~3 dosings might be explained by the higher reactivity of manganese precursor with the surface OH groups in the thin native oxide at higher temperature, which was the reason for the fast growth for the deposition at 600K. But the reason for the much faster growth of MnO at 425K, almost saturation for oxidized manganese at 600K, and the appearance of new peaks are unknown, and more experiments need to be carried out to find an explanation. As a result, a series of experiments were designed to gain a better understanding of the unknown results in the preliminary experiments above.

4.3 Results

4.3.1 Deposition of $MeCpMn(CO)_3$ at different temperatures

From the preliminary results at 425K, the main components for the thin film were identified with MnO. The temperature range for this series of experiments was set between 500 and 775K to find the proper temperature for this deposition. The left panel of Figure 4.4 displays the Mn 2p XPS data obtained after dosing $MeCpMn(CO)_3$ at 0.15 mTorr for 2000 s on the Si with native oxide (~1 nm) at different temperatures.

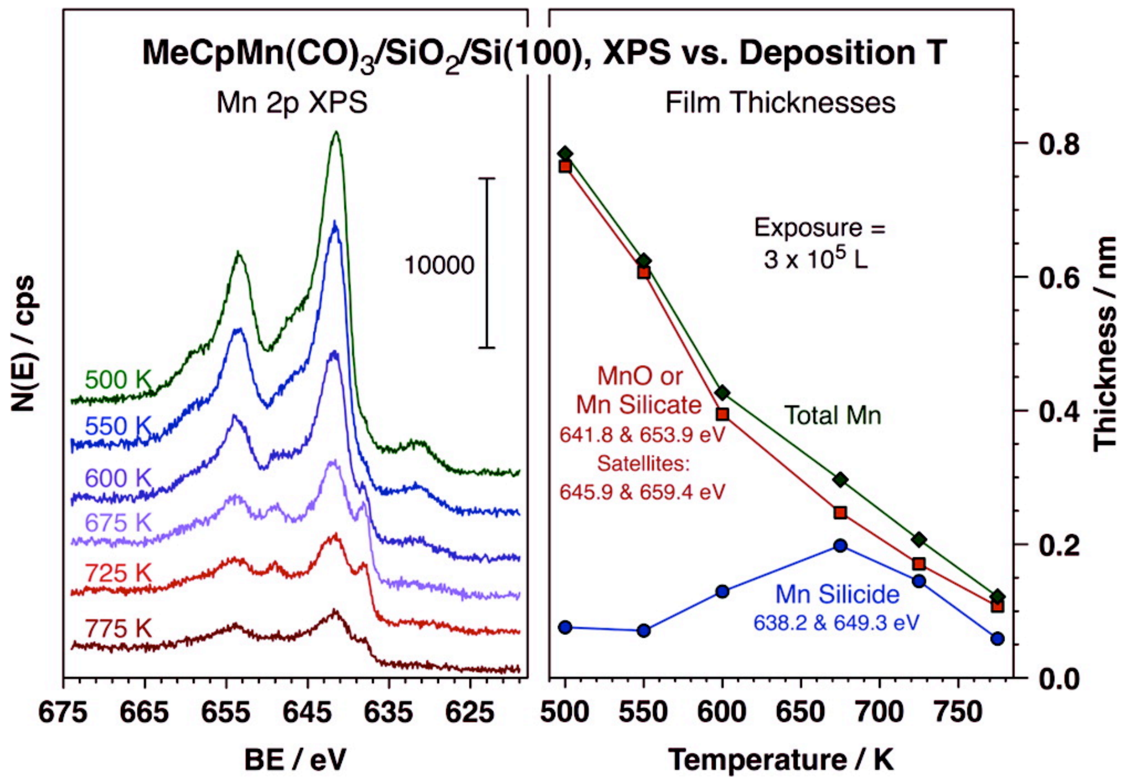

Figure 4.4 Left: Mn 2p XPS for MeCpMn(CO)$_3$ (0.15 mTorr for 2000 s) on a Si(100) sample covered with its native oxide layer(~1 nm) as a function of temperature. Right: Summary of peak intensities for the Mn species identified in the data on the right, converted to film thicknesses.

Similar to the charts in the preliminary results above, in all traces, the main peaks for all the depositions at different temperatures are centered at 641.8 and 653.9 eV, typical binding energies for Mn $2p_{3/2}$ and Mn $2p_{1/2}$ photoelectrons from oxidized manganese, given the additional appearance of satellite peaks at ~645.9 and 659.4 eV for manganese in a +2 oxidation state. The spectra obtained at low temperatures, below ~550 K, are typical of MnO. The peaks for Mn^{2+} in the data obtained after deposition at higher temperatures shift slightly toward lower binding energies and are accompanied by less intense satellites, and are therefore likely to be due to a different species.

The same to the data for the last dosing in the deposition of $MeCpMn(CO)_3$ at 600K in the preliminary results above, a new pair of peaks develops in the Mn XPS traces in Figure 4.4 upon deposition at temperatures of 600 K or above, at 638.2 and 649.3 eV for the Mn $2p_{3/2}$ and Mn $2p_{1/2}$ photoelectrons. Low binding energies are typically associated with reduced species, possibly metallic manganese in this case, but are also consistent with manganese silicide [11]. The appearance of additional broad and weak peaks at ~660 and 670 eV in some of the spectra (in particular for manganese deposited on sputtered silicon without native oxide, see Figure 4.8 below) has been reported to originate from plasmon losses in Mn silicide [12]. Here, we would like to assign the 638.2 and 649.3 eV features in these films mainly to manganese silicide, although a small component from Mn(0) may also be present in some instances. As a result, the three pairs of peaks for Mn 2p XPS observed are assigned to manganese silicide (638.2 and 649.3 eV), MnO or manganese silicate (641.8 and 653.9 eV), and satellites of the

oxidized manganese (645.9 and 659.4 eV). As it can be seen in the right panel of Figure 4.4, the signal for Mn silicide first grows with increasing temperature, the peaks at about 625~650 K, but decreases again at higher temperatures. Meanwhile, the signal intensities for the Mn^{2+} species decrease monotonically all throughout the temperature range discussed here, from 500 to 775 K.

4.3.2 Angle-resolved XPS for $MeCpMn(CO)_3$ on Si with native oxide

Additional angle-resolved spectra were obtained for a film grown at 625 K to better interpret the distribution of the different manganese species within the films deposited at the intermediate temperatures where manganese silicide is formed. 625 K was chosen because the maximum intensity was obtained for the low-binding-energy peak associated with the Mn silicide at 625 K. Figure 4.5 shows the data for the Mn 2p (left) and Si 2p (right) XPS peaks obtained from the single deposition at 625 K, and Figure 4.6 displays a summary of the signal intensities of the main features in those data. Considering the experience after these experiments, a note is that the temperature range where the signal for the Mn silicide is maximized is fairly sharp and somewhat difficult to reproduce because of a kinetic effect by which Mn is first deposited on top and then diffuses into the film and forms the Mn silicate and Mn silicide (see discussion in connection with the data in Figure 4.9). The spectra for 625 K shown in Figure 4.5 do display a much larger contribution from the low-binding-energy peaks associated with the manganese silicide than those in Figure 4.4, but were not added to the sequence in that figure because the sample was prepared under slightly different conditions (half pressure and doubled time compared to the

data in Figure 4.5). This kinetic effect is less significant at the high or low temperature ends of the range in Figure 4.4 and does not change the qualitative trends reported here, as the dosing time was shorter.

The deconvolution of the Mn 2p XPS data in Figure 4.5 (left) clearly shows pairs of peaks for each of the three components discussed above, namely, for Mn silicide and for the main and satellite features of the manganese silicate. Two clear components at approximately 99.1 and 103.0 eV, corresponding to Si (0) and SiO_2, are displayed in the Si 2p XPS traces in Figure 4.5 (right). In fact, each of those peaks is composed of two ($2p_{3/2}$ and $2p_{1/2}$) spin split peaks and was fitted accordingly with peak separations of 0.5 eV and fixed 2:1 area ratios. The goodness of the overall fits is illustrated by the results for the original SiO_2/Si(100) surface, before any Mn deposition, shown in the top trace of Figure 4.4 (right); a SiO_2 film thickness of ~1 nm was estimated from those data. For the samples after Mn deposition, a third species becomes evident at ~101.7 eV (for the Si $2p_{3/2}$ peak), which becomes more intense at glancing detection angles. This new binding energy matches that of metal silicates [13,14] and is consistent with the discussion provided above in connection with the interpretation of the Mn 2p XPS data.

Figure 4.6 indicates that carbon on the top surface as the intensities of carbon in particular, increase with increasing detection angle (measured from the surface normal). The angular dependence of the intensities of the different Mn and Si

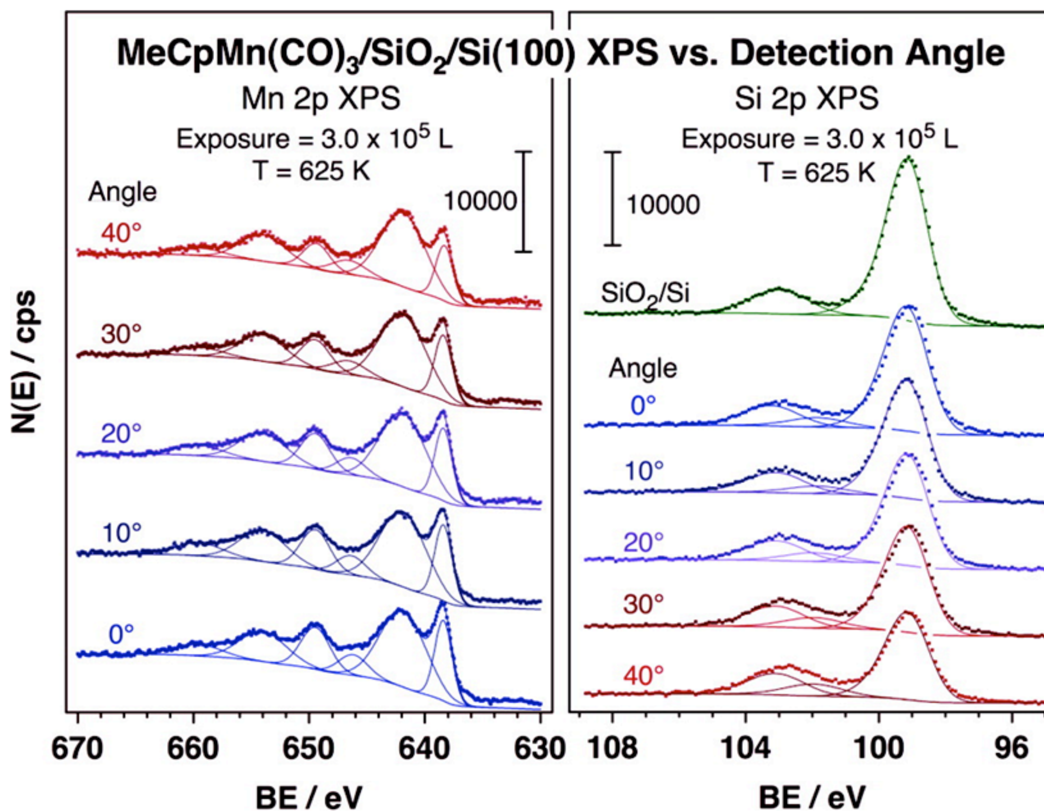

Figure 4.5 Angle-resolved Mn 2p (left) and Si 2p (right) XPS for $MeCpMn(CO)_3$ (0.08 mTorr for 3780 s) on a Si(100) sample covered with its native oxide layer(~1 nm) at 625 K as a function of detection (takeoff) angle, measured from the surface normal.

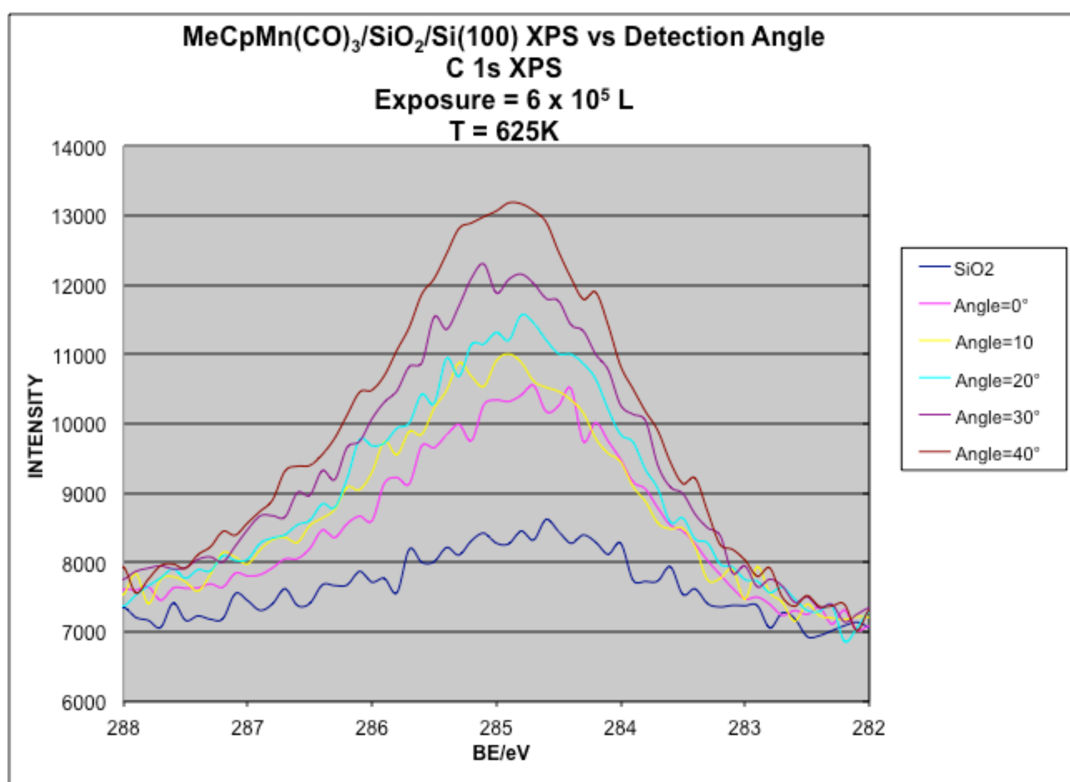

Figure 4.6 Angle-resolved C 1s XPS for $MeCpMn(CO)_3$ (0.08 mTorr for 3780 s) on a Si(100) sample covered with its native oxide layer(~1 nm) at 625 K as a function of detection (takeoff) angle, measured from the surface normal.

XPS features, shown in Figure 4.7 clearly points to a layered structure of the final films. The intensity of the C 1s XPS peaks increases with increasing detection angle, indicating that those atoms are placed close to the surface, whereas other peaks decrease in intensity, indicating that they originate from species buried underneath other layers. The latter include the signal for Si (0) (the Si 2p peak at 99.1 eV), which is initially below the SiO_2 native layer and covered by all other films after manganese deposition, and also the signals from Mn silicide (Mn $2p_{3/2}$ peak at 638.2 eV), which follows a similar, albeit less pronounced, trend than Si (0), indicating that the Mn silicide film is formed right above the Si (0) substrate but below all other components. The signals associated with the manganese silicate (average of Si $2p_{3/2}$ peak at 101.7 eV and Mn $2p_{3/2}$ peak at 641.8 eV) and silicon oxide (Si 2p peak at 103.0 eV) show an intermediate behavior, with a weak angular dependence (increasing somewhat with detection angle), indicating that those layers are present at intermediate depths in the overall manganese plus silica system.

A schematic representation of the proposed layered structure formed by deposition of Mn on SiO_2/Si (100) at 625 K is Figure 4.7. All of these layers are relatively thin, corresponding to only a few monolayers. Calculations using reported photoelectron mean free paths [15,16] and exponential attenuation of the signals [17] yielded the following approximate thicknesses for the different layers: C = 0.23 $\pm$ 0.05 nm, Mn silicate = 0.32 $\pm$ 0.05 nm, SiO_2 = 0.78 $\pm$ 0.05 nm, and Mn silicide ~0.50 $\pm$ 0.15 nm. The angular dependence estimated by using

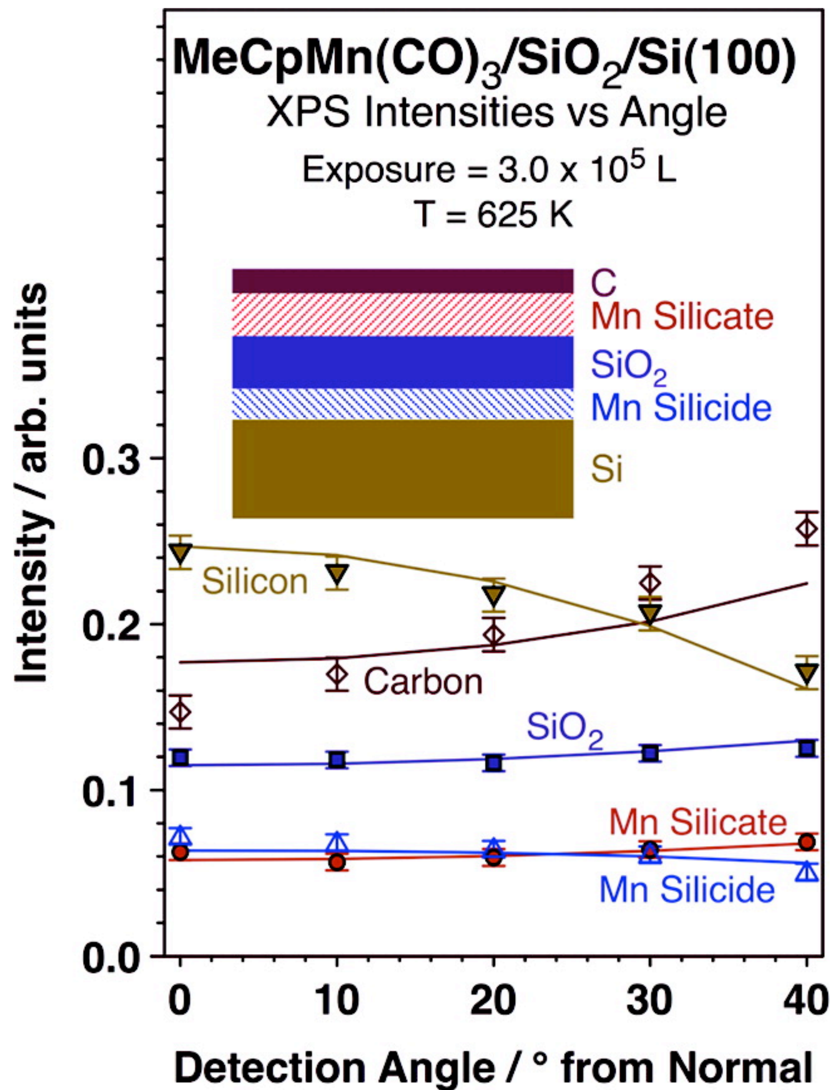

Figure 4.7 Summary of XPS peak intensities in Figure 4.5 and 4.6 as a function of detection angle (symbols with error bars) and a proposed layered model structure on the basis of the angular dependence displayed in this figure.

this layered model and a simple exponential attenuation equation for the photoelectron signal as a function of thickness, provided as solid lines in Figure 4.7, are within experimental error of the data for all layers except the topmost carbon layer, providing further support for the validity of our model, at least at a semi-quantitative level. At the same, any other ordering of the layers could not explain the angular trends with detection angle seen in our experiments. Large deviations from the calculation are seen for the carbon signal, because of this topmost layer being in fact a molecular monolayer of adsorbed methylcyclopentadienyl ligands, not a homogeneous carbon film. It should also be noted that our model assumes sharp and flat interfaces between each layers.

Although we have no direct evidence of the layering proposed in our model, several arguments can be made in its favor. First, the original SiO_2/Si films are fairly flat. In addition, similar silicon-manganese mixed oxide films made in other laboratories do show good monolayer-resolved interfaces [18,19]. The rather good agreement of our angular dependent data to the layered model structure is also consistent with typical self-made layers produced by diffusion of one element into a solid film. Of course, this is only a simplified model; some degree of roughness and other defects are expected in the real samples at these interfaces. However, it has been shown that the effect of roughness on the estimation of film thicknesses is negligible at detection angles of $\sim 40^{0}$ [20-22].

4.3.3 Uptake study of $MeCpMn(CO)_3$ on Si with native oxide

An interesting aspect of this manganese-silicon mixed oxide system is the fact that although the manganese silicide layer is buried in the interface in between the SiO_2 and Si (100) components, it grows only after saturation of the more superficial manganese silicate layer. This is indicated by the uptake data shown in Figure 4.8. It is clear from the figure that the first Mn 2p XPS peaks to grow are those associated with the silicate, with the main Mn $2p_{3/2}$ features centered at 641.8 eV; only after that signal reaches saturation do the Mn silicide signals (at lower binding energies) appear. Presumably, these manganese-containing layers form via diffusion of the Mn atoms through the top layers of the substrate, first reacting with the SiO_2 film to make the silicate and later traveling through that layer to react with Si (0) and produce the Mn silicide film. One thing to notice in Figure 4.8 is the fact that the total Mn uptake at 675 K asymptotically reaches a saturation value at high exposures, in this case at the equivalent of ~0.25 nm of manganese silicate and another 0.25 nm of manganese silicide. This self-limiting growth is a behavior highly desirable in ALD processes and may produce a thin diffusion barrier film, even after one single deposition cycle. It should be indicated, though, that the manganese silicide may keep growing slowly if the exposure of the surface to the $MeCpMn(CO)_3$ precursor is continued.

4.4 Uptake of $MeCpMn(CO)_3$ on Si with different thick silicon oxide

The sequence of events discussed above is supported by the data in Figure 4.9, which correspond to the Mn 2p XPS traces obtained from films produced via Mn deposition on silicon substrates with silicon oxide films of different thicknesses.

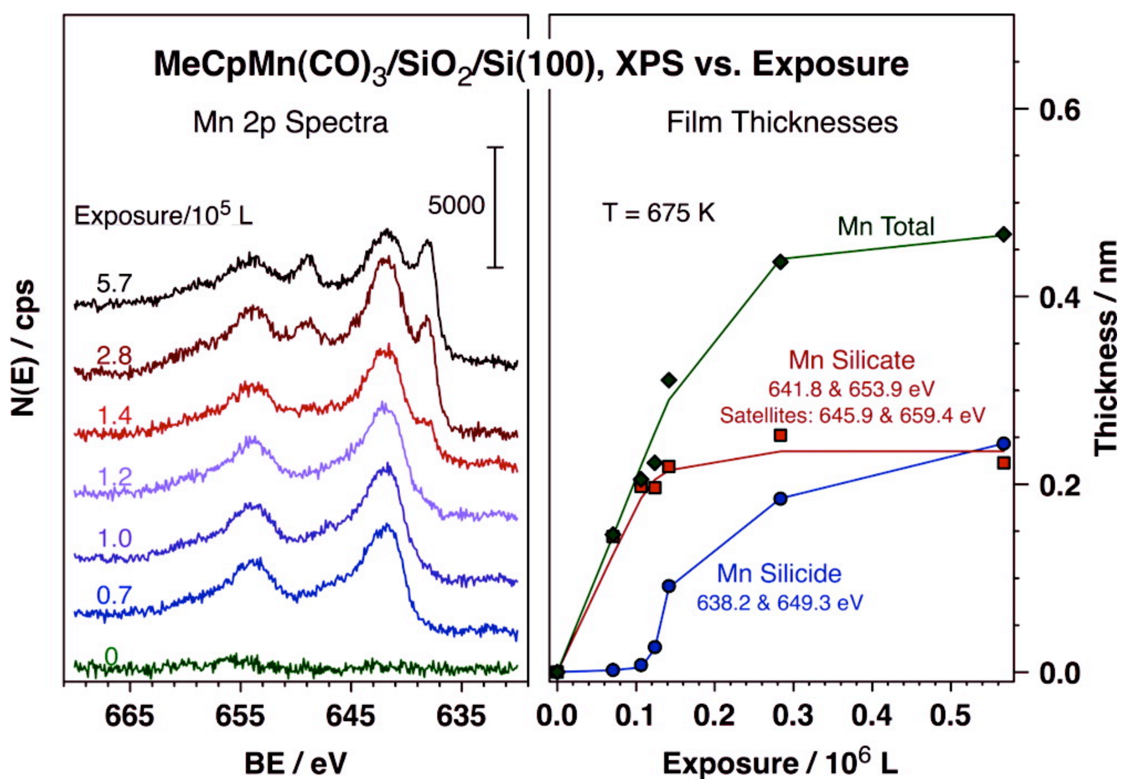

Figure 4.8 Left: Uptake Mn 2p XPS data from a SiO_2/Si(100) surface dosed with 0.15 mTorr of $MeCpMn(CO)_3$ at 675 K as a function of dosing time. Right: Summary of peak intensities for the Mn species in the left panel.

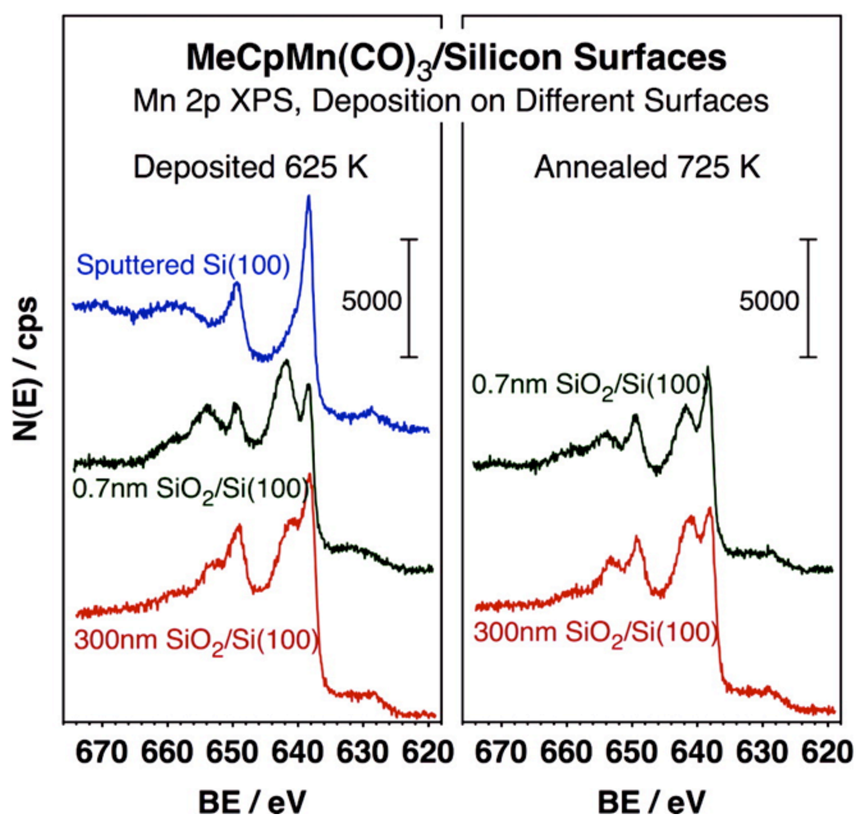

Figure 4.9 Mn 2p XPS for $MeCpMn(CO)_3$ on silicon surfaces dosed with ~2 x10^6 L at 625 K (left) and after annealing at 725 K (right).

The left panel shows the spectra recorded after deposition at 625 K on (from top to bottom): (1) a sputtered silica surface, with all SiO_2 removed, (2) a Si (100) wafer with ~1 nm thick native oxide, and (3) a Si (100) wafer covered with a 300 nm thick SiO_2 layer. Only Mn silicide is made on the sputtered surface because there is no oxygen or OH for further oxidation; the identification of the low binding energy peaks with Mn silicide is helped by the observation of the plasmon losses at 660 and 670 eV. Oxidized Mn is also seen on the surfaces covered with native oxide films, but even on the substrate with the thick oxide, where the Si (0) is not visible in the Si 2p XPS traces, a low binding energy peak is still observed in the Mn 2p XPS traces. That peak does become smaller upon annealing to 725 K, as shown in the right panel of Figure 4.9, while the opposite of what is seen on the thin silicon dioxide film. This suggests that the Mn atoms may first be reduced upon adsorption on the surface. The low-binding-energy peak seen in the thick SiO_2 surface may correspond to metallic manganese, which may diffuse into the oxide films at higher temperatures to make the silicate species (which grows in thickness at the expense of the SiO_2 layer as the Mn diffuses in). On the thin (native) SiO_2 film, a mixture of Mn (0) and Mn silicide may be seen instead.

4.5 Discussions and conclusions

The results presented here were obtained by depositing manganese chemically using $MeCpMn(CO)_3$ as a precursor, but we believe that the conclusions based on the surface chemistry in the manganese deposition to SiO_2/Si substrates are

general. We have recently reported some of the same behavior during the deposition of Mn using $Mn_2(CO)_{10}$ instead, and the buried nature of the manganese silicide layer was proven by depth profiling XPS experiments in that case[23]. The formation of a silicate layer has also been inferred in chemical vapor deposition (CVD) studies using a manganese acetamidinate precursor [24] and mixed manganese silicate/manganese silicide films have been produced via Mn ion implantation on silica glass [11]. A study where Cu-Mn alloys were deposited by simultaneous sputtering of both elements on a SiO_2 substrate lead to the observation of a silicate phase as well [25-28]. It should be noted that the formation of manganese silicates from mixtures of MnO and SiO_2 is thermodynamically quite favorable [29-31]. On the other hand, to the best of our knowledge, no formation of manganese silicide films at the SiO_2/Si(100) interface has been reported. A low binding energy peak in films deposited by CVD using $(EtCp)_2Mn$ was assigned to metallic manganese in one report [19], but we suspect that such feature may have corresponded to the same buried manganese silicide layer characterized in our study. Manganese silicide is thermodynamically favored over separate Mn and Si phases but is much less stable than the silicates [32], a fact that may explain why the silicide is only produce after saturation of the silicate.

The combined manganese silicate/silicon dioxide/manganese silicide films reported here are only 1 to 2 nm in total thickness, and their growth by chemical means is self-limiting. The implication is, that thin self-forming diffusion barriers can be made this way, much thinner than the barriers used at present, typically

metal nitrides, mixed carbide-nitrides, or late transition metals [33-36], and also thinner than the dimensions required for the current and near-future technology nodes in the microelectronic industry (~22 nm) [37]. Deposition of these self-limiting Mn-based diffusion barriers by CVD (or by atomic layer deposition) also solves the problem of conformality often found with physical deposition methods on complex surface topologies in modern microelectronic circuits and devices production. The precursor is believed to be activated by OH surface groups, which can occur after adsorption on any exposed silicon oxide surface regardless of orientation.

The one remaining challenge with this approach is the need to develop a way to clean the top layer from the organic matter, the methylcyclopentadienyl ligand in this case, that is co-deposited during the exposure of the surface to the $MeCpMn(CO)_3$ precursor. In an atomic layer deposition (ALD) type process, this could potentially be achieved by using a cleaning reagent in the second half of the cycle, either a reducing agent such as hydrogen or an oxidizing compound such as ozone or N_2O. Our laboratory has explored these alternatives to complete a chemical deposition procedure designed to deposit these self-forming diffusion barriers cleanly on SiO_2 films. In more general terms, our results from the characterization of this system indicates the possible complexity of films prepared by simple deposition of one element on top of a solid layer, because a combination of kinetic and thermodynamic driving forces can lead to the diffusion of certain elements through, and reaction with, specific layers, leading to the development of multiple mixed phases. Based on the results and analysis

above, what I learned was that choosing appropriate metal organic precursor and substrates is very important. The carbonyl precursor can be used to deposit the MnSixOy complex after hours of dosing, finding another precursor, which might be deposited faster on the substrates, is necessary. Meanwhile, substrates are also playing an important role in the deposition, and substrates covered with thick SiO_2 thin films might enable the surface chemistry involved easier.

To sum up, we reported on X-ray photoelectron spectroscopy (XPS) studies on the nature of films prepared by chemical means using $MeCpMn(CO)_3$ as the precursor. It was found that at the temperatures typically used for deposition, between approximately 550 and 750 K, a manganese silicate layer grows first upon reaction with the top SiO_2 surface, and a thin manganese silicide film develops latter at the SiO_2/Si(100) interface in Fig 3.10. The combined manganese silicate/silicon dioxide/manganese silicide films reported here are only 1 to 2 nm in total thickness, and their growth by chemical means is self-limiting, which is very promising. The performance of these structures, of the silicide in particular, in microelectronic applications is still to be determined.

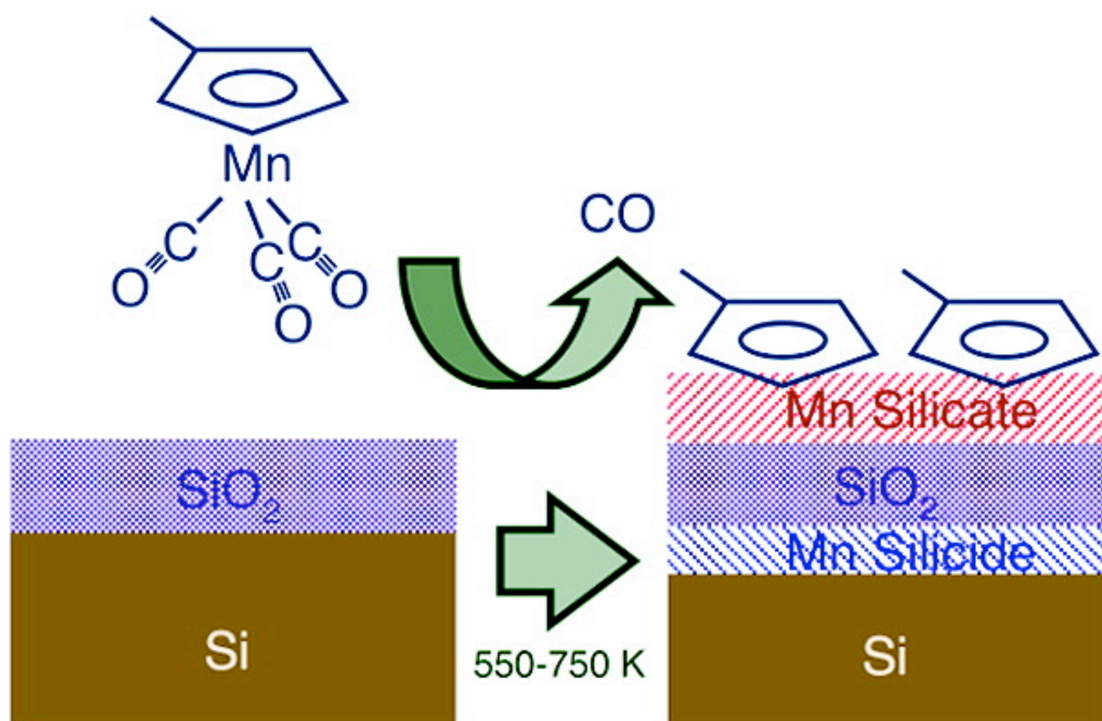

Figure 4.10 Schematic chart for the formation of the layered structure in the uptake of $MeCpMn(CO)_3$ on the Si with native oxide substrate

4.6 References:

[1] S. Wen-bin, K. Durose, A.W. Brinkman, B. K. Tanner, *Mater. Chem. Phys.* **1997**, 47, 75;

[2] S. I. Raider, R. Fitsch, M. J. Palmer, *J. Electrochem. Soc.* **1975**, 122, 413;

[3] M. Morita, T. Ohmi, E. Hasegawa, M. Kawakami, M. Ohwada, *J. Appl. Phys.* **1990**, 68(3), 1272;

[4] M. Morita, T. Ohmi, E. Hasegawa, M. Kawakami, K. Suma, *Appl. Phys. Lett.* **1989**, 55(6), 562;

[5] R.G. Gordon, H. Kim, Y. Au, H. Wang, H. Bhandari, Y. Liu, D. K. Lee, Lin, Y. *Advanced Metallization Conference 2008 proceedings*, **2009**, 321;

[6] H. W. Nesbitt, D. Banerjee, *Am. Mineral.* **1998**, 83, 305;

[7] M. Chigane, M. Ishikawa, *J. Electrochem. Soc.*, **2000**, 147, 2246;

[8] M. Oku, K. Wagatsuma, T. Konishi, J. *Electron Spectrosc. Relat. Phenom.* **1999**, 98, 277–285;

[9] F. Parmigiani, L. Sangaletti, *J. Electron Spectrosc. Relat. Phenom.* **1999**, 98, 287;

[10] M. Oku, S. Suzuki, N. Ohtsu, T. Shishido, K. Wagatsuma, *Appl. Surf. Sci.* **2008**, **254**, 5141;

[11] S. Barison, G. Battaglin, R. Bertoncello, E. Cattaruzza, A. Mascolo, P. Mazzoldi, M. Ruzzi, F. Trivillin, *J. Mater. Chem.* **1999**, 9, 2929;

[12] N. Ohtsu, M. Oku, A. Nomura, T. Sugawara, T. Shishido, K. Wagatsuma, *Appl.Surf. Sci.* **2008**, 254, 3288;

[13] M. J. Guittet, J. P. Crocombette, M. Gautier-Soyer, *Phys. Rev. B,* **2001**, 63,

125117;

[14] V. P. Zakaznova-Herzog, H. W. Nesbitt, G. M. Bancroft, J. S. Tse, X. Gao, W. Skinner, *Phys. Rev. B,* **2005**, 72, 205113;

[15] K.N. Dalby, H.W. Nesbitt, V. P. Zakaznova-Herzog, P. L. King, *Geochim. Cosmochim. Acta,* **2007**, 71, 4297;

[16] M.P. Seah, W.A. Dench, *Surf. Interface Anal.* **1979**, 1, 2;

[17] S. Tanuma, C. J. Powell, D. R. Penn, *Surf. Interface Anal.* **1991**, 17, 911;

[18] P. J. Cumpson, *J. Electron Spectrosc. Relat. Phenom.* **1995**, 73, 25;

[19] K. Neishi, S. Aki, K. Matsumoto, H. Sato, H. Itoh, S. Hosaka, J. Koike, *Appl. Phys. Lett.* **2008**, 93, 032106;

[20] P. L. J. Gunter, O.L. J. Gijzeman, J. W. Niemantsverdriet, *Appl. Surf. Sci.***1997**, 115, 34;.

[21] P. Kappen, K. Reihs, C. Seidel, M. Voetz, H. Fuchs, *Surf. Sci.* **2000**, 465, 40;

[22] C. J. Powell, A. Jablonski, *J. Electron Spectrosc. Relat. Phenom.* **2010,** 178, 331;

[23] X. Qin, H. Sun, F. Zaera, *J. Vac. Sci. Technol., A* **2012**, 30(1), 01A112;

[24] Y. Au, Y. Lin, H. Kim, E. Beh, Y. Liu, R. G. Gordon, *J. Electrochem. Soc.* **2010**, 157, D341;

[25] J. Koike, M. Wada, *Appl. Phys. Lett.* **2005**, 87, 041911;

[26] T. Usui, H. Nasu, S. Takahashi, N. Shimizu, T. Nishikawa, M. Yoshimaru, H. Shibata, M. Wada, J. Koike, *IEEE Trans. Electron Devices,* **2006**, 53, 2492;

[27] J. Koike, M. Haneda, J. Iijima, Y. Otsuka, H. Sako, K. Neishi, *J. Appl. Phys.* **2007**, 102, 043527;

[28] M. Haneda, J. Iijima, J.Koike, *Appl. Phys. Lett.* **2007**, 90, 252107;

[31] B. Rao, D. Gaskell, *Metall. Mater. Trans. B* **1981**, 12, 311;

[32] G. Eriksson, P. Wu, M. Blander, A. D. Pelton, *Can. Metall. Q.* **1994**, 33, 13;

[33] A. I. Zaitsev, B. M. Mogutnov, *Inorg. Mater.* **1997**, 33, 823;

[34] O. Knacke, O. Kubaschewski, K. Hesselmann, *Thermochemical Properties of Inorganic Substances*, 1st ed. Springer-Verlag: Berlin, **1973**;

[35] A. E. Kaloyeros, E. Eisenbraun, *Annu. Rev. Mater. Sci.* **2000**, 30, 363;

[36] I. Goswami, R. Laxman, *Semicond. Int.* **2004**, 27, 49;

[37] W. Koh, D. Kumar, W. M. Li, H. Sprey, I. J. Raaijmakers, *Solid State Technol.* **2005**, 48, 54;

[38] H. Kim, *Surf. Coat. Technol.* **2006**, 200,3104;

[39] *International Technology Roadmap for Semiconductors*, **2011.**

CHAPTER FIVE

Chemical Vapor Deposition of Manganese Metallic Films on Silicon Oxide Substrates

5.1 Introduction

It was shown in Chapter 4 that the deposition of manganese thin films on Si with native oxide substrates may induce the formation of a complex layered structure that includes manganese silicates and also possibly manganese silicides, and the growth rate for this manganese thin films is very slow as it takes several hours doing to obtain about 1-2 nm thick manganese thin films at 625 K. It's expected that this carbonyl precursor, $MeCpMn(CO)_3$, can also react with thick oxide to form manganese silicates, but what's really going to happen might be different and needs to be investigated, given that the SiO_2 is too thick that the diffusion through the manganese silicate/SiO_2 films to react with the S(0) almost impossible. Meanwhile, Finding a new manganese precursor that might have higher deposition rates is necessary. It was found that manganese acetamidinate compounds could be used as a manganese precursor to grow manganese thin films fast [1]. The manganese acetamidinate precursor, provided by Intel, was deposited to the thick SiO_2 surface to study the surface chemistry involved in the chemical deposition.

In this chapter, the deposition of Mn films using two precursors, two Mn complexes containing acetamidinate and methylcyclopentadienyl ligands, respectively, was characterized and contrasted by X-ray photoelectron spectroscope (XPS).

All the conditions were discussed in Chapter 2, and it should be pointed out that a nude ion gauge, placed on the side of the auxiliary chamber, was used for electron-impact excitation in the case of the deposition of the $MeCpMn(CO)_3$ precursor to enhance its reactivity.

5.2 Results

5.2.1 Deposition of Mn Amidinate on Si with 300 nm silicon oxide

Figure 5.1 displays typical Mn 2p XPS data obtained for the uptake of the Mn Amidinate on the thick silicon oxide film at 625 K. The left panel shows the raw data as a function of both exposure and detection angle, whereas the right panel displays the differential increases in signal between consecutive exposures to highlight the incremental changes that occur on the surface. Fits to Gaussian peaks are reported as thin lines for the main Mn features in the data in the left panel.

The initial stages of the Mn deposition lead to the development of broad peaks at 641.50 and 645.35 eV in the Mn $2p_{3/2}$ XPS data. Those can be easily assigned to the formation of manganese silicate and/or manganese oxide surface species, a

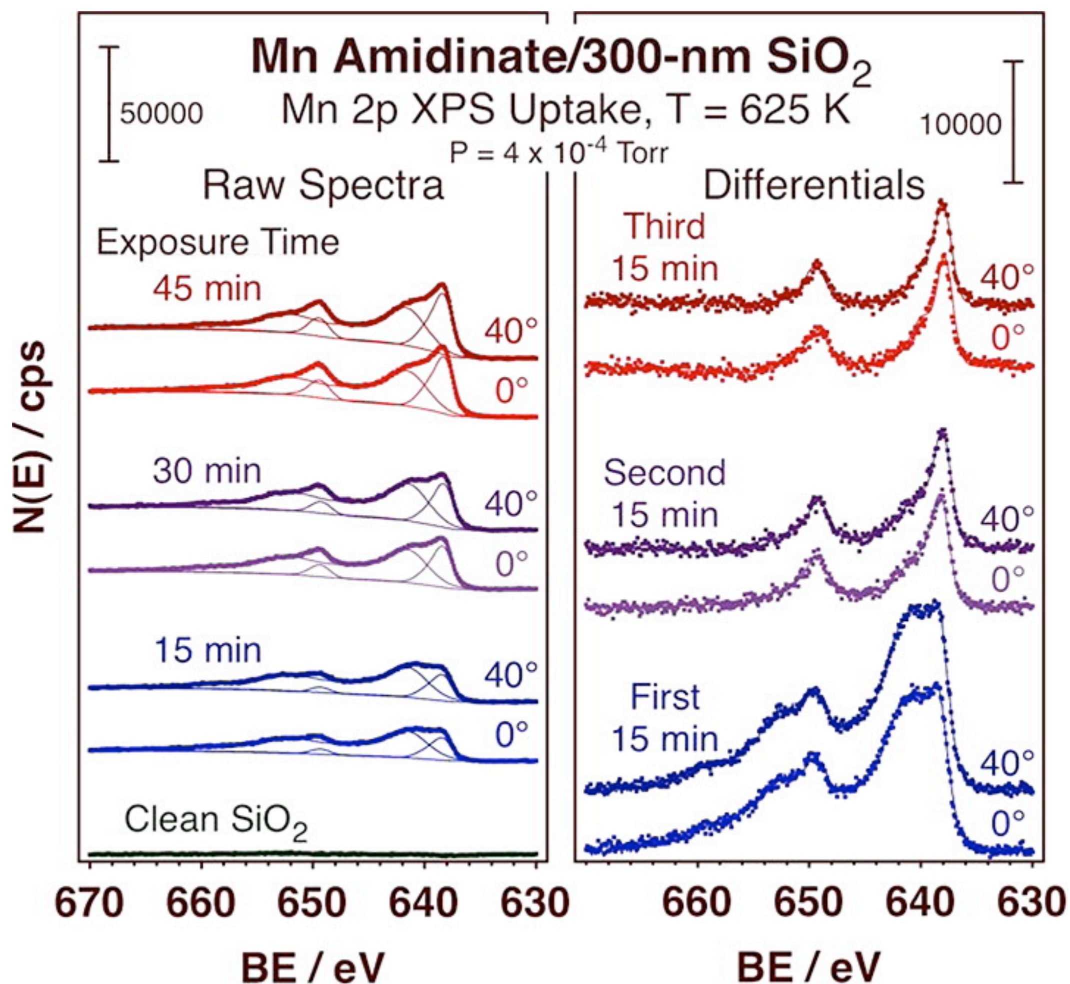

Figure 5.1 Mn 2p XPS data for the evolution of a silicon oxide substrate upon exposure to 0.4 mTorr of Mn Amidinate at 625 K. Data are presented for the clean surface as well as for the substrate after 15, 30, and 45 minutes doses, and for photoelectron detection at directions normal (0°) and glancing (40°) from the surface.

similar process that has been reported before by us in Chapter 4 and others [2, 3] with other precursors and on other similar surfaces. It is difficult to differentiate between these two possible compounds in this system by using the Mn 2p XPS data exclusively, but previous Si 2p data from experiments in Chapter 3 using silicon wafers covered with a thin native oxide film indicated the clear formation of at least some manganese silicate in addition to the oxide.

Besides the peaks for manganese silicate/oxide, a second set of sharper peaks is also observable already in the data in Figure 5.1 after the first 15 min of exposure. The Mn 2p $_{3/2}$ XPS components of this growing signal are centered at 638.35 and 639.40 eV, and are associated with metallic manganese and/or manganese silicide. Differentiating between those two species is again difficult, since both display similar Mn XPS features. However, these new low-binding features are more prominent in the trace taken normal to the surface in the angle-resolved XPS experiments. The comparison of the data from detection at 0° versus 40° off normal in the two lower traces of both panels of Figure 5.1, indicates that the new compound is located underneath the surface, below the Mn silicate layer. This behavior was also seen on SiO_2/Si(100) wafers before, where a Mn silicide subsurface layer was identified by the additional plasmon loss features seen in the Mn 2p XPS at approximately 660 and 670 eV binding energy in the deposition of manganese thin films on Si with native oxide in Chapter 4, and similar spectra was also observed on sputter-clean Si(100) surfaces in Chapter 3.

By analogy, we propose that the initial signal in the low binding energy features seen in the XPS traces in Figure 5.1 may correspond to a thin subsurface Mn silicide layer, which appears right after saturation of the Mn silicate/Mn oxide layer that forms during the initial exposure of SiO_2 surfaces to the Mn Amidinate precursor. Further exposure of the surface to this precursor leads to the almost exclusive growth of the low binding energy Mn 2p XPS features (30 and 45 minutes exposures in Figure 5.1). The additional Mn deposited during the second and third 15 minutes dosing is in fact detected at the surface, and is accompanied with a slight shift to lower binding energies, to approximately 638.20 eV in the data in Figure 5.1 and to values as low as 639.75 eV upon the growth of thicker films. It is possible that the newly deposited manganese is in metallic form, as Mn(0), at these later stages of film growth, but it should be indicated that the growing films often contain low levels of carbon and nitrogen impurities(see below) and could therefore be considered as diluted Mn nitrides and/or carbides instead.

A quantitative analysis of the Mn 2p XPS data in terms of the growth of these Mn films as a function of exposure is displayed in Figure 5.2. Data are reported for four different substrate temperatures. The average film thicknesses were estimated by assuming a layer-by-layer distribution of species, assuming exponential attenuation of the signals, and using published photoelectron mean free paths, and are reported in terms of monolayers (ML)[4]. Film thicknesses are reported separately for the Mn(0) (together with any Mn silicide, left panel) and Mn silicate (and Mn oxide, center panel) films as well as for the total Mn

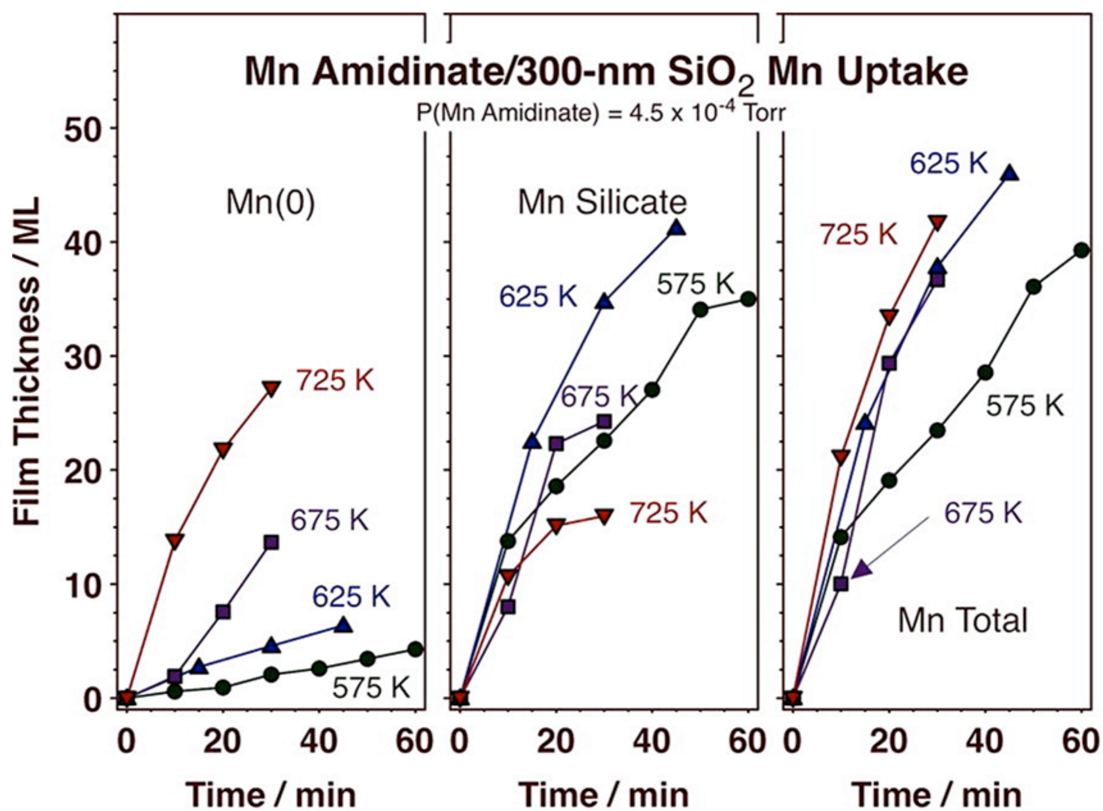

Figure 5.2. Summary of the Mn 2p XPS signal intensities obtained in Mn uptake studies such as that illustrated in Figure 5.1 as a function of substrate temperature using the Mn Aamidinate precursor.

deposition. Film thicknesses were also estimated from the attenuation of the Si 2p and O 1s XPS signals, and were consistent with the results shown in this Figure (data not shown). The data in Figure 5.2 confirm the conclusion for the sequences of the formation of the different manganese species reached above , namely, that the Mn silicate film is formed first and is followed by the additional growth of a Mn(0) film on top. Notice, however, that the Mn silicate film may in fact keep growing even after the Mn(0) film starts to form due to the diffusion of oxidized manganese to the thick silicon oxide at the bottom. This Mn silicate can become quite thick, possibly amounting to approximately 50 monolayers, although the accuracy of thickness determinations by XPS with thick films is not reliable. In any case, the development of the Mn silicate film is similar at all deposition temperatures within the range reported here, between 575 and 725 K, with somewhat thicker films possibly forming at 625 K. The decrease in film thickness with increasing temperature beyond 625 K seen in Figure 5.2 may be related to a higher diffusivity of the Mn into the SiO_2 bulk (see below). Multilayer Mn(0) films can then be grown on top of the Mn silicate layer, at faster rates if higher temperatures are employed. Films of thickness of up to ~30 ML were grown in our experiments (at 725 K), at which point the Si 2p and O 1s signals are barely detectable.

One potential limitation of the use of metalorganic precursors in chemical deposition applications is that the organic ligands may decompose during the deposition process and leave undesired contaminating elements in the growing film. In the case of the Mn Amidinate, the ligand contains carbon and nitrogen

atoms. In our study, the fate of both those elements was followed by XPS. In terms of the signal for carbon, the C 1s XPS spectra were dominated by two features, at 282.70 and 284.20–285.45 eV, characteristic of metal carbide and organic (aliphatic) carbon, respectively (data shown in Figure 5.3). Three Gaussian peaks, at 282.70, 284.20 and 285.45 eV, were used to fit the metal carbide and two organic components in order to reflect the different chemical environment experienced by the carbon atoms bonded to other carbons versus to nitrogen in the acetamidinate ligand respectively. Angle-resolved experiments indicated that the latter, dominant feature (that is, the combination of the two organic C peaks) is located at the signal, on the other hand, appears to be spread throughout the grown Mn film, surface and amounts to approximately 10–20% of a monolayer. The carbidic C signal, on the other hand, appears to be spread throughout the Mn film, and amounts to the equivalent of ~5% of a monolayer in the film deposited at 625 K. Figure 5.4 reports equivalent N 1s XPS data obtained during deposition with Mn Amidinate at 625 K. In this case, three components are again identified, at 396.20 and 397.85 eV, corresponding to metal nitride and organic nitrogen atoms; a third, small and constant feature at 399.60 eV, was detected in all spectra, an impurity in the SiO_2 film. The organic N XPS signal grows first, but saturates already after 15 minutes, at a value equivalent to a few percent of a monolayer. The nitride N XPS peak, on the other hand, develops at a later time but continues to grow with Mn deposition. The intensities of both peaks versus Mn Amidinate exposure time is summarized in Figure 5.5 for three deposition temperatures: 575, 625, and 725 K. In all three cases, the organic N signal quickly reaches the same asymptotic value, approximately 0.15 - 0.20 ML.

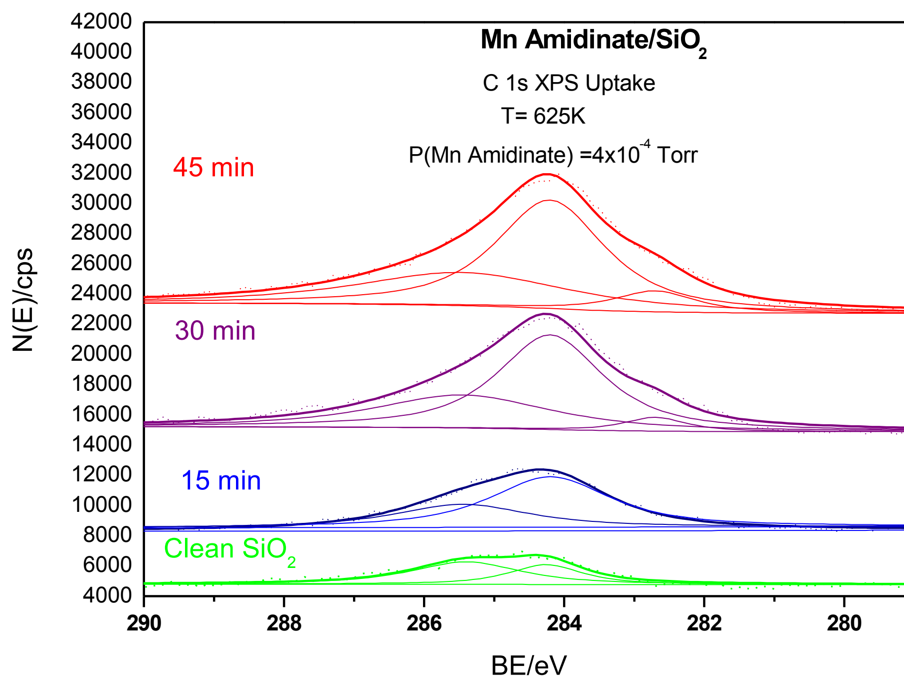

Figure 5.3. C 1s XPS data for the same experiment reported in Figure 5.1. The raw data were deconvoluted into three Gaussian components, corresponding to, from low to high binding energies: carbidic, and two organic components.

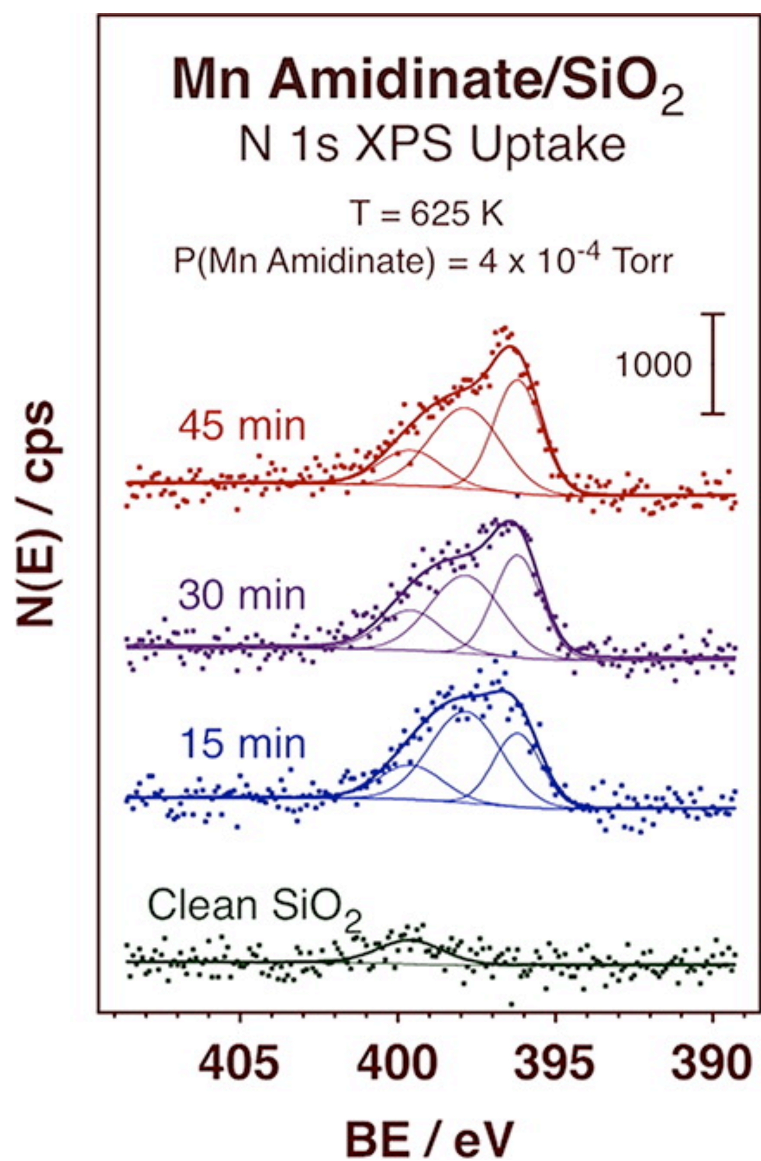

Figure 5.4 N 1s XPS data for the same experiment reported in Figure 5.1. The raw data were deconvoluted into three Gaussian components, corresponding to, from low to high binding energies: nitride, organic, and impurity nitrogen.

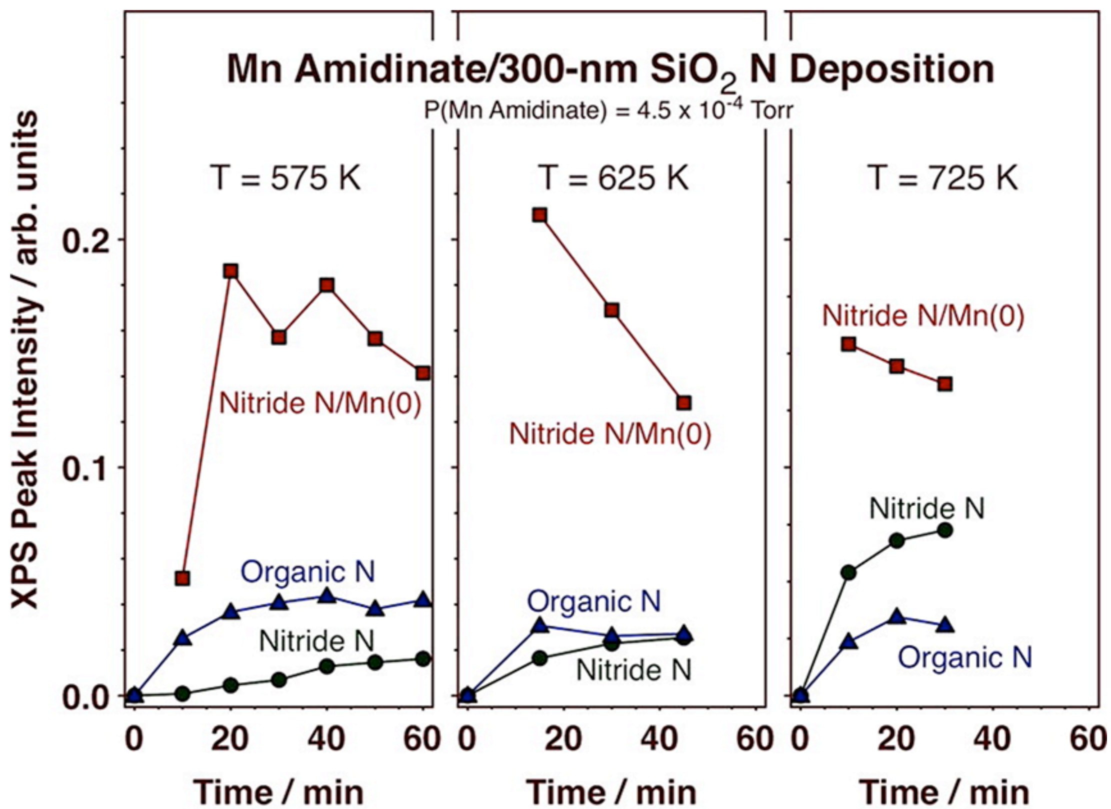

Figure 5.5 Summary of the N 1s XPS signal intensities obtained in Mn Amidinate uptake experiments such as that shown in Figure 5.4 for three substrate temperatures. The evolution of the organic (blue triangles) and nitride (green circles) nitrogen signals is reported as a function of exposure.

The nitride N 1s XPS signal, by contrast, grows continuously, and reaches higher values at higher deposition temperatures. That signal roughly tracks the intensity of the Mn(0) signal: the red squares in Figure 5.5 show that the corresponding nitride N/Mn(0) XPS signal ratios (normalized to equivalent monolayers) always amount to approximately 17 ± 4 atomic%.

It is interesting to note that a recent report describes the CVD of Mn4N (20% N atomic%), a good diffusion barrier material, on the surfaces inside silicon by using the same manganese acetamidinate precursor [5]. This suggests that Mn_4N may be what grows in the experiments reported here as well. Unfortunately, we could not find any reference Mn 2p XPS data for Mn_4N to check this hypothesis directly. Our expectation is for the binding energy of the Mn $2p_{3/2}$ peak in Mn_4N to be somewhere between those of metallic Mn and the manganese oxides and silicates, to reflect the partial positive charge created by association with such an electronegative element as nitrogen is, but the high Mn/N ratio in Mn_4N could explain the lack of significant blue shifts in the XPS signals. Certainly, the binding energy of the N 1s XPS signal associated with this Mn containing film is characteristic of metal nitrides. We here refer to the low binding energy peaks in the Mn 2p XPS as to correspond to Mn(0) and/or Mn silicide, but the possibility of Mn nitride formation should be considered as well.

5.2.2 Deposition of $MeCpMn(CO)_3$ on Si with 300 nm silicon oxide

Contrasting experiments were performed by using the $MeCpMn(CO)_3$ precursor. Two important differences can be identified between the Mn Amidinate and this

second precursor: (1) the methylcyclopentadienyl compound does not have nitrogen-containing ligands, which means that nitrogen contamination in the growing films is not an issue, and (2) it is significantly less reactive, a fact that may potentially afford greater control on the deposition. In fact, $MeCpMn(CO)_3$ is so stable that it is, in general, quite difficult to deposit any Mn on silicon-based surfaces with it. Luckily, we have developed an electron-impact gas-phase excitation method, using an ion gauge inside the chemical vapor deposition chamber, to help activate the precursor via ionization and partial decarbonylation prior to adsorption, as discussed in Chapter 3. This ion-gauge-based excitation method was used in all the experiments reported here.

Figure 5.6 displays Mn 2p XPS spectra from uptake experiments on SiO_2 using $MeCpMn(CO)_3$ at three different temperatures (625, 675, and 725 K). The data were fitted and analyzed in similar fashion as in the experiments with the Mn Amidinate, and the same components for Mn silicate/Mn oxide and Mn(0)/Mn silicide were identified, with Mn $2p_{3/2}$ XPS peaks at (641.50, 645.35) and (638.35, 639.40) eV, respectively. A sequential build up of Mn containing species was observed too, with the Mn silicate/Mn oxide saturating first and the Mn(0)/Mn silicide film growing afterward. There are, however, some significant differences between these and the previous results. The most noticeable is the fact that the deposition of Mn appears to be slower, not faster, at higher temperatures. This certainly applies to the buildup of the Mn(0) film, which can be barely started at 725 K but reaches thicknesses above 10 ML after 300 minutes of exposure at 625 K. In addition, the signal for the oxidized Mn also decreases with increasing

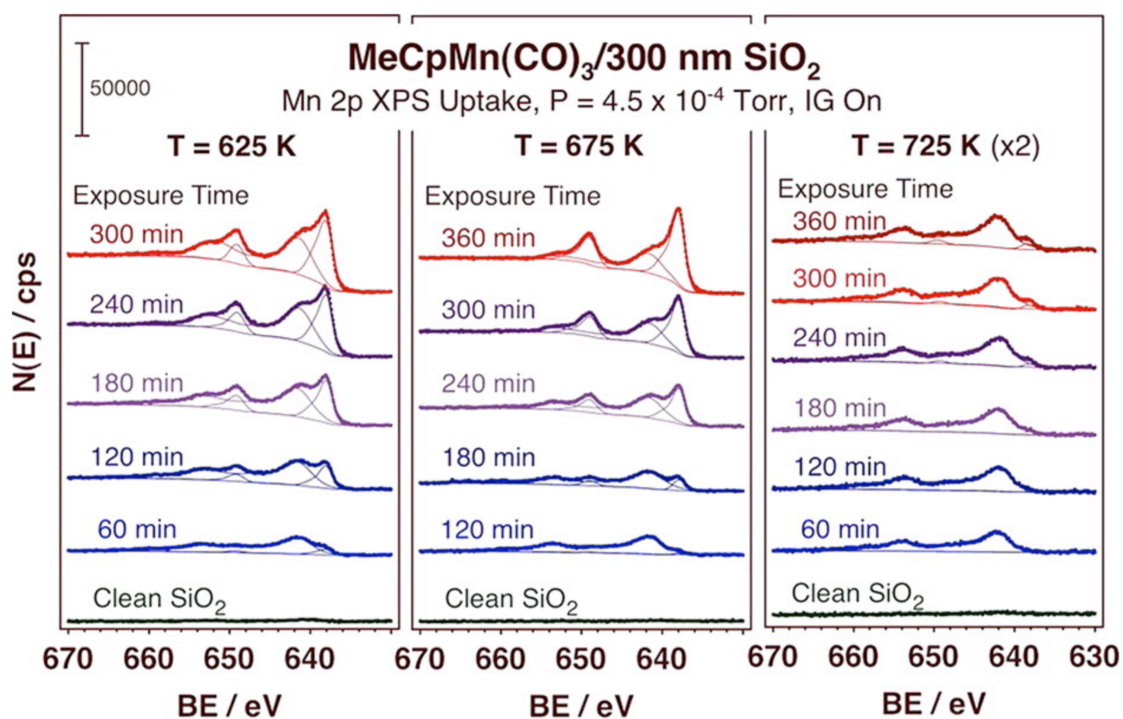

Figure 5.6 Mn 2p XPS uptake spectra for films grown on SiO_2 by using (MeCpMn(CO)3) at three deposition temperatures: 625 (left), 675 (center), and 725 (right) K. An ion gauge located on the side of the reactor was kept on during the deposition to induce electron-bombardment activation of the compound in the gas phase, to facilitate deposition.

deposition temperature. As discussed later, this behavior was ascribed to the faster diffusion of Mn into the bulk of the silicon oxide substrate at higher temperatures. Thick Mn silicate films seem to be made, in these cases, several tens of monolayers thick, with nonstoichiometric compositions and increasing Mn dilution with increasing temperature.

Additional information on the sequence of events involved in the build up of these Mn films can be extracted from Si 2p and O 1s XPS data. The spectra for those elements are dominated by the signals from the SiO_2 substrate, which manifests itself in peaks centered at 103.5 and 532.7 eV, respectively. No evidence could be extracted for the formation of Mn silicide, as it was possible in experiments using Si (100) wafers cover with their thin native oxide film. Nevertheless, information on the thicknesses of the Mn films being deposited could be estimated by the accompanying attenuation of the intensities of the Si 2p and O 1s XPS features.

Figure 5.7 summarizes the data obtained for all relevant elements as a function of exposure time for the case of Mn deposition with $MeCpMn(CO)_3$ on SiO_2 at 725 K. A few observations are worth highlighting from these data. First, the sequential deposition of Mn silicate and Mn(0) is evident in this case as well: the latter only starts building up after approximately 200 minuntes deposition, and by that time, the signal for the Mn silicate has already reached a value close to its saturation. Notice, however, that the signal for Mn silicate does continue to grow after that point, albeit at a much slower rate. Second, both Si 2p and O 1s XPS

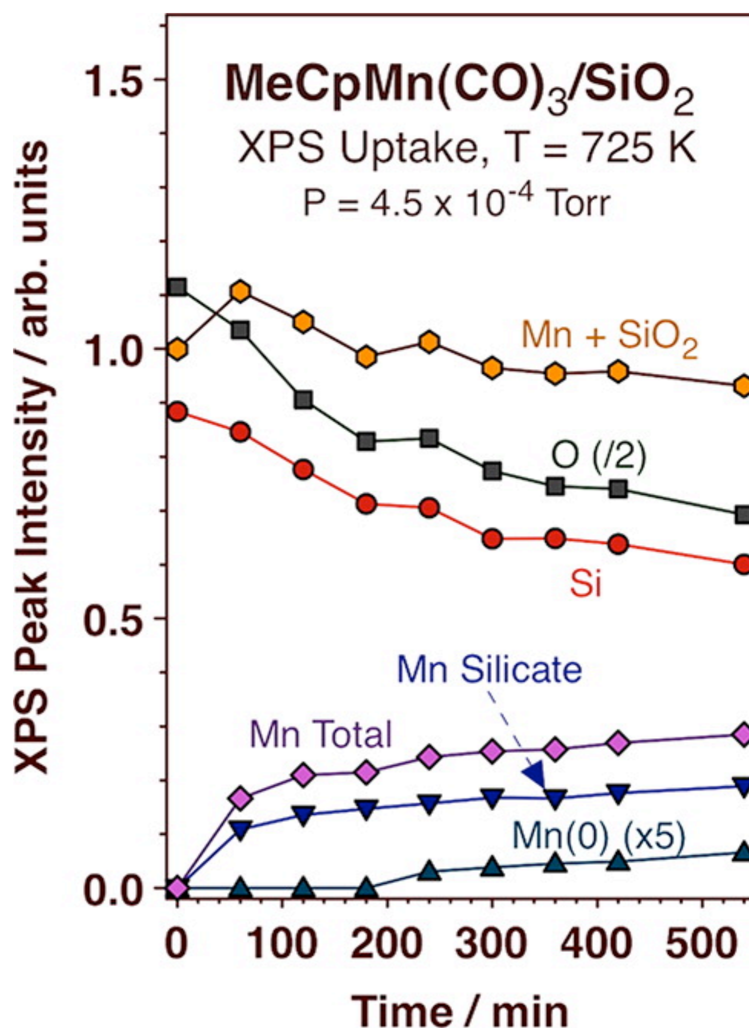

Figure 5.7 Summary of the XPS signal intensities seen during the uptake of $MeCpMn(CO)_3$ on SiO_2 at 725 K. Data are reported for the O 1s, Si 2p, and Mn 2p XPS signals. The Mn data were also divided into contributions from the Mn silicate/Mn oxide and Mn(0)/Mn silicide films, estimated from the Gaussian fits shown in Figure 6.6. The data clearly highlight the sequential formation of the Mn silicate, Mn silicide, and Mn(0) layers.

signals decrease with $MeCpMn(CO)_3$ exposure. This is the case from the very beginning, even before the start of the growth of the Mn(0) film, a fact that indicates that the silicon and oxygen atomic densities in the film decrease as the Mn is incorporated in the topmost layers, to form a combination of Mn silicate and Mn oxide. In fact, the combined Mn + Si XPS signals, reported as orange hexagons in Figure 5.7, remains roughly constant all throughout the Mn deposition experiment. Finally, both Si 2p and O 1s signals remain unchanged during the first stages of the growth of the low-binding energy Mn 2p peaks that we assign to a mixture of Mn(0) and Mn silicide. Combined with the other pieces of evidence provided throughout this dissertation, this observation is consistent with the formation of a thin subsurface Mn silicide layer. The Mn(0) film only starts to grow after that layer is formed. Also, as mentioned before, the Mn 2p XPS peaks corresponding to these species red-shift slightly as the deposition progresses.

One key difference between the deposition results with the Mn Amidinate versus with $MeCpMn(CO)_3$ is that the film growth is much faster with the former. Moreover, thicker Mn(0) films can also be grown with it at higher temperatures. This is to be contrasted with the behavior seen with $MeCpMn(CO)_3$, with which the growth is slow, and slower at higher temperatures: virtually no Mn(0) can be deposited with this precursor at 725 K. We explain these different trends in terms of the relative rates of Mn deposition, via precursor adsorption and decomposition on the surface, versus those for Mn diffusion into the bulk. In our model (illustrated in the schematics in the graphical abstract), Mn(0) films can

only start to grow once a threshold Mn density is reached in the Mn silicate layer that forms first, and possibly after a thin subsurface Mn silicide barrier is formed as well. With $MeCpMn(CO)_3$ and at high temperatures, it seems that Mn diffusion into the bulk is faster than deposition of new Mn, and that this ordering of relative rates precludes the system from ever building the Mn silicate/Mn silicide structure needed for Mn(0) film growth.

The extent of Mn diffusion into the bulk in the films prepared with $MeCpMn(CO)_3$ at 725 K was probed by performing depth profiling analysis, by acquiring XPS spectra at different stages during the sputtering of the film using Ar^+ ions. Figure 6.8 shows a summary of the data in terms of XPS signal intensities as a function of sputtering time for a film prepared by exposing a clean SiO_2 surface to 9 hours of $MeCpMn(CO)_3$ at a pressure of 4.6×10^{-4} Torr. The attenuation of the Si 2p and O 1s XPS signals resulting from that deposition were used to estimate the Mn(0) film thickness at approximately 5 ML, and their recuperation during the early stages of sputtering were employed to estimate the rate of film removal by the Ar^+ ion beam at approximately 1 ML/min. It can be seen in Figure 5.8 that the carbon signal comes from species on the topmost surface, which are removed within the first few minutes of sputtering. The Si 2p and O 1s XPS signals are restored relatively early on within the depth profiling experiment as well. The Mn 2p XPS intensity, on the other hand, decreases at a much slower pace, and shows detectable signal even after 40 min of sputtering. This indicates deep diffusion of the Mn within the SiO_2 substrate during deposition, down to several tens of monolayers, as inferred in the experiments discussed before. Caution

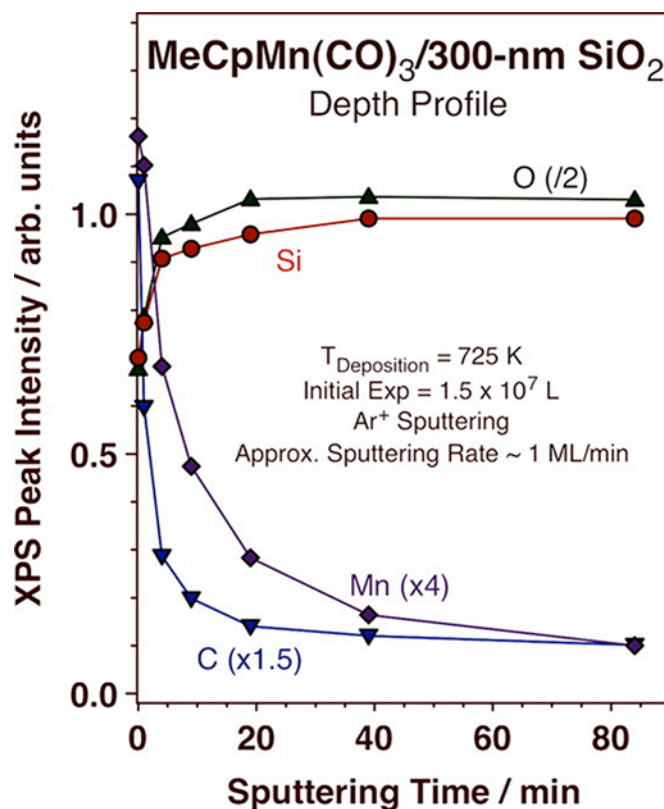

Figure 5.8 Depth profile for the as-formed thin films with Ar^+ sputtering as function of time. The Si 2p, O 1s, C 1s, and Mn 2p XPS signal intensities measured as a function of sputtering time starting with a Mn film prepared by exposure of the SiO_2 substrate to 4.6×10^{-4} Torr of $MeCpMn(CO)_3$ at 725 K for 9 h.

must be taken when quantitating these depth profiling data, because there is always some degree of layer intermixing during ion sputtering (which explains why the C and Mn signals never fully disappear) and the sputtering also tends to reduce some surface species (the reason why we do not report the Mn silicate and Mn(0) signals separately; there is always a residual Mn(0) signal in the XPS spectra obtained after sputtering).

5.2.3 Deposition vs diffusion in manganese deposition

The role of Mn diffusion into the bulk of the substrate in these Mn film deposition processes was tested by a couple of independent experiments. In the first, a Mn(0) film was first grown at 625 K using the Mn Amidinate precursor (a 60 minutes exposure at a pressure of 4×10^{-4} Torr) and then annealed at 725 K for 1 hr. The relevant Mn 2p XPS data from that experiment are reported in Figure 5.9. The net result from the high-temperature annealing is a decrease in signal intensity in the Mn(0) $2p_{3/2}$ XPS peaks at 638.10 and 639.40 eV (and a shift of the first to a value of 638.35 eV), indicating the loss of some of that film to the bulk. The Mn(0) XPS peak reduction is compensated in part by the growth of the peaks at 641.50 and 645.35 eV associated with the oxidized Mn. It should be noted that the gain in the Mn silicate/Mn oxide signal does not fully account for the loss of the Mn(0)/Mn silicide peak intensity, so there is a net loss of overall Mn 2p XPS signal. This is explained by two factors: (1) the Mn silicate XPS photoelectrons are partially shielded by the Mn(0) film on top (the placement of the Mn(0) on top and the Mn silicate beneath it was corroborated by the angle-dependent XPS

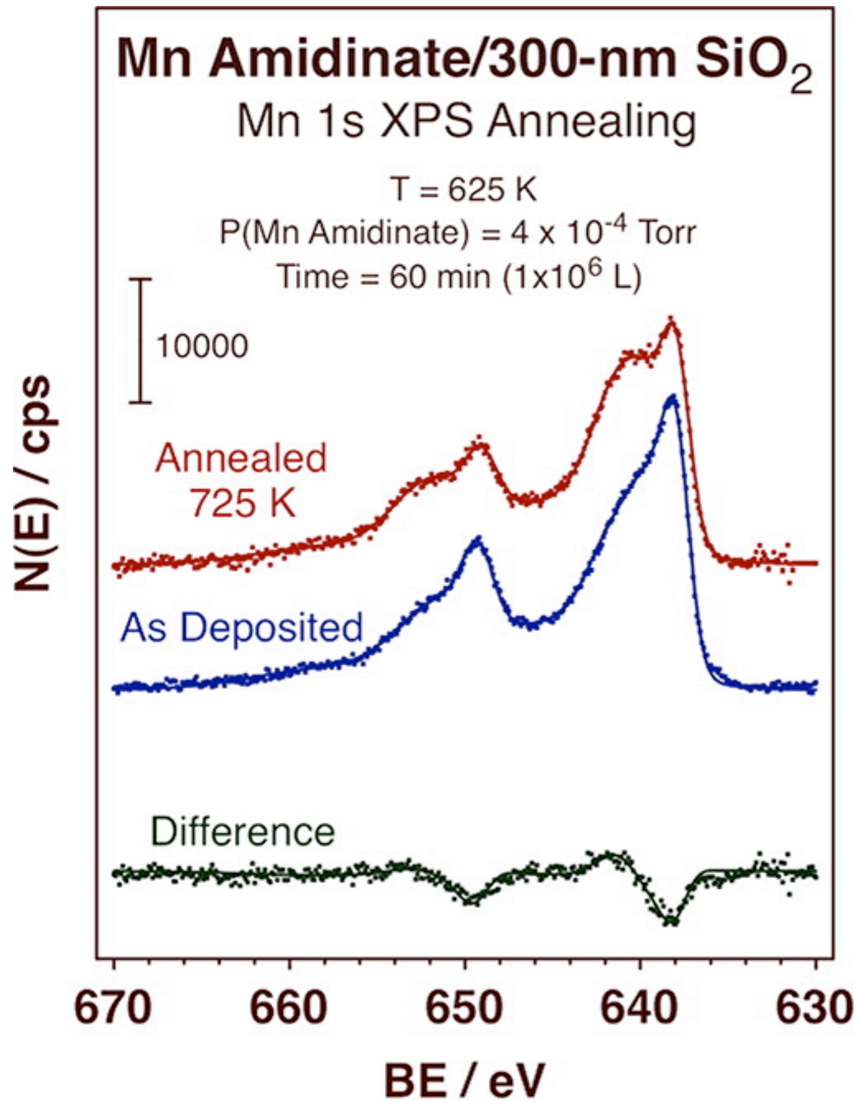

Figure 5.9 Mn 2p XPS for the annealing of the as-deposited thin film grown by Mn Amidinate precursor. The green trace at the bottom shows the difference between the two raw spectra.

XPS analysis, data not shown), and (2) the Mn density within the Mn silicate layer may be reduced as the Mn atoms diffuse deeper into the bulk.

A second experiment was performed with $MeCpMn(CO)_3$ by varying the partial pressure of the precursor during film growth, from 4.6×10^{-4} (Figure 5.10, filled symbols) to 9.2×10^{-4} Torr (Figure 5.10, open symbols). This affords a change in the rate of deposition independently from that of Mn diffusion into the bulk. The deposition temperature was set at 625 K in both cases. A summary of the data, in the form of XPS peak intensities as a function of exposure of the SiO_2 substrate to the precursor, is given in Figure 5.10. It can be seen there that the evolution of the Si 2p (red circles) and O 1s (green squares) XPS signals were comparable in both cases, regardless of the pressure used. In fact, the overall Mn 2p XPS signal intensities (purple diamonds) were also similar in both runs. The data show a steady growth of the Mn XPS signal. The main difference upon changing precursor pressure during Mn deposition was observed in the distribution of the Mn XPS intensity: more Mn silicate was seen to form at any given exposure when the lower precursor pressure was used. This behavior takes place at the expense of a lower Mn(0) formation. Accordingly, the opposite trend was identified at the higher pressure (which corresponds to a doubling of the deposition rate): the Mn(0) XPS signal is larger, by about 50% after a 5×10^6 L exposure, while the Mn silicate XPS intensity is reduced, to about 75% of the value seen after low-pressure deposition. It appears that a faster deposition rate facilitates the build up of the minimum Mn silicate layer need to trigger the start of the Mn(0) growth.

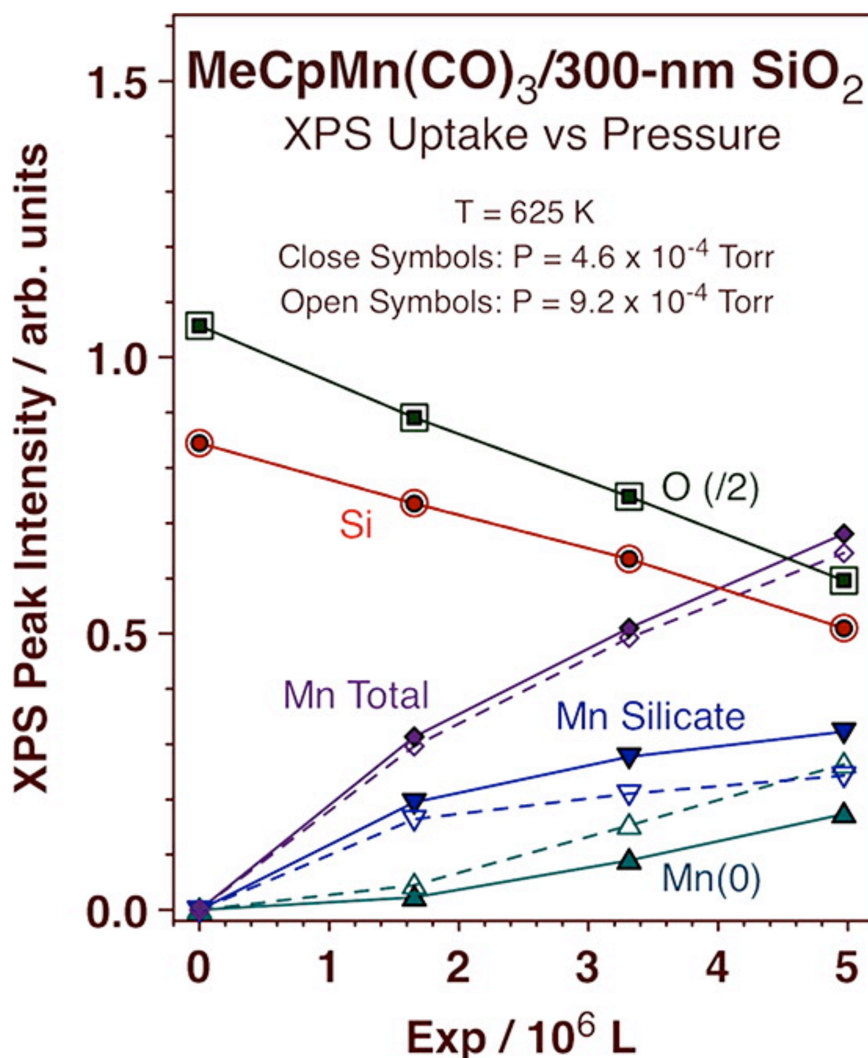

Figure 5.10 Summary of the XPS signal intensities seen during the uptake of $MeCpMn(CO)_3$ on SiO_2 at 625 K at different dosing pressures. Two sets of data are presented, for doses using 4.6×10^{-4} (close symbols) and 9.2×10^{-4} (open symbols) Torr of the precursor while keeping all other parameters the same.

5.2.4 Optimized deposition sequence

Although the first precursor, Mn Amidinate, provides faster Mn deposition and therefore affords the growth of Mn(0) films even at high temperatures, its use needs to be minimized because it also leads to the incorporation of nitrogen impurities. Meanwhile, methylcyclopentadienyl compound does not have nitrogen-containing ligands, which means that nitrogen contamination in the growing films is not an issue, but the deposition rates was much slower. It is possible to combine the two depositions to take advantage of the merits of both, fast growth rate as well as less nitrogen contaminant. At the same time, the hypothesis that a Mn silicate/Mn silicide barrier needs to be formed on the substrate before the growth of Mn(0) films can start could be tested by combining deposition cycles using the Mn Amidinate and $MeCpMn(CO)_3$. Accordingly, deposition sequences were designed to first provide a limited amount of Mn by using the Mn Amidinate, sufficient to build up the Mn silicate/Mn silicide barrier mentioned above, after which further deposition was carried out using $MeCpMn(CO)_3$. Mn 2p XPS data from three of such experiments are shown in Figure 5.11, for runs carried out at 725 K with three different initial Mn Amidinate exposures. As opposed to depositions where the $MeCpMn(CO)_3$ precursor was used alone, in which case virtually no Mn(0) could be deposited (at 725 K in Figure 5.6, right panel), the deposition of Mn(0) films was possible in all three examples reported in Figure 5.11. Particularly noteworthy is the case reported on the left panel of that figure, where the Mn deposition using the Mn Amidinate was stopped right after the very start of the appearance of the Mn(0)/Mn silicide XPS peaks. Significant Mn(0) signal is seen there after the first

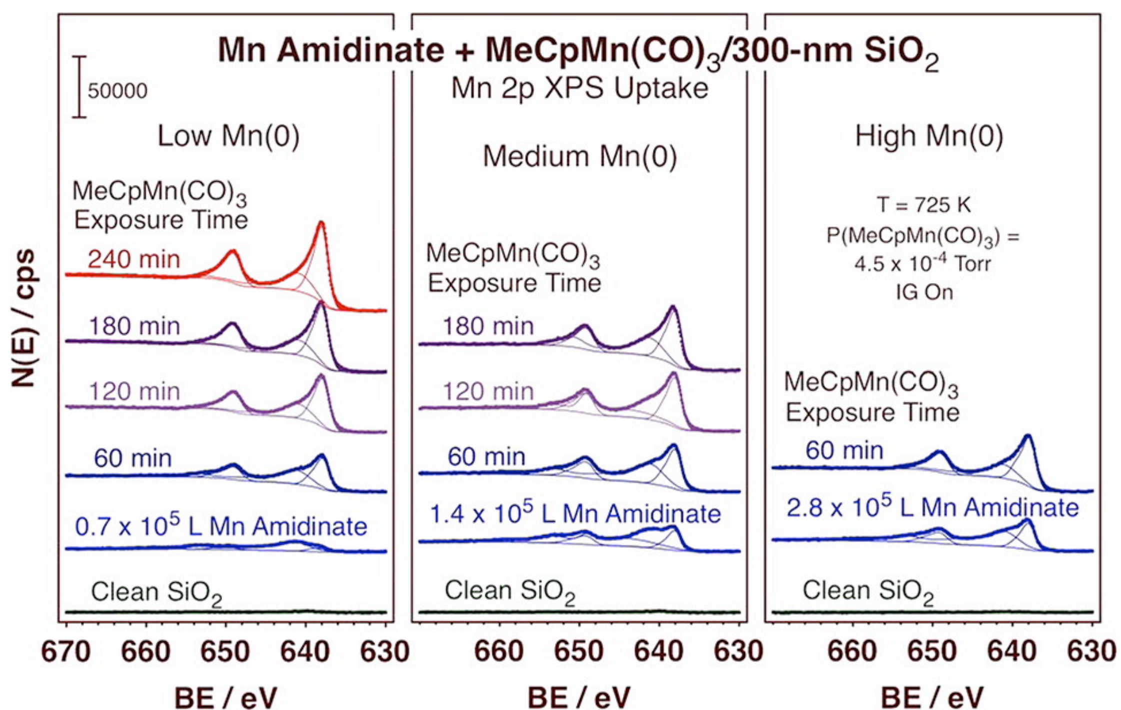

Figure 5.11 Manganese deposition using Mn Amidinate first, and then $MeCpMn(CO)_3$ on Si with 300 nm thick silicon oxide. Three sets of data are shown in the respective three panels with three different initial exposures of Mn Amidinate.

60 minutes of exposure to $MeCpMn(CO)_3$, even though the signal for the Mn silicate layer also continues to grow, slightly. The transition from Mn silicate/Mn silicide saturation to Mn(0) growth is not sharp, the two processes overlap in time.

5.3 Discussion

The experiments reported here were directed at developing an understanding on the mechanism for the deposition of manganese films on silicon oxide substrates by chemical means. As mentioned in the introduction in Chapter 1, there has been some interest recently in developing an effective method for growing such films as self-forming diffusion barriers for copper interconnects. Chemical deposition methods may be preferred for this purpose due to their isotropic nature, but developing the proper chemistry for this is challenging. Besides the possible impurities from decomposition of the ligands in the Mn precursors used, a problem common to most CVD and ALD processes, it is also not easy to deposit manganese films in metallic form, which is very easy to oxidize. Most manganese precursors contain Mn atoms in a nonzero valence state, and manganese oxides are quite stable and difficult to reduce. One possibility to overcome this limitation is to use $Mn_2(CO)_{10}$ as the starting material, because that is a compound with Mn(0) centers, but such a precursor has proven to be quite reactive and to display surface chemistry not easy to control [6].

Most other Mn metalorganic compounds identified as candidates for CVD and ALD require the reduction of the Mn center [7-11]. Usually, it is conceivable to design ALD processes where an oxidized metal layer deposited in the first half of the cycle is reduced by a second agent in the second half. However, this is not a promising approach for manganese, because, as mentioned above, oxidized manganese atoms are quite difficult to reduce to their metallic state. On the other hand, it has become evident that in several ALD processes the metalorganic compound used in the first half-cycle has the ability to undergo disproportionation reactions by itself, during adsorption [12,13]. This chemistry often leads to the reduction of the metal center at the expense of the oxidation of the organic ligands and of their decomposition into smaller fragments. This type of chemistry has been reported even when an oxidizer such as O_2 is used in the second ALD halfcycle, in which case the resulting oxide films are presumably reduced by the metalorganic precursor in the subsequent ALD cycle, and has also been reported for metal acetamidinates similar to that tested in this work [14-16]. Evidence of disproportionation and of the reduction of the metal center during dissociative adsorption was also obtained in our present studies with the two Mn precursors reported above.

When dealing with the deposition of Mn films on silicon oxide, it is often that additional surface chemistry takes place after adsorption leading to the formation of complex layered structures. Manganese films tend to react with silicon oxide to produce manganese silicates, a process driven by the particularly thermodynamic stability of such layer. The results in Chapter 4 have shown that

a thin Mn silicide layer also forms at the interface between the SiO_2 and Si phases on the Si with native oxide substrate. The picture of the final structure developed in that study consisted of a sequence of silicon, Mn silicide, mixture of Mn silicate and MnOx + SiOx, and organic-matter layers. Much of this behavior has been reproduced in the studies on thick silicon oxide films reported here.

Above the results from our characterization of the deposition of Mn films using two possible metalorganic precursors, a Mn Amidinate and $MeCpMn(CO)_3$ were discussed. Amidinate and cyclopentadienyl metalorganic compounds have proven to be promising precursors in CVD for the deposition of Mn as well as of other transition metals, and have been considered for ALD as well [17, 18]. A contrasting study of the surface chemistry of both compounds was carried out to investigate the reactivity upon adsorption in defining the nature of the grown films. Of these two precursors, the Mn Amidinate is more reactive; it easily dissociates and adsorbs on surfaces even at low temperatures. The experiments above showed that the use of such compound does indeed lead to the deposition of Mn on silicon oxide at relatively fast rates. On the other hand, they also indicated that the acetamidinate ligands undergo a degree of decomposition leaving carbon and nitrogen contaminants in the thin films. Reported studies with a similar copper acetamidinate precursor on silicon oxide led to the conclusion that the metal deposition is clean and that the ligands are removed by straight hydrogenation to form the corresponding acetamidine [19], the work finished by our lab with the same compound on nickel, cobalt, and copper substrates identified a stepwise decomposition mechanism involving the

formation of smaller acetamidines, alkenes, amido surface moieties, and HCN, among other species [14-16]. It appears that at least some of that or equivalent surface chemistry may take place on the Mn Amidinate/silicon oxide system too. This high and complex thermal reactivity of metal acetamidinates is likely to explain the CVD component that is often observed in ALD processes with such precursors.

The reactivity of the $MeCpMn(CO)_3$ precursor is another story. This is a fairly stable compound that decomposes thermally only at relatively high temperatures: an early report indicates decomposition only above 685 K [10], although a more realistic estimate of that temperature from GC-MS experiments in our laboratory may be about 575 K (data not shown). It is also quite difficult to dissociatively adsorb the $MeCpMn(CO)_3$ precursor and to deposit Mn films with it at reasonable rates. Thankfully, we have recently identified a method for pre-activating this compound in the gas phase, before deposition, based on electron bombardment. It was shown that this induces the ionization and decarbonylation of the gas-phase molecules, leading to the formation of highly reactive $MeCpMn(CO)_x{}^+$ cations (x = 0, 1, or 2), which can then form MeCpMn(ads) moieties on the surface. Even with such pre-activation, reactivity and film growth with $MeCpMn(CO)_3$ proved to be much slower than with the Mn acetamidinate. On the positive side, the $MeCpMn(CO)_3$ precursor does not contain nitrogen atoms and, therefore, does not lead to any nitrogen incorporation in the growing films. Moreover, the methylcyclopentadienyl ligand is quite sturdy and survives intact up to relatively high temperatures, which

means that it may be quite possible to induce its hydrogenation in the second half of ALD cycles, to remove it from the surface as either methylcyclopentadiene or as a related species. If that chemistry can be identified and implemented, clean ALD processes could be achieved without the complications arising from the deposition of impurities. The drawback identified in these studies is that the deposition rate achievable with $MeCpMn(CO)_3$ as a precursor is slow and may compete unfavorably with other surface steps, diffusion into the bulk in particular. This is perhaps one of the most relevant and novel observations from our work.

Initial evidence for a competition among Mn deposition, Mn diffusion into the bulk, and Mn film growth steps was provided by the evolution of the Mn 2p XPS signal recorded in uptake experiments with $MeCpMn(CO)_3$ on SiO_2 at different temperatures (Figure 5.6). The counterintuitive observation from those data is that Mn deposition appears to occur at a slower rate with increasing substrate temperature. This is the opposite of what is seen with the Mn Amidinate, and not what is expected from thermally activated processes. However, the interpretation of the data may not be straightforward because of the fact that the film deposition goes through a number of sequential steps, starting with the formation of a mixture of Mn oxides, intermixed with the silicon oxide, and Mn silicate. On Si(100) wafers covered with their native oxide, saturation of that layer is followed by formation of a Mn silicide at the SiO_2/Si interface and, after that, of a metallic Mn film. A similar sequence of events appears to take place on the SiO_2 substrates as well (Figures 5.6 and 5.7).

Indeed, the Mn 2p XPS spectra in Figure 5.6 clearly show the early formation of oxidized Mn, most likely containing silicate species. However, a new aspect of the chemistry seen on the thick silicon oxide is that the intensity of that signal decreases with increasing temperature. Our interpretation is that a nonstoichiometric mixture of Mn silicates and MnOx + SiOx is formed and that some of the deposited Mn diffuses into the bulk (depth profiling experiments such as that in Figure 5.8 support this conclusion). Diffusion is faster at higher temperatures, and may not be fully compensated by the rate of deposition of new Mn for the deposition of $MeCpMn(CO)_3$ on thick silicon oxide. It is also evident in the Mn $2p_{3/2}$ XPS data in Figure 6.6 that a new low-binding-energy feature develops after a minimum of Mn silicate has build up on the surface, and that such feature can then grow indefinitely as a metallic Mn film is deposited on top of the substrate. A couple of observations, including a slight shift in the position of the low-binding-energy Mn 2p XPS peaks as it develops and the fact that the Si 2p and O 1s XPS signals decrease in the intermediate uptake period right after the saturation of the Mn silicate, suggest that the new Mn 2p XPS peak is initially associated with a thin subsurface Mn silicide layer that the Mn(0) film starts to grow only afterward. Possibly, it is the Mn silicide, or a combination of that layer and the initial Mn silicate film (after reaching a minimum Mn density), that acts as a diffusion barrier and allows for the build-up of the Mn(0) film in the following deposition using $MeCpMn(CO)_3$.

The diffusion of Mn into the silicon oxide bulk at high temperatures and the competition of the rate of that process with the deposition of new Mn was tested

by the two independent experiments reported in Figures 5.9 and 5.10. In Figure 5.9, Mn 2p XPS data are contrasted for a thick Mn(0) film grown using the Mn Amidinate precursor at 625 K before versus after annealing to 725 K. Conversion of Mn(0) from the top film into an oxidized Mn form and diffusion into the bulk are demonstrated by the decrease in signal intensity seen in the low binding energy region of the spectra and the partial compensation of that loss by an increase in the signal associated with Mn silicate/Mn oxide. The competition between adsorption and film growth versus diffusion into the bulk is illustrated by the data in Figure 5.10, where a summary of the Mn 2p XPS signal intensities is reported as a function of exposure of the SiO_2 film to the $MeCpMn(CO)_3$ precursor for two cases where the only difference was the pressure of the precursor used during deposition. The data show that more Mn(0) is deposited, at the expense of the formation of Mn silicate (the total amount of Mn remaining approximately the same) at the higher precursor pressure, presumably because of an increase in deposition rate while maintaining all other processes, including the diffusion of Mn into the bulk, the same.

Finally, the role of the Mn silicate/Mn silicide layer as a barrier to prevent the diffusion of newly deposited Mn into the bulk is highlighted by the results shown in Figure 5.11. Here, the diffusio barrier was first prepared by using the Mn Amidinate precursor, after which further Mn deposition was carried out with $MeCpMn(CO)_3$. Thick Mn(0) films could be grown by following that deposition sequence in spite of the low deposition rates afforded by the $MeCpMn(CO)_3$ precursor and the high temperature (725 K) used: although no significant Mn(0)

growth could be achieved at this temperature with $MeCpMn(CO)_3$ alone, metallic Mn deposition was possible once the Mn silicate/Mn silicide was made. One interest in depositing Mn films on silicon oxide substrates in the microelectronics industry is to generate a diffusion barrier for copper interconnects. It is tempting to suggest that the Mn silicate/Mn silicide barrier identified here, which prevents further diffusion of Mn into the SiO_2 bulk, may also act as barrier for copper: it may be that there is no need to deposit additional Mn(0) layers for this purpose.

It was concluded here that the chemistry associated with Mn deposition on silicon oxide films is complex and leads to the sequential formation of Mn silicate, Mn silicide, and metallic Mn layers, much as reported in related systems before. This in itself needs not to be a problem, since the Mn silicate/Mn silicide layers formed appear to be able to act as a diffusion barrier by themselves, and could most likely be used to prevent copper electromigration in integrated circuits, for instance. On the other hand, the Mn-based layers in these applications need to be thin and clean, and their chemical deposition using metalorganic precursors may not always achieve such thickness and composition requirements. Mn acetamidinate compounds afford acceptable deposition rates but tend to decompose and leave carbon and nitrogen contaminants behind. $MeCpMn(CO)_3$ is a cleaner precursor, but it leads to fairly slow deposition rates, even if electron-impact gas-phase activation is used to accelerate the process. Slow deposition rates are undesirable, among other reasons, because they compete with diffusion of Mn into the bulk, although that can be prevented, or at least

minimized, by using lower deposition temperatures. Note, however, that we were able to develop a optimized deposition sequence using a combination of both precursors to take advantage of their good properties and minimize their side effects (Figure 5.11). Conceivable, such ideas may be implemented in practical CVD processes.

Another issue deriving from the data presented above is that, once reactivity of the Mn precursor is observed on the surface and dissociative adsorption is promoted, no self-limiting behavior seems to ever occur, as required for ALD applications. That is, once the Mn deposition starts, the growth of both Mn silicate and Mn(0) films can be sustained for long times, and thick films can be deposited this way. Such behavior is in general not desirable for ALD, but could be controlled by limiting the precursor exposures in CVD-type processes (albeit with a concomitant imposition of somewhat stringent requirements in the design of the deposition). In such a case, a second appropriate coreactant needs to be added to ensure that the Mn precursor ligands, the methylcyclopentadienyl moiety in the case of $MeCpMn(CO)_3$, is removed cleanly from the surface, to avoid carbon deposition. More research is needed to design a viable CVD process for the formation of Mn silicate/Mn silicide/ Mn(0) diffusion barriers.

5.4 Conclusion:

The deposition of Mn-based films on silicon oxide thick films using metalorganic precursors was tested and characterized by using XPS. The behavior of two

different precursors, bis(N,N'-diisopropylpentylamidinato)Mn(II) (Mn Amidinate) and methylcyclopentadienylmanganese(I) tricarbonyl ($MeCpMn(CO)_3$), was contrasted for this chemical deposition.

With the Mn Aamidinate precursor, deposition was shown to be relatively fast, faster at higher substrate temperatures. Several distinct stages were identified during the deposition, starting with the formation of a mixture of Mn silicate and Mn oxide, and followed by the eventual growth of reduced Mn(0)(or Mn nitride) on top. The rate of development of the Mn silicate layer was found not to differ much as a function of temperature, leveling off after reaching a threshold concentration, but growth of that film was optimum at about 625 K; the corresponding Mn 2p XPS signal intensity was seen to decrease somewhat at higher temperatures. The Mn(0) contribution to the Mn 2p XPS spectra, by contrast, clearly grows at faster rates at higher temperatures, and can easily reach intensities corresponding to tens of monolayers. Carbon and nitrogen deposition was detected as well. The N 1s XPS traces, in particular, identified two types of species, one from the organic nitrogen originating from the acetamidinate ligands adsorbed on the surface, and a second associated with a metal nitride that forms throughout the film. The first saturates at about the same coverage in all cases, whereas the second grows in proportion to the amount of Mn(0) deposited and accounts for a level of approximately 15–20 N atomic% contamination in all cases.

Mn film growth is much slower with $MeCpMn(CO)_3$, even if electron-impact gas-phase excitation is used to promote the deposition. Moreover, the apparent total amount of Mn deposited after a given exposure decreases with increasing substrate temperature. In fact, the same sequence of Mn silicate and Mn(0) formation seen with the Mn Amidinate is seen with $MeCpMn(CO)_3$. However, lower Mn densities in the Mn silicate layer are observed at higher temperatures, and the last Mn(0) deposition stage is suppressed almost completely at 725 K. Evidence was also obtained to suggest the intermediate formation of a thin subsurface Mn silicide layer right after Mn silicate saturation and before Mn(0) growth.

It was determined that Mn deposition competes kinetically with Mn diffusion into the bulk, and that the higher rates of the latter step with $MeCpMn(CO)_3$ at high temperatures explain the slower Mn XPS signal intensity evolution seen in the experiments. Independent evidence was obtained for the diffusion of manganese from Mn(0) films into the Mn silicate layer underneath upon annealing at 725 K, and a competition between the rates of Mn deposition and Mn diffusion was highlighted by contrasting Mn uptakes using different pressures of the $MeCpMn(CO)_3$ precursor. Finally, the role of the Mn silicate/Mn silicide self-forming layer as a barrier against metal diffusion into the bulk was successfully tested by showing that Mn(0) films can indeed be grown with $MeCpMn(CO)_3$, even at 725 K, as long as such barrier is made first by using the

Mn Amidinate precursor. A brief discussion was provided on the implications of these results to the design of viable CVD or ALD processes.

5.5 References:

[1] R.G. Gordon, H. Kim, Y. Au, H. Wang, H. Bhandari, Y. Liu, D. K. Lee, Lin, Y. *Advanced Metallization Conference 2008 proceedings*, **2009**, 321;

[2] Y. Au, Y. Lin, H. Kim, E. Beh, Y. Liu, R. G. Gordon, *J. Electrochem. Soc.* **2010**, 157, D341;

[3] T. Usui, H. Nasu, S. Takahashi, N. Shimizu, T. Nishikawa, M. Yoshimaru, H. Shibata, M. Wada, J. Koike, *IEEE Trans. Electron Devices*, **2006**, 53, 2492;

[4] Y. Au, Y. Lin, R. G. Gordon, *J. Electrochem. Soc.* **2011**, 158, D248;

[5] Y. Au, Q. Min Wang, H. Li, J. S. M. Lehn, D. V. Shenai, R. G. Gordon, *J. Electrochem. Soc.* **2012**, 159, D382;

[6] X. Qin, H. Sun, F. Zaera, *J. Vac. Sci. Technol., A* **2012**, 30(1), 01A112;

[7] G.N.Pain, N. Bharatula, G.I. Christiansz, M.H. Kibel, M.S. Kwietniak, C. Sandford, T. Warminski, R.S. Dickson, R.S. Rowe, K. McGregor, *J. Cryst. Growth,* **1990**, 101, 208;

[8] D.K. Russell, I.M.T. Davidson, A.M. Ellis, G.P. Mills, M. Pennington, I.M. Povey, J.B. Raynor, S. Saydam, *Chem. Vap. Dep*. **1998**, 4, 103;

[9] M.J. Almond, H. Redman, D.A Rice, *J. Mater. Chem.* **2000**, 10, 2842;

[10] S.Wen-bin, K. Durose, A.W. Brinkman, J. Woods, *J. Cryst. Growth*, **1991**,13, 1;

[11] B.B. Burton, F.H. Fabreguette, S.M. George, *Thin Solid Films*, **2009**, 517, 5658;

[12] H. Tiznado, F. Zaera, *J. Phys. Chem. B*, **2006**, 110, 13491;

[13] M. Bouman, F. Zaera, *J. Electrochem. Soc.* **2011**, 158, D524;

[14] Q. Ma, H. Guo, R. G. Gordon, F. Zaera, *Chem. Mater.* **2011**, 23, 3325;

[15] Q. Ma, F. Zaera, R. G. Gordon, *J. Vac. Sci. Technol., A* **2012**, 30, 01A114;

[16] Q. Ma, H. Guo, R. G. Gordon, F.Zaera, *Chem. Mater.* **2010**, 22, 352;

[17] M. Leskelä, M. Ritala, *Angew. Chem., Int. Ed*. **2003**, 42, 5548;

[18] B. S. Lim, A. Rahtu, R. G. Gordon, *Nat. Mater.* 2003, 2, 749;

[19] M. Dai, J. Kwon, M. D. Halls, R. G. Gordon, Y. J. Chabal, *Langmuir*, **2010**, 26, 3911.

CHAPTER SIX

Chemical Deposition of Copper on the As-deposited Manganese Films

6.1 Introduction

As discussed in Chapter 2, using chemical means, especially atomic layer deposition, to deposit Cu thin film on the as-deposited Mn thin films is necessary to produce the self-forming barriers. But the deposition of manganese precursors on Si with thick oxide was complicated, and the roles of Mn silicate, Mn silicide or metallic manganese in the later deposition of Copper on the as-deposited manganese surfaces were unknown. For the structure Cu/Ta/TaN structure in current technology, the seed layer Ta is needed to enhance the adhesion of Cu onto to the barrier layer TaN. Given the complex MnSixOy, which might include different amount of metallic Mn, Mn silicate and Mn silicide, the deposition of Cu on the as-deposited Mn thin films needs to be explored to illustrate the roles of each manganese componts in the as-deposited Mn thin films.

Recently, the copper acetamidinate precursor was found to be an potential copper precursors to produce thin, completely continuous and highly conductive copper films [1], and extensive work has been finished by my colleague in our lab using the same compound on nickel, cobalt, and copper substrates identified a stepwise decomposition mechanism involving the formation of smaller

acetamidines, alkenes, amido surface moieties, and HCN, among other species [2-4]. As a result, copper (I)-*N,N'*-di-*sec*-butylacetamidinate (CuAM) in Figure 6.1, was chosen to investigate its deposition on the as-deposited manganese thin films in. It should be noted that CuAM is air sensitive, and caution should be taken to do the experiments. It was filled into a manifold, and heated to 90°C to have sufficient dosing pressure.

6.2 Results

6.2.1 Preparation of as-deposited Mn thin films

Fortunately, we successfully developed one method to enhance the deposition of manganese thin film on Si with thick silicon oxide through gas phase activation of the precursor, $MeCpMn(CO)_3$, by electron bombardment, discussed in previous chapters . In this method, manganese thin film with different ratios of metallic Mn, Mn silicate/oxide and Mn silicide could be controlled to study the deposition of copper on such as-deposited surfaces. Figure 6.2 shows the thin films we deposited on Si with thick silicon oxide at 625 K with different ratios of metallic Mn, Mn silicate/oxide and Mn silicide on the surface.

6.2.2 CuAM on MnSiOx/300 nm SiO_2 at 625K

A silicon substrate with only a Mn silicate (MnSiOx) was made using $MeCpMn(CO)_3$ on a 300nm SiO_2 film at 625 K. The Mn 2p XPS in Figure 6.3, which corresponds to the surface before and after copper deposition, clearly shows again that only Mn silicate was on the surface before deposition of the copper

Figure 6.1 Copper precursor: copper(I)-*N,N'*-di-*sec*-butylacetamidinate.

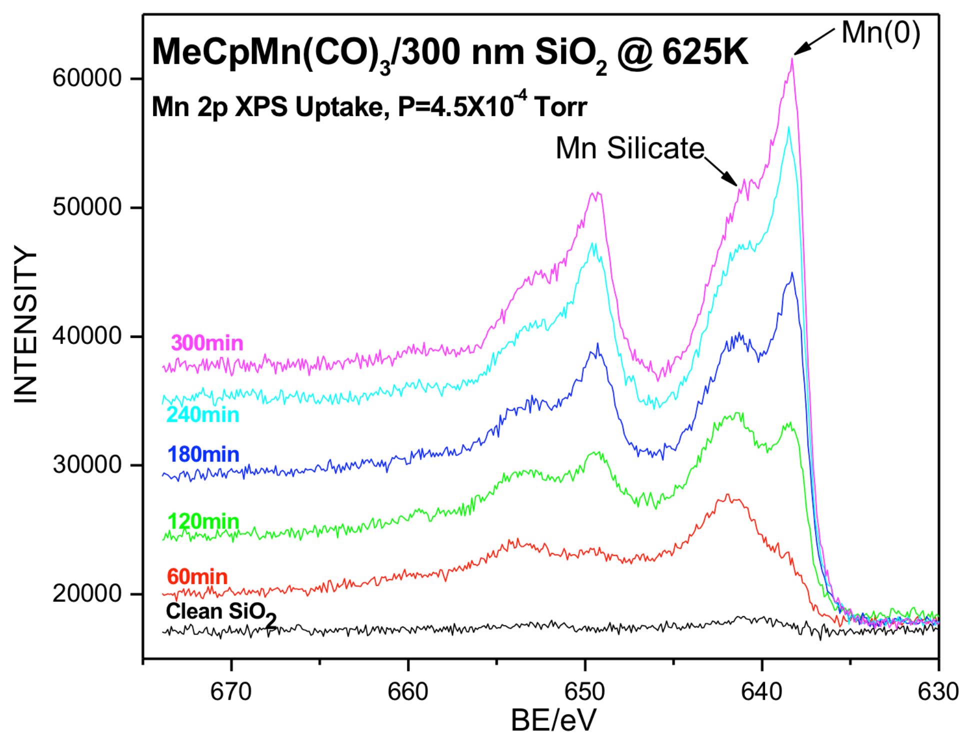

Figure 6.2 Mn 2p XPS for the deposition of $MeCpMn(CO)_3$ on 300nm SiO_2 at 625 K as function of dosing time(60, 120, 180, 240, and 300 minutes).

precursor, but that, after deposition of the manganese(a, black line in Figure 6.3), the sample was transferred into the main chamber to collect XPS data, and then transferred back to the preparation chamber to deposit CuAM on it at 625K, using a dosing pressure of 0.05 mTorr for 30 mintues(b, red line). Finally, the sample was sputtered using Ar+ ions for 5 minutes with emission current at the ion gun of 25 mA. The evolution of XPS peaks, Mn 2p, Cu 2p, and N 1s during the above process was shown in Figure 6.3, 6.4 and 6.5.

The black line in Figure 6.3 shows the formation of Mn silicate on the surface, based on the analysis of the binding energies for Mn 2p 3/2 peaks centered at 641.8 and 653.9 eV and the shoulder peaks at ~ 645.9 eV and 659.4 eV, decribed in Chapter 4. After the deposition of 30 minutes CuAM, the intensity of the Mn 2p XPS features decrease in intensity, but no obvious shift of binding energy was observed. Finally, 5 minutes sputtering could effectively remove the Mn silicate layers. The Cu 2p XPS signal intensity is very strong compared to that of Mn, in terms of its XPS cross section, and the fast increase in those peaks after 30 minutes dosing of CuAM, with the central peaks at 932.5 eV, typical of metallic Cu according the work in our lab [2-4], is clear evidence of copper deposition. Ar sputtering could remove most of the Cu from the surface. However, both Mn and Cu traces could be seen after sputtering, and this is most likely because some interlayer mixing always occurs during sputtering, which is not strictly layer by layer. The good news for the deposition of CuAM, which has nitrogen inside the molecule, is that no notable increase in the intensity of the N 1s XPS peaks at 399

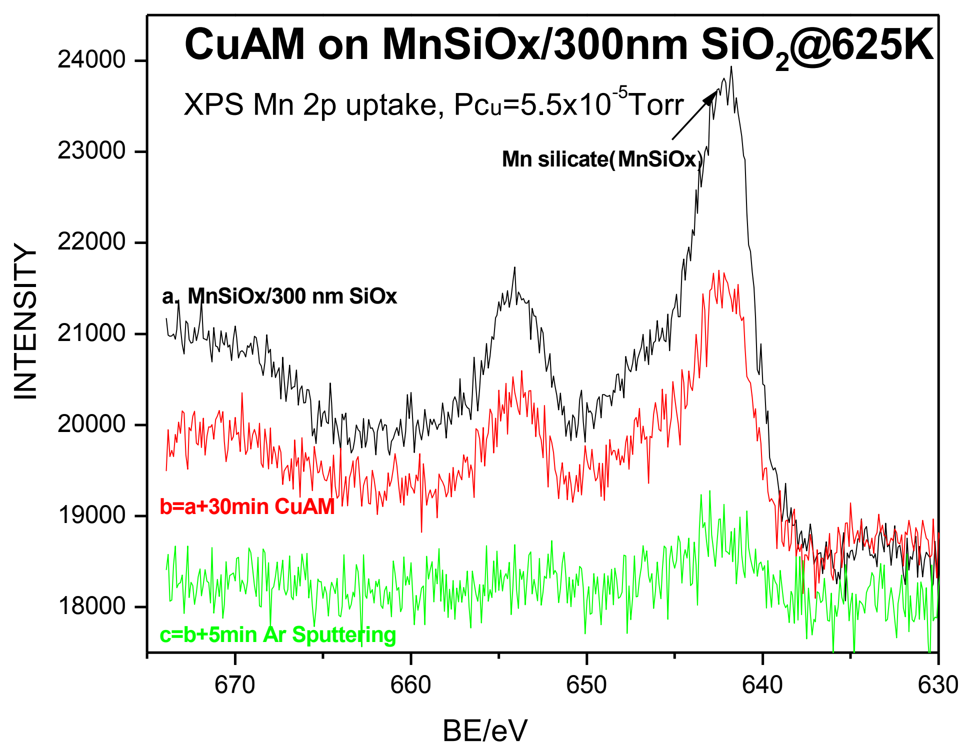

Figure 6.3 XPS Mn 2p for CuAM deposition on 300n SO_2 covered by Mn silicate at 625 K and sputtering after deposition.

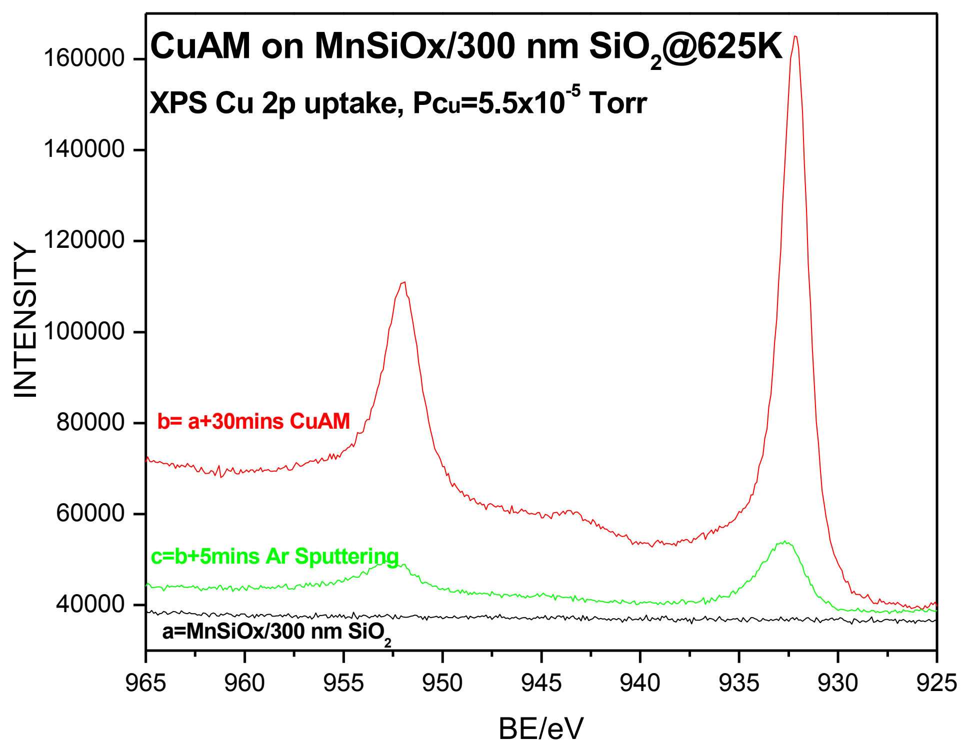

Figure 6.4 XPS Cu 2p for CuAM deposition on 300n SO_2 covered by Mn silicate at 625 K and sputtering after deposition.

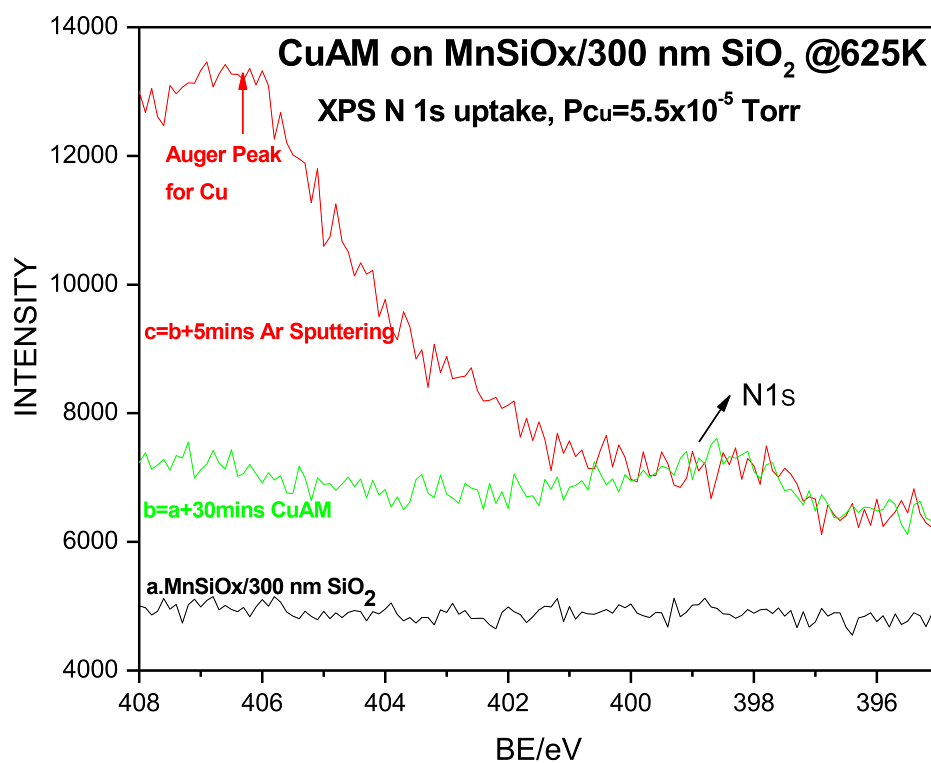

Figure 6.5 XPS C 1s for CuAM deposition on 300n SO_2 covered by Mn silicate at 625 K and sputtering after deposition.

eV was seen in Figure 6.5, indicating minimal incorporation of N in the growing of Cu films.

To summarize, the deposition of CuAM on Mn silicate is fast and clean, leaving only metallic Cu on the surface at 625 K. This means that the Mn silicate might be a diffusion barrier for Copper at 625 K, as well as fast growth of copper. Estimates about the thickness of Cu from decrease in Mn signal upon Cu addition, using the inelastic mean free path of manganese (kinetic energy of electron is about 611.7 eV using Mn $2p_{3/2}$ XPS peaks) from the database [5], is 0.7 $\pm$0.2 nm, about 3 monolayers according to the results of Cu an Ni[4]. The deposition is a chemical vapor deposition, rather an atomic layer deposition.

As discussed in the introduction, the copper wires need to be surrounded by diffusion barriers. As a result, it is also necessary to study the deposition of manganese on Cu surfaces. This is explored by the results in Figure 6.6. After a 30 minutes dosing of CuAM on the 300 nm SiO_2, only a little Cu was formed on the surface, but the following 60 minutes dosing of $MeCpMn(CO)_3$ showed faster growth of manganese with much more metallic Mn, compared to what is obtained by deposition under the same conditions on a clean 300 nm SiO_2 film, as shown in Figure 6.2 . This fast growth of Mn on Cu, combined with the fast growth of Cu on Mn silicate, points to the potential for the use of such depositions of Mn and Cu in producing self-forming diffusion barriers for copper interconnects in microelectronics. On the other hand, it also provides a method

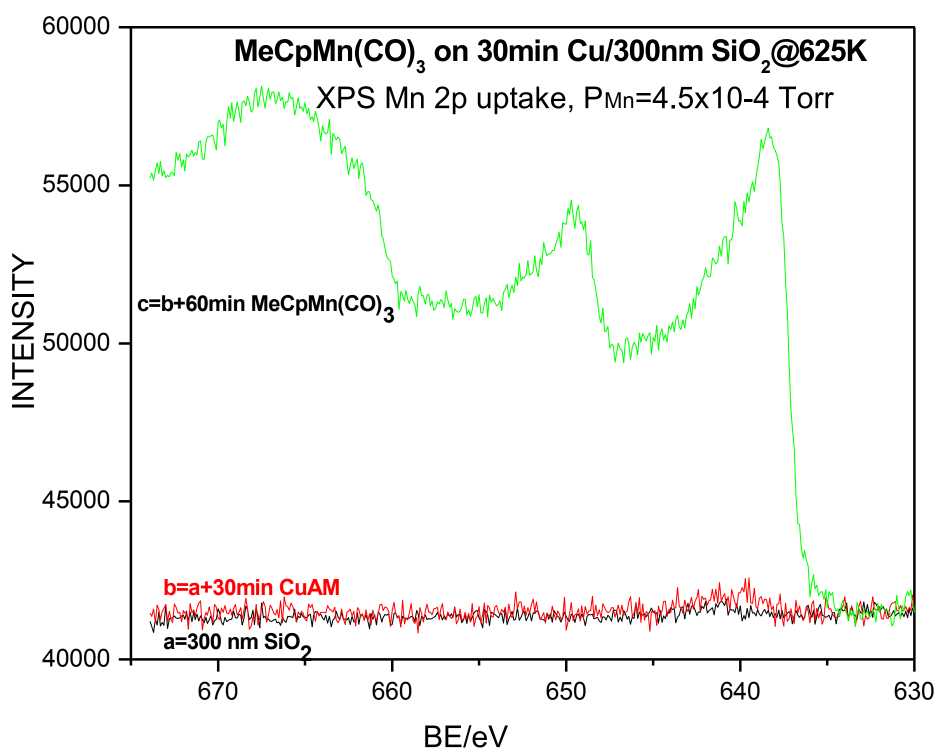

Figure 6.6 XPS Mn 2p for $MeCpMn(CO)_3$ on the as-deposited Cu thin film made by 30 minutes dosing of CuAM.

to deposit metallic Mn on silicon oxide substrates, by depositing some Cu first, possibly to act as nucleation sites. However, the nature for such behavior is still unclear, and the role of Mn silicates in the deposition of Cu needs more work.

6.2. 3 CuAM on Mn(0)/MnSiOx/300 nm SiO_2 at 625K

The experiments in section 6.2.2 were done on substrates with only Mn silicate on; and it was found that Cu can be easily deposited on such surfaces. Since the deposition of $MeCpMn(CO)_3$ on this 300 nm SiO_2 surface was shown before to be complex, it is important to investigate the deposition of Cu on the surfaces with more than just Mn silicate on. Figure 6.7 shows that the ratio of metallic Mn (Mn(0)) could be tailored to fit this need. In this case, the deposition of Cu was carried out first on a surface with both Mn(0) and Mn sliciate (~ 3:4 ratio of Mn(0): Mn silicate) after 240 minutes deposition of Mn (a, black line). That was followed by a 30 minutes dosing of CuAM, which yield the spectra shown by a red line (b), this was followed by an addition 60 minutes deposition of $MeCpMn(CO)_3$, to yield the XPS green line (c). That blue (d) and light blue l (e) lines were obtained after the last two 30 minutes dosings of CuAM. Figure 6.8 shows the results of the Cu 2p XPS, same sequence of the deposition (a to e).

From comparison between the black and red lines in Figure 6.7, it is concluded that Mn can be buried by the Cu film grown on top, and more metallic Mn is lost after the deposition of Cu on top of it. Afer the first 30 minutes dosing of CuAM on the substrate with both Mn(0) and Mn silicate on, the red line (b) in Figure 7.8 indicates a slower Cu growth rate compared to the results in 7.4 (~30% lower

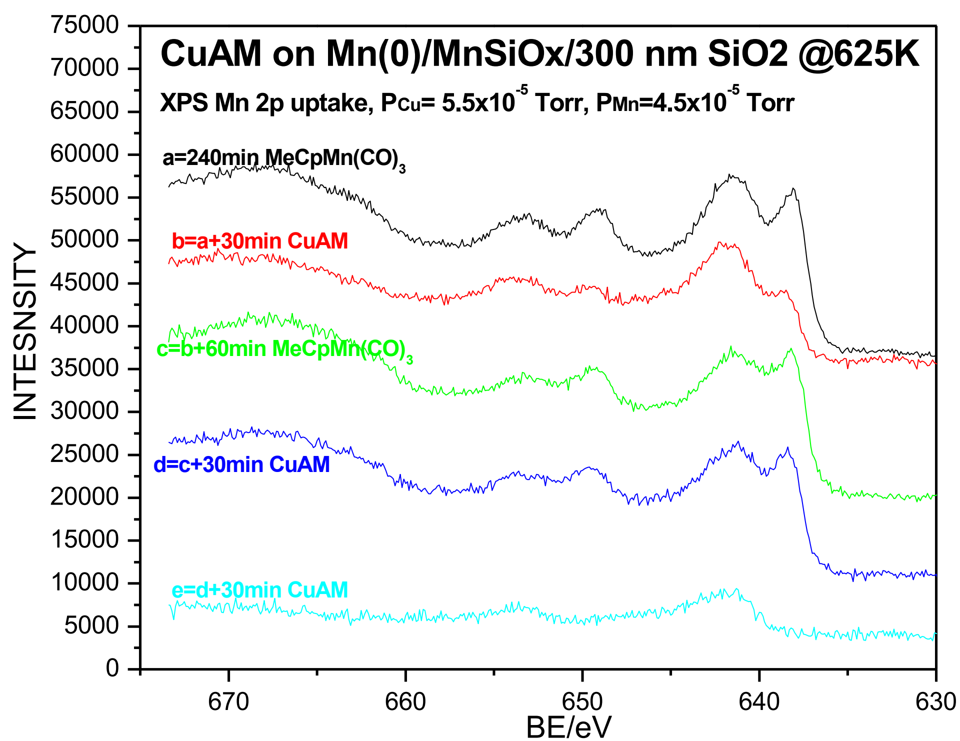

Figure 6.7 XPS Mn 2p for the mixed depositions(a to e) using $MeCpMn(CO)_3$ and CuAM.

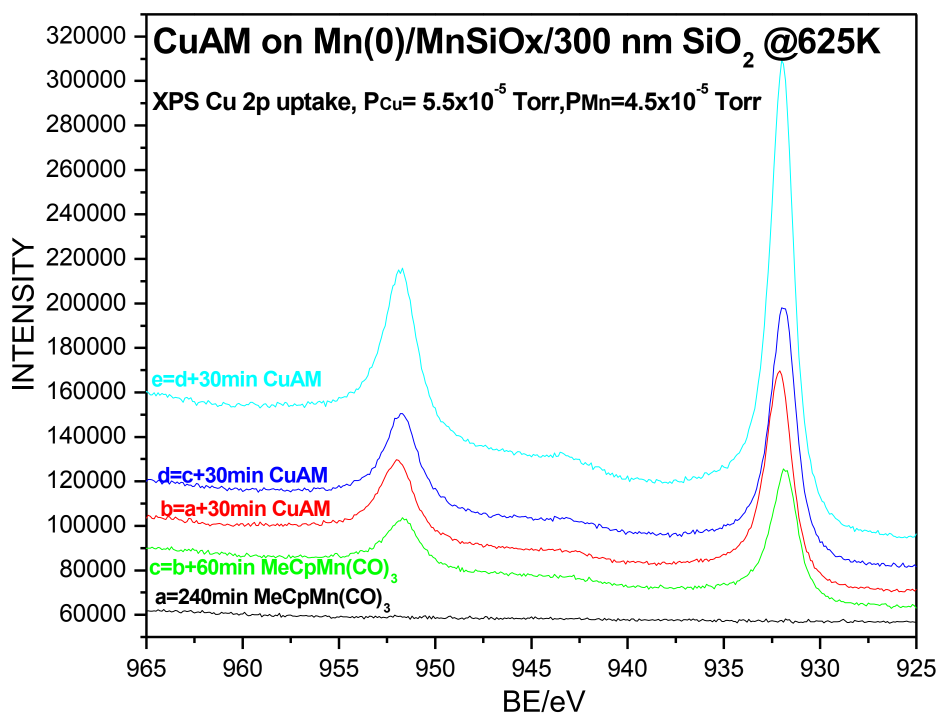

Figure 6.8 XPS Mn 2p for the mixed depositions(a to e) using $MeCpMn(CO)_3$ and CuAM.

than that in Figure 6.4). The following 60 minutes dosing of $MeCpMn(CO)_3$ regnerates both the Mn(0) and Mn silicates, similar to what was seen in Figure 6.4, from 60 minutes to 120 minutes dosing. This means that the Cu formation on the surface does not change the behavior of manganese deposition. Which is contrasted with the results in Figure 6.6. However, after the second dosing of CuAM, the intensity of Mn 2p did not decrease much, and after the third dosing of CuAM, the Mn signal did become significantly reduced. This is consistent with the slow growth of Cu in the second dosing of CuAM, and much faster growth of Cu in the third dosing of CuAM. One interesting observation here is that Mn(0) almost disappears after the third dosing of CuAM, which means that the diffusion of Mn(0) is fast and much less Mn (0)could be detected with a thick Cu layer on top.

6.2.4 CuAM on 300 nm SiO_2 vs Mn(0)/MnSiOx/300 nm SiO_2 at 425K

From the above experiments, we can see that the deposition rates for CuAM at 625 K are fast, and follow CVD behavior, as the CuAM precursor is easy to decompose at higher temperature (the same as with Mn Amidinate). On the other hand, the behavior of the bare 300 nm SiO_2 surface in ALD without any Mn, also needs to be investigated. Some results from work in this direction are shown in Figure 6.9 and 6.10.

The inset in Figure 6.9 provides the background data for the case where the deposition of Cu was finished on a surface almost fully cover with metallic Mn, only metallic Cu was observed after the following CuAM deposition. By contrast, the deposition of CuAM on the bare 300 nm SiO_2 was much slower, and oxidized

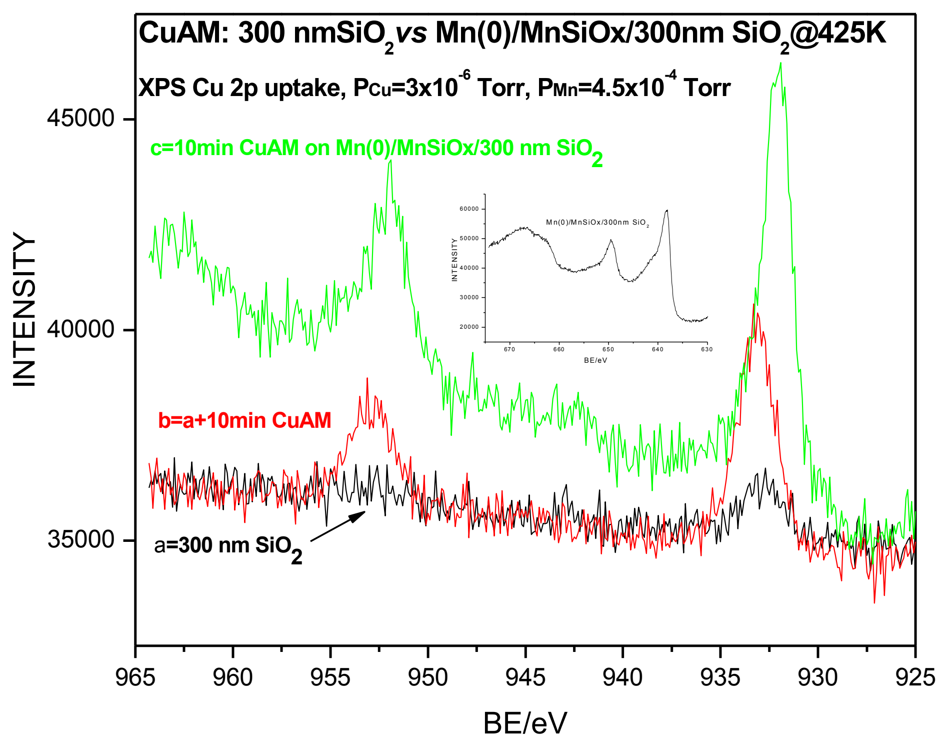

Figure 6.9 XPS Cu 2p for CuAM on bare 300 nm SiO_2 vs Mn(0)/MnSiOx/300 nm SiO_2 at 425 K.

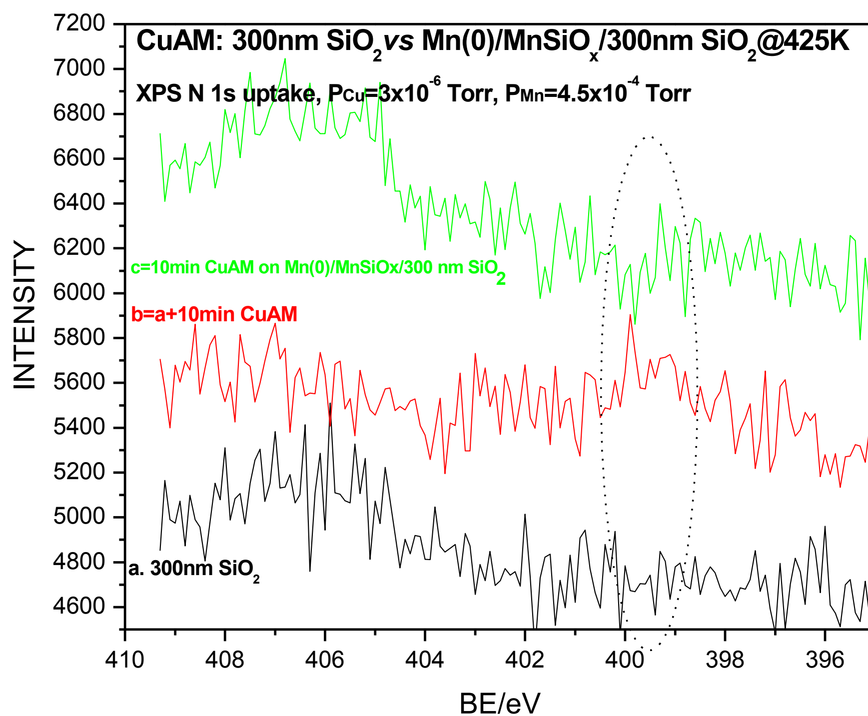

Figure 6.10 XPS N 1s for CuAM on bare 300 nm SiO_2 vs Mn(0)/MnSiOx/300 nm SiO_2 at 425 K.

copper was grown on the surface. These data indicate that Cu containing species might be oxidized on the bare surface, perhaps because the relatively high reactivity of OH groups on the top. No obvious increase in XPS signal for N 1s seen in Figure 6.10 for the deposition of CuAM on a surface almost fully covered by Mn(0) surface, indicating that almost no acetamidinate ligand was left on the surface, while some ligands were left on the surface after Cu deposition on the bare 300 nm SiO_2 surface. The positions of the XPS peaks expected from organic nitrogen are highlighted by the circles in Figure 6.10 to show the difference. Another point derived from these data is that the Cu deposition rate at 425 K is slower than at 625 K, which might be easy to explain by assuming the activated process. But the amount of Mn (0) seen on the surface is also different, which also affect the deposition rates. Refer to the comparison provided between sections 6.2.2 and 6.2.3, silicate only in the samples reported in section 6.2.2 may facilitate the deposition of Cu at a faster pace, and more Mn(0) might not promote the formation of metallic Cu on the surface.

More work needs to be done to find out the roles of Mn(0) and Mn silicate in the future. For example, the Cu precursor can be deposited on the as-deposited manganese thin films with completely covered by Mn(0) after hours of dosing of $MeCp(CO)_3$, and bare 300 nm SiO_2 at 625K, making the results comparable to the results in section 6.2.2 and section 6.2.3. The copper deposition at lower temperatures from 375 K to 575 K can be carried out to find a possible ALD temperature window. Then a series of experiments at the same temperature on the-deposited thin films with no Mn, only Mn silicate, both Mn silicate and Mn

silicide but different ratios, and only Mn(0) on the surface should be done to find the role of these species. At the same time, annealing these samples might be useful to solve the issue.

6.3 Discussion and conclusion

Cu deposition on the as-deposited manganese thin films is complicated, because the surface is covered by the manganese complex. From the results obtained non a surface with only Mn silicate, metallic Cu can be grown fast without increasing the nitrogen contaminants left on the surface, which means such self-forming Mn silicate films might be used as a diffusion barrier layer for copper interconnects. At the same time, metallic manganese can be easily deposited on the surface with metallic Cu films. Mn oxides are fairly stable, much more stable than metallic Mn and Cu, also stable than CuO [6], which might explain the fast growth of metallic Cu on the surface with only Mn silicate.

For the deposition of Cu on a surface with both Mn(0) and Mn silicate, the growth rate is a little slower than that on only silicate, because longer nucleation period is needed for this deposition, which can be seen clearly from Mn 2p XPS data in in Figure 6.8 after the second and third 30 mintues dosing of CuAM, as the growth of Cu during the second 30 minutes dosing is much slower than that during the third 30 minutes dosing. It might be expected that a seed layer, respectively, a metallic Mn layer, is not a must in this self-forming manganese thin films to enhance the deposition of Cu, like Ta seed layer to TaN barrier layer.

For the deposition of Cu at lower temperature (425K), it can be seen in Figure 6.9 that a film is needed to prevent the oxidation of Cu on the SiO_2 surface, and temperatures (from 375 K to 600K) might be tried to find a possible temperature window for this Cu precursor. Though growth rates are slower, surface chemistry involved in these depositions at lower temperatures might be easier as the decomposition of the Cu precursor is avoided.

To sum up, Cu can be easily deposited on surfaces covered with different ratios of Mn(0) to Mn silicate, easier than on the bare SiO_2 surface. For the surface with only Mn silicate on, it seems that Cu displays higher deposition rates, and Mn deposition is also much faster in consecutive dosings. This might be one of the most important findings from the experiments reported in this chapter. This behavior has the potential to be applied in producing self-forming manganese barrier in microelectronics. On the other hand, for the deposition of CuAM on the surfaces with both Mn(0) and Mn silicate, the growth rates are slower than that on the Mn silicate film alone. It seems that the initial phase for Cu deposition takes longer, and the Mn(0) disappears at much higher rates than the Mn silicate. Finally, even at 425 K, it is still possible to deposit copper on the surfaces with almost all the Mn(0) covered and on bare 300 nm SiO_2, although the deposited copper ends up in an oxidized state on the bare SiO_2 . Organic ligands are left on the bare SiO_2, while no obvious increases in C 1s XPS signals were found after deposition on Mn(0).

6.4 References:

[1] M. Dai, J. Kwon, M. D. Halls, R. G. Gordon, Y. J. Chabal, *Langmuir*, **2010**, 26, 3911.

[2] Q. Ma, H. Guo, R. G. Gordon, F. Zaera, *Chem. Mater.* **2011**, 23, 3325;

[3] Q. Ma, F. Zaera, R. G. Gordon, *J. Vac. Sci. Technol., A* **2012**, 30, 01A114;

[4] Q. Ma, H. Guo, R. G. Gordon, F.Zaera, *Chem. Mater.* **2010**, 22, 352;

[5] *NIST Electron Inelastic-Mean-Free-Path Database 7.1*;

[6] O. Knacke, O. Kubaschewski, K. Hesselmann, Eds. *Thermochemical Properties of Inorganic Substrates*, 1st ed. Spring-Verlag, Berlin, **1973**.

CHAPTER SEVEN

General Conclusions and Future Work

7.1 General conclusions

The work in this dissertation is part of a continuous effort in our group to understand the mechanisms involved in chemical vapor deposition (CVD) and atomic layer deposition (ALD) from the point view of surface chemistry. A lot of work has been done in our lab related to issues in CVD or ALD to provide insights into the reaction mechanisms at a molecular level [1-5]. Our contribution here is on the chemical deposition of manganese films, which are used as potential materials for self-forming diffusion barriers for copper interconnects in microelectronics.

Here, we found that gas-phase activation of $MeCpMn(CO)_3$, which was accomplished by using a typical nude ion gauge employed in many ultrahigh-vacuum (UHV) studies, enhances its dissociative adsorption on silicon surfaces, affording the design of ALD cycles with more extensive Mn deposition and at lower temperatures. Significantly higher Mn uptakes were demonstrated by X-ray photoelectron spectroscopy (XPS) on both silicon dioxide films and on Si(100) wafers Ar+- sputtered to remove their native oxide layer. The effectiveness of this electron-impact activation approach in ALD is explained in terms of the

cracking patterns seen in mass spectrometry for the metal–organic precursor used.

The nature of films prepared on Si with native oxide film by chemical means using $MeCpMn(CO)_3$ as the precursor was also investigated. It was found that at the temperatures typically used for deposition, between approximately 550 and 750 K, a manganese silicate layer grows first upon reaction with the top SiO_2 surface, and a thin manganese silicide film develops latter at the SiO_2/Si (100) interface. The combined manganese silicate/silicon dioxide/manganese silicide films reported here are only ~1 nm in total thickness, and their growth by chemical means is self- limiting, which is very promising. The performance of these structures, of the silicide in particular, in microelectronic applications is still to be determined.

For the deposition of Mn on thick SiO_2, the behavior of two different precursors, Mn Amidinate and $MeCpMn(CO)_3$, was characterized and contrasted using XPS. The acetamidinate precursor proved highly reactive, affording the deposition of Mn at reasonable rates, higher at higher temperatures, but also leading to the incorporation of approximately 15% of nitrogen and additional carbon in the grown Mn(0) films. The methylcyclopentadienyl compound, by contrast, proved quite unreactive, even if an electron-impact gas-phase preactivation step recently developed in our laboratory was used. Slow deposition rates were seen with this precursor, appearing to be slower at higher temperature because of an unfavorable kinetic competition with Mn diffusion into the bulk. In both cases, a

nonstoichiometric mixture of MnOx + SiOx and Mn silicate is formed first, possibly followed by the formation of a thin subsurface Mn silicide layer. The combined Mn silicate/Mn silicide structure acts as an effective diffusion barrier, after which Mn(0) metallic films can be grown on top.

Optimized deposition sequence using two different manganese precursors, $MeCpMn(CO)_3$ and Mn Amidinate, was developed on the thick SiO_2 surfaces: first, Mn Amidinate, was deposited on the surface after a few mintues of dosing to form a combined Mn silicate/Mn silicide layer which serves as an effective diffusion layer for the M(0) films growth later ; then, $MeCpMn(CO)_3$ was introduced to the as-deposited surfaces to obtain a slow growth of metallic Mn with a cleaner surface after all the depositions.

Depositions of both $MeCpMn(CO)_3$ and Amidiante on thick SiO_2 substrates are typical of chemical vapor deposition (CVD), with much higher growth rates than that of $MeCpMn(CO)_3$ on Si substrates with native oxides. However, Mn silicate formed on Si substrates with native oxide reaches saturation, which is a typical feather of atomic layer deposition (ALD), though the growth of Mn silicide formed after the saturation of Mn silicate between the interface of Mn silicate and Si(100) continues all the time.

Cu thin films on the surfaces with different ratio of Mn(0) to Mn silicate were also studied. It was found that metallic Cu can be fast grown on the surfaces with only Mn silicate on. On the other hand, CuAM on the surfaces with both Mn(0)

and Mn silicate, displays lower growth rates. Finally, even at 425 K, it is still possible to deposit copper on the surfaces with almost all the Mn(0) covered. The roles of each manganese component in the as-deposited manganese thin films need to be clarified by a series experiments, and this is helpful to understand the nature of the complex, MnSixOy, and to produce such a self-forming barrier layer in microelectronics.

7.2 Future work

7.2.1 Studies using temperature programmed desorption

TPD, also called TDS (Thermal Deposition Spectroscopy), is an excellent technique to study the surface chemistry of precursors during deposition processes [6]. In a typical TPD experiment, specific amounts of chemicals are dosed onto the solid surface at low temperature, and then the surface is heated at a fast but steady rate while the desorbing species are monitored by using mass spectrum. I have been working on the TPD apparatus on my system, but I have not been successful due to limitations of the present system, such as, slow and unstable heating of the sample, lower resolution Mass Spectrum and high water and contaminants level in the chamber. TPD experiments for these manganese precursors, especially for methylcyclopentadieny manganese tricarbonyl, might be helpful to understand the reaction mechanism.

7.2.2 Studies on manganese thin film deposition

It became clear from our studies that none of the two manganese precursors are ideal for ALD applications on Si wafers. The surface chemistry involved in the deposition for both precursors are complicated and the competition between manganese films formation and diffusion, making the choosing of the reaction conditions difficult. New precursors might be identified from the previous CVD studies, since ALD is still a modified version of CVD. In terms of H_2 and N_2O were found in studies in our laboratory to be not good for the deposition of manganese thin films. Azocompound has proven to be a good reducing agent in previous work in our lab [8], and could be used as an alternative. This was considered, but I did not succeed in the synthesis of azopropane. More work should be done in this direction in the future. A better ALD reactor may be needed to carry out the ALD reactions using similar reaction conditions as in other labs. The preparation chamber in our system equipped with a tubormolecular pump, limits the maximum dosing pressure that can be used in our expriments.

7.2.3 Studies on Cu deposition on the manganese thin films

The preliminary results in Chpater 6 indicate the complexity of this deposition. First of all, future work should be directed to reproduce the control of the ratio of Mn(0) and Mn silicates on the surfaces used to start these studies. Second, parameters for the deposition of Cu precursor on such substrates need to be narrowed down, including as a proper temperature window.

7.2.4 Electronic properties measurements

The results in Chapter 5 suggest the possibility of a simply self-forming manganese barrier that may be used as a barrier for Cu. This conclusion is based in part on the observation of a fast growth of the metallic Mn after the saturation of Mn silicate layer. We can make this argument more convincing if we were able to develop a device and measure its electronic properties using a 4-point probe [8]. The combined results from both the chemistry and electronic studies would make the selection of appropriate precursor fast and efficient.

7.3 References:

[1] Q. Ma, H. Guo, R. G. Gordon, F. Zaera, *Chem. Mater.* **2011**, 23, 3325;

[2] Q. Ma, F. Zaera, R. G. Gordon, *J. Vac. Sci. Technol., A* **2012**, 30, 01A114;

[3] M. Bouman, F. Zaera, *ECS Trans*. **2010**, 33, 291;

[3] Q. Ma, H. Guo, R. G. Gordon, F.Zaera, *Chem. Mater.* **2010**, 22, 352;

[4] H. Tiznado, F. Zaera, *J. Phys. Chem. B*, **2006**, 110, 13491;

[5] F. Zaera, *J. Mater. Chem.* **2008**, 18, 3521;

[6] G. A. Somorjai, *Introduction to Surface Chemistry and Catalysis*, New York, Wiley, **1994**;

[7] N.R. Gleason, C.J. Jenks, C.R. French, B.E. Bent, F. Zaera, *Surf. Sci.***1998**, 405, 238;

[8] R. G. Gordon, H. Kim, Y. Au, H. Wang, H.B. Bhandari, Y Liu, D. K. Lee, Y Lin, *Advanced Metallization Conference 2008 Proceedings*, **2009**, 321.